eman ta zabal zazu

Universidad del País Vasco
Euskal Herriko Unibertsitatea

FACULTY OF ENGINEERING BILBAO
UNIVERSITY OF THE BASQUE COUNTRY

PhD Thesis

LASER METAL DEPOSITION ENHANCEMENT BY HOLISTIC SIMULATION OF POWDER MASS FLOW AND DEPOSITION INTO THE MELT POOL

Presented by
Dipl. Ing. Jon Iñaki Arrizubieta Arrate

At the
Department of Mechanical Engineering

Of the
University of the Basque Country

For obtaining the degree on
International PhD in Mechanical Engineering

Supervised by
Prof. Dr.-Ing. Aitzol Lamikiz
Dr.-Ing. Kristian Arntz

June 2017

(c) 2017 JON IÑAKI ARRIZUBIETA ARRATE

Nire gurasoei,

momentu oro nire alboan egon izanagatik

Acknowledgements

Once I have finished writing the present dissertation work, I look back and notice the huge effort its accomplishment has required me for the last four years. During this period, I have learned how to research, but I have also learned how to work in team and more important, to be part of a team. Therefore, I would like to thank all those people who have encouraged me.

First of all, I would like to express my sincere gratitude to my supervisors, Prof. Lamikiz and Dr. Arntz, for their continuous encourage and motivation. Without their support, the accomplishment of this work would have been impossible.

Besides, I would like to thank “La Caixa” Foundation for the financial support during this period. My heartfelt gratitude for their trust and confidence placed in my PhD work from the very beginning.

Special thanks to the staff at the Mechanical workshop of the University of the Basque Country, thank you; especially to Silvia, Exe, Mario, Iñigo, Amaia, Adrian, Alvaro, Asier, Gorka, Octavio, Rober, Iker, Izaro, Ivan, Haizea, Olatz, Leire, Aintzane, Egoitz and Unai. Many of the best ideas and resolutions to the toughest problems came up in the brainstorming sessions carried out during the coffee breaks. Also to my office colleague Andoni, who has been by my side during this whole period. Neither could I forget those professors that have been an inspiration and a real assistance during this journey: Eneko, Soraya, Naiara, Berti, Frank and Jose Antonio.

I would like to express my gratitude to the Fraunhofer IPT, for welcoming and taking care of me during my stay in Aachen. To all the friends I have done there. Besides offering the opportunity of improving my researching skills in one of the most recognized worldwide researching centers, you made me feel part of it. Thanks to you, I enjoyed my time.

I would like to thank Mada, for being by my side during this time. You have encouraged me every time the horizon was obscured and helped me to give my best.

But most of all, I would like to thank my parents. Who have been always by my side, not only for these last four years, but also along my whole studies. I am deeply grateful for all of the sacrifices that you have made on my behalf.

Summary

The present research work is focused on the development of a holistic model of the Laser Metal Deposition (LMD) and the improvement of the process based on the obtained knowledge. For this purpose, the whole additive process is simulated in different stages. First of all, a new laser cladding nozzle that fulfils the process requirements is designed using a Computational Fluid Dynamic (CFD) commercial software. Afterwards, the designed nozzle is manufactured and validated by means of an improved version of an already existing mechanical method for measuring the powder distribution.

Moreover, with the aim of enhancing the efficiency of the nozzle and increase the stability of the process, a new powder regulation system based on a solenoid is developed and installed. The nozzle is used satisfactorily for the repair of hot and cold stamping dies. Additionally, typical parts of the aeronautical sector are manufactured: initially a 3 axis blade is built, afterwards a 5 axis blade and lastly a whole Blisk is manufactured. Thus, the good performance of the developed nozzle is demonstrated.

Regarding the LMD process, the melt pool stability is a critical factor when obtaining high quality parts. Therefore, a proper modeling of the melt pool is required for obtaining an accurate LMD model. A model that considers the fluid-dynamic phenomena that occur inside the melt pool is developed using the Matlab environment. After the model validation, the importance of considering or neglecting the melt pool fluid-dynamics phenomena is evaluated. To this end, different LMD situations and parameter combinations are simulated and the relevance of considering or neglecting the melt pool fluid-dynamics is evaluated in each case by comparing the experimental results with the outcome provided by the model. On the basis of the obtained results, an empirical coefficient that determines the influence of the movement of the molten material during the LMD process is defined. The results show that the influence of the fluid-dynamics phenomena is minimal for the conventional LMD process parameters and they can be omitted without losing accuracy.

On the basis of the previous statement, a 3D thermal model that simulates the LMD process is developed. Heat transfer inside the workpiece by means of conduction is considered and the model calculates the dimensions of the melt pool where material is added. Filler material is added according to the powder distribution at the nozzle exit and the model simulates the generation of the clad and the subsequent solidification. On the basis of the heating and cooling cycles of the base and filler materials during the LMD process, the model is able to predict the

mechanical properties of the deposited material, such as the hardness of the material, and the resulting microstructure.

To sum up, this work presents a methodology to enhance the Laser Metal Deposition process based on a holistic simulation of the powder mass flow, filler material deposition and the generation of the clad. Obtained results pretend to facilitate the inclusion of the LMD process in CAD/CAM/CAE tools, introducing knowledge based functions into these tools.

Main Index

Chapter I. Introduction 3

I.1. Background and motivation 3

I.2. Objectives 5

I.3. Memory organization 6

Chapter II. State of the art of the Laser Metal Deposition process and the latest developments.. 11

II.1. Introduction to the lasers 11

II.1.1. Laser generation principles 11

II.1.2. Main parameters of the laser based processes 15

II.1.3. Industrial laser market and revenue numbers.. 16

II.2. Introduction to the Laser Metal Deposition process 18

II.2.1. LMD and SLM comparison 18

II.2.2. Laser Metal Deposition process basics 23

II.2.3. Nozzle design for the Laser Metal Deposition process 24

II.2.4. Different filler systems: wire and powder.. 25

II.3. Latest machines for the LMD and hybrid processes 28

II.4. Laser manufactures and market numbers 30

II.5. Characteristics of the filler material and different delivery systems.............. 33

II.5.1. Powder characteristics 33

II.5.2. Powder feeder types used in Laser Metal Deposition 36

II.5.3. Review of the evolution of designs and patents of industrial LMD nozzles 40

II.6. Latest developments for predicting the geometry of the deposited material and process monitoring.. 48

II.6.1. Latest CAM developments 49

II.6.2. Process monitoring 51

II.6.3. Control systems of the powder feeders 56

II.7. Industrial applications 58

II.7.1. Aeronautical sector 58

II.7.2. Die & Mold 62

II.7.3. Naval industry and heavy industry 64

II.8. LMD process model 66

II.8.1. Powder particle modeling 66

II.8.2. Melt pool model 79

II.8.3. Filler material addition and material deposition 84

II.9. Main highlights after the analysis of the state of the art of the Laser Metal Deposition 90

Chapter III. Coaxial nozzle design for the Laser Metal Deposition process based on CFD simulation results 95

III.1. Introduction 95

III.2. Coaxial continuous nozzle design 96

III.2.1. LMD nozzle specifications 96

III.2.2. Mathematical background of the CFD model and considerations 98

III.2.3. Conceptual design of the nozzle 103

III.2.4. Description of the used mesh and boundary conditions 103

III.2.5. Analysis of the obtained results after the CFD simulations 106

III.2.6. Manufacturing and final assembly of the EHU-Coax 2015 nozzle 111

III.2.7. Validation tests of the EHU-Coax2015 nozzle 113

III.2.8. Determination of the efficiency of the EHU-Coax2015 nozzle 117

III.3. Powder flux regulation system 119

III.3.1. Aim of the regulation system 119

III.3.2. Development of the regulation system 120

III.3.3. CFD simulation of the powder flux regulation system 122

III.3.4. Validation of the powder flux regulation system 125

III.4. Real applications of the nozzle EHU-Coax2015 133

III.4.1. Die and mold manufacturing 133

III.4.2. Aeronautical sector 135

III.4.3. High resistance coatings 137

III.4.4. Copper electrodes 137

Chapter IV. Evaluation of the importance of melt pool fluid-dynamics in Laser Metal Deposition modeling 141

IV.1. Introduction 141

IV.2. Methodology proposed to analyze the influence of the fluid-dynamic phenomena inside the melt pool 141

IV.3. Description of the developed model 142

IV.3.1. Melt pool dynamics governing equations 142

IV.3.2. LMD model considering melt pool dynamics 147

IV.3.3. LMD model without considering melt pool dynamics 150

IV.4. Experimental validation of the influence of the melt pool fluid-dynamics in the LMD process 151

IV.4.1. Analysis of the melt pool generated by a stationary laser beam 152

IV.4.2. Analysis of the material deposition in the LMD process 155

IV.4.3. Influence of the melt pool fluid-dynamics in the LMD process 158

IV.5. Analysis of the results obtained 160

Chapter V. Development and validation of a 3D model for LMD based on finite differences 165

V.1. Introduction 165

V.2. Mathematical development of the numerical model 166

V.2.1. Computational assumptions 166

V.2.2. Model basis 167

V.2.3. Initial and boundary conditions 169

V.2.4. Central finite differences 170

V.2.5. Convergence criteria 171

V.2.6. Material addition 172

V.3. Post-processing of the data obtained from the model 172

V.3.1. Microstructure of the deposited material 173

V.3.2. Hardness prediction 173

V.3.3. Porosity modeling 173

V.3.4. Solidification front rate and direction 175

V.4. Experimental procedure for the validation of the model 176

V.4.1. Spiral test 177

V.4.2. Corner test 178

V.5. Discussion on the results obtained 180

V.5.1. Spiral test 180

V.5.2. Corner test 188

Chapter VI. Contributions and future works 195

VI.1. Contributions 195

VI.2. Future works 199

Bibliography 201

Figures Index

Figure I. 1: Additive manufacturing revenue (in millions of dollars) for AM products and services worldwide. The lower (blue) represent the products revenue, whereas the upper (garnet) represents the services revenue [Wohlers, 2016]................................ 3

Figure I. 2: Evolution of the number of publications related with the additive manufacturing [Sciencedirect, 2016].. 4

Figure II. 1: Scheme of a fiber laser generator [Heston, 2010].. 13

Figure II. 2: Scheme of a diode bar. 13

Figure II. 3: Fast axis (FAC) and Slow axis collimation (SAC) of the diode laser......................... 14

Figure II. 4: Different alternatives for multiplexing the diode lasers....................................... 14

Figure II. 5: Comparison of the efficiency of different lasers [Trumpf, 2015]. 15

Figure II. 6: a) An array of subplots containing the various Hermite-Gaussian modes; b) 3D view of multi-mode Hermite-Gaussian beam consisting of 80% TEM_{00}, 10% TEM_{10}, and 10% TEM_{01}; c) Profile and Gaussian fit of the multi-mode Hermite-Gaussian beam in b) [DataRay, 2017]... 16

Figure II. 7: Laser revenue evolution and future expectations [M&M, 2017] (left) and market segments in the year 2016 [Overton, 2016] (right)....................................... 17

Figure II. 8: General function principle of laser sintering [EOS, 2017]. 19

Figure II. 9: Different alternatives to generate overhung geometries [Renishaw, 2017]. 20

Figure II. 10: An Aorta pendant on small build plate with supports (left) and an image of a SLM manufactured bridge model (right) [Renishaw, 2017].. 20

Figure II. 11: LMD process using a coaxial continuous nozzle. 21

Figure II. 12: Different alternatives for LMD systems, a Cartesian hybrid machine from Ibarmia (left) [Ibarmia, 2017] and an anthropomorphic robot (right).......................... 22

Figure II. 13: LMD process step by step. 23

Figure II. 14: Different types of nozzles used in the LMD, a) Lateral; b) Discrete coaxial; c) Continuous coaxial nozzle. 24

Figure II. 15: Schemes of powder and wire LMD processes including the physical phenomena involved.. 26

Figure II. 16: Final shape of powder (left) and wire (right) LMD manufactured parts. 27

Figure II. 17: a) Tensile test of a powder LMD manufactured part. b) The same part after the breakage. c) Detail of the tested. d) Average results of the tensile tests for Wire and Powder LMD test probes. 27

Figure II. 18: a) Designed wire-LMD nozzle; b) Flange built in AISI 316L; c) Front view of a flange built in AISI 316L. 28
Figure II. 19: The hybrid machine LASERTEC 65 3D developed by DMG-Mori (left) and an additive operation (right) [DMG Mori, 2017]. 29
Figure II. 20: The hybrid machine Integrex i-400AM developed by Mazak (left) and a demonstration part (right) [Mazak, 2017]. 29
Figure II. 21: Rebuilding the surface using AMBIT™ laser cladding head (left) and in-process finishing via grinding (right) [Hybrid, 2017]. 30
Figure II. 22: Revenue of the laser manufacturer companies. 30
Figure II. 23: Made in China 2025 Roadmap for Building China into a Manufacturing Powerhouse [HKTDC, 2016]. 32
Figure II. 24: Inconel 718 powder: SEM image and particle size distribution. 33
Figure II. 25: AISI D2 material deposition over an AISI D2 substrate using an Inconel 718 intermediate material. 34
Figure II. 26: Microhardness vs depth measurement for a 30% WC and 70% AISI 316L (400W laser power and 2050mm·min^{-1} machine feed rate) [Iglesias, 2014]. 34
Figure II. 27: Mixture of filler materials directly in the LMD nozzle. 35
Figure II. 28: Comparison between the nozzle functioning with humid (left) and preheated (right) powder. 36
Figure II. 29: Scheme of a gravity based powder feeder with a rotating wheel. 37
Figure II. 30: Relation between the powder feeder rotation speed and the measured powder mass flow. 38
Figure II. 31: Scheme of a mechanical wheel powder feeder. 38
Figure II. 32: Scheme of a fluidized-bed powder feeder. 39
Figure II. 33: Hosokawa Mikro® Vibratory Feeders, Model PF 7.5/1-U. Rates from 20 grams per hour to 5 kg per hour [Hosokawa, 2017] 40
Figure II. 34: Flowmotion powdef feeder from Medicoat [Medicoat, 2017]. 40
Figure II. 35: Design of the nozzle patented by Miyagi et al. [Miyagi, 2011]. 43
Figure II. 36: Design patented by Nowotny et al. [Nowotny, 2012]. 43
Figure II. 37: Design patented by Iwatany et al. [Iwatani, 2014]. 44
Figure II. 38: Powder flux control system patented by Miyagi et al. [Miyagi, 2014]. 45
Figure II. 39: LMD nozzle and laser focusing variation system patented by Whitfield et al. [Whitfield, 2016]. 45
Figure II. 40: LMD processing head VarioClad (left) and the control unit (right) [Reis, 2017]. 46

Figure II. 41: The continuous coaxial nozzle YC52 from Precitec [Precitec, 2017]. 46

Figure II. 42: The LMD nozzle Ambit^{TM} from Hybrid Manufacturing Technologies [Ambit, 2017]. 47

Figure II. 43: LMD nozzles COAX12 (left) and COAX8 (right) developed by the IWS [IWS, 2017]. 47

Figure II. 44: Appearance of pores in an AISI 316L clad. 49

Figure II. 45: In-process workpiece and verification works for both additive and subtractive modes [Siemens, 2017]. 50

Figure II. 46: Coaxial photo of the melt pool. 51

Figure II. 47: Melt pool length and width size measurement during straight line deposition [Ocylok, 2014]. 52

Figure II. 48: Variations of the measured melt pool size due to the differences in the fixed threshold value [Ocylok, 2014]. 52

Figure II. 49: Schema of the closed-loop process control based on the IR signal measurement [Bi, 2006_1]. 53

Figure II. 50: Process destabilization when building thin walls using LMD. Both base material and filler material are Inconel 718. 53

Figure II. 51: Retained particles for velocity calculation, source [Smurov, 2013] (left) and projected velocity due to viewing the particles in 2D (right). 54

Figure II. 52: Empirical dependence of the laser track height “H” and width “w” on combined processing parameters observed for coaxial and lateral cladding setups for Ni and Co based alloy cladding; from [Ocelík, 2007] (left) and from [de Oliveira, 2005] (right). 55

Figure II. 53: Flow chart of the sensing and control of the powder flow rate [Ding, 2016]. 56

Figure II. 54: Response of a powder feeder for a determined set value. 56

Figure II. 55: Closed–Loop System Schematic with Modified PI Controller Implemented in a SPCS (Smith Predictor Corrector Structure) [Thayalan, 2006]. 57

Figure II. 56: Experimental Results for Step Inputs. Experimental Results for Controller Implemented in SPCS (multiple step references) [Thayalan, 2006]. 57

Figure II. 57: Integral NGV manufactured using PBF technology [ILT, 2017]. 59

Figure II. 58: BR718 HPT case (left) and a detail of a locally repaired flange using LMD (right) [Gasser, 2010]. 59

Figure II. 59: V2500 high-pressure turbine vane repair process. Photos from MTU [Martens, 2010]. 60

Figure II. 60: Turbine blade edges repair using the LMD technology [IWS, 2017] 60

Figure II. 61: Repair of worn-out areas in a car lamp mold [Propawe, 2011]............................ 63

Figure II. 62: Co-based alloy coating using different laser powers. 63

Figure II. 63: A scheme (left) and a real photo (right) of the reparation of a gas turbine shaft using the LMD [Andolfi, 2012].. 64

Figure II. 64: a) Laser cladding head attached to a 6 axis robot; b) Bottom side at lower dead center position of a crankshaft; c) Crankshaft segment around oil bore [Koehler, 2010]. 65

Figure II. 65: Sample produced with an unsteady powder feed rate [Liu, 2005] 66

Figure II. 66: Powder particle trajectories colored according to their velocity magnitude [Zekovic, 2007]. 68

Figure II. 67: Image of the powder particles at the exit of the nozzle when depositing on a flat surface (left) and when depositing on a previously deposited thin wall (right) [Zekovic, 2007]. 69

Figure II. 68: (A) Concentration and (B) velocity fields obtained after simulation for AISI D2 [Tabernero, 2010]... 69

Figure II. 69: NT-20 powder stand-off distance comparison between (a) experimental and (b) numerical results at a carrier gas flow rate of 3.94×10^{-5} $m^3 \cdot s^{-1}$ and a powder flow rate of 0.06 $g \cdot s^{-1}$ [Balu, 2012]. 70

Figure II. 70: Schematic setup used for obtaining the powder distribution at the nozzle exit and the subsequent digital analysis [Pinkerton, 2007] 71

Figure II. 71: Experimental measurement system of the powder flux [Tabernero, 2010] 71

Figure II. 72: Particle stream structure where a) pre-waist; b) waist; c) post-waist stages can be distinguished (left) and powder jet temperature profile for a 300 W laser power and a 1.5 mm laser beam diameter (right) [Wen, 2009]... 73

Figure II. 73: Temperature of the particle stream when no substrate is considered (left) and temperature of the particle stream when the substrate is situated at a 10mm distance from the nozzle tip (right). In both cases same process parameters are used. Power 1000 W, powder flow rate: 0.58 $g \cdot s^{-1}$, carrier gas: 5 $l \cdot min^{-1}$, protective gas: 4 $l \cdot min^{-1}$ [Ibarra-Medina, 2010]. 73

Figure II. 74: a) Powder flux at standard gas flow parameters without laser radiation. b) Optimal zone with the highest concentration of particles formed by crossing divergent particle streams [Kovalev, 2010].. 74

Figure II. 75: Thermal state of the powder particles at the outlet of the nozzle: The schematic of the laser beam interaction with the particles in two different trajectories (left) and the varying particle temperature along their trajectories (right) [Kovalev, 2010]. 75

Figure II. 76: Effect of the laser power and the powder mass flow on the particle heating before arriving in to the substrate surface (left) and laser beam attenuation due to different powder mass flows (right) [He, 2007]. 76

Figure II. 77: Laser beam attenuation. 77

Figure II. 78: Melt pool dynamics without powder injection [Han, 2004] 79

Figure II. 79: Comparison between the predicted and experimental profiles of the melt pool [Safdar, 2013]. 80

Figure II. 80: Comparison between an experimental cross section and a simulated clad geometry (900 W of laser power, 10 mm·s^{-1} of cladding speed, 0.1585 g·s^{-1} of powder feeding rate with 69% of powder efficiency) [Ya, 2016]. 81

Figure II. 81: Microhardness profile of clad, together with simulated clad height, melt depth and HAZ [Ya, 2016]. 81

Figure II. 82: Influence of the oxidation on the formation of the multi-vortex in the molten pool (P=180W, v=400mm·s^{-1} and t= 0.275ms) [Dai, 2016]. 82

Figure II. 83: Influence of the existence of rust at the surface of the molten material in the surface tension coefficient. 83

Figure II. 84: Screenshot of the melt pool for a Gaussian intensity distribution laser beam [Gibson, 2009] 83

Figure II. 85: Multiscale methodology for fast prediction of part distortion and residual stress [Li, 2016]. 84

Figure II. 86: Schematic diagram of transverse sections of a clad layer [Zhao, 2003]. 85

Figure II. 87: Scheme of a typical laser track with its main geometric characteristics. 85

Figure II. 88: Superposition of the experimental results (continuous line) and the simulated results obtained with linear relationships (dashed line) [El Cheick, 2012]. 86

Figure II. 89: Comparison between the experimental and calculated profile (black line) using a parabolic profile function; single clad (left) and multiple clad overlapping (right) [Ocelík, 2014]. 86

Figure II. 90: Schematic view of the clad profile in 2D [Ya, 2016]. 87

Figure II. 91: Sequence of calculation in the proposed numerical model [Toyserkani, 2004]. 88

Figure II. 92: Material deposition procedure [Tabernero, 2012_2]. 89

Figure II. 93: Modeling of continuous double line bead during the second laser heating pass [Chew, 2015]. 90

Figure III. 1: Simulation based nozzle design process 96

Figure III. 2: Required power to melt the substrate (P_{ms}) and the particle (P_{mp}) as a function of the velocity of the powder particles. Powder mass feeding rate 8.5 g·min^{-1} and machine feed rate 280.2 mm·min^{-1} [de Oliveira, 2005]. 97

Figure III. 3: 3D view of the designed nozzle. 103

Figure III. 4: Cross sections of the designed nozzle and a list of the different components that comprise the nozzle. 103

Figure III. 5: Drag and protective gas flows drawn over the mesh of the nozzle. 104

Figure III. 6: Boundary conditions defined for the nozzle CFD simulation. 105

Figure III. 7: Simulation result: Contours of DPM concentration [kg·m^{-3}]. 106

Figure III. 8: Simulation result: Contours of powder flux [kg·m^{-2}·s^{-1}]. 107

Figure III. 9: Simulation result: Contours of Total pressure [Pa]. 107

Figure III. 10: Simulation result: Contours of Turbulence intensity [%]. 108

Figure III. 11: Simulation result: DPM concentration in the OZ axis at different distances from the nozzle tip 108

Figure III. 12: Simulation result: DPM concentration in the OX axis at a 15mm distance from the nozzle tip 109

Figure III. 13: Simulation result: DPM concentration in the OX axis at different distances from the tip of the nozzle. 110

Figure III. 14: Powder particle paths inside the LMD coaxial nozzle colored according to their instantaneous velocity. 110

Figure III. 15: Kondia A6 milling center (left) and CMZ-TC25BTY turning center (right). 111

Figure III. 16: Different stages of the manufacture of the cooling sleeve in the Kondia A6 milling center. 111

Figure III. 17: Different stages of the manufacture of the inner cone (upper image row) and the outer cone (lower image row). 112

Figure III. 18: Different nozzle parts (left) and the whole assembly of the nozzle (right). 112

Figure III. 19: Planes of the container (left), 10 mm diameter entrance cover (center) and 1 mm diameter entrance cover (right). 114

Figure III. 20: Powder distribution at the nozzle exit. Focal plane is situated at a 15 mm distance. 114

Figure III. 21: Container base, container and the set of different covers (up). Powder collecting process (down-left) and the weight measuring precision scale (down-right). 115

Figure III. 22: Comparison between the experimental and simulated powder concentration in the X axis at the focal plane (situated at a 15mm distance from the nozzle tip)..... 116

Figure III. 23: Experimental test to check the sealing of the nozzle (left) and a thermal image of the nozzle after the thermal equilibrium is reached for a 1 kW laser power (right). 117

Figure III. 24: Determination of the laser beam diameter for the nozzle efficiency tests. 118

Figure III. 25: Theoretical powder catchment calculation based on the CFD simulation results. 118

Figure III. 26: Examples of over-deposited areas due to the reduction of the machine feed rate. 120

Figure III. 27: Diagram of the designed powder flux regulation system. The solenoid is shown in position 1. 121

Figure III. 28: Scheme of the designed control system and an example of the velocity vectors and the generated PWM signal. 122

Figure III. 29: Powder concentration in [kg·m^{-3}] for the three simulated cases in the XZ plane that comprises the rotation axis of the nozzle and the corresponding XY cross sections at a 15mm distance from the nozzle tip. 124

Figure III. 30: Comparison of the DPM concentrations in the rotation axis of the nozzle for the three simulated cases. The Z=0 is located at the nozzle tip. 124

Figure III. 31: Powder particle distribution at the nozzle exit when extra gas is used (case 2) and when no extra gas is used (case 3). The diagram in the right shows the DPM concentration in the X axis at a 15 mm distance from the nozzle tip......................... 125

Figure III. 32: Different working situations: a) Solenoid in position 1; b) Solenoid in position 2; c) 50 Hz commutation frequency of the solenoid.. 126

Figure III. 33: Experimental setup of the solenoid inside the LMD machine........................... 127

Figure III. 34: Lines 1, 2 and 3 with their respective average cross section profiles. 128

Figure III. 35: The deposited right angles. 129

Figure III. 36: Obtained velocity vectors when an “L” shaped trajectory is followed and the generated PWM signal based on the velocity error. 131

Figure III. 37: Analysis of the height of the deposited material at the beginning of the line, with and without powder control. 132

Figure III. 38: Deposited material over-height analysis when the LMD direction is changed. . 132

Figure III. 39: Generation of a 5-axis Inconel 718 blade over an Inconel 718 substrate. 133

Figure III. 40: DIN 1.2379 material deposition over a 1.2379 substrate using an Inconel 718 intermediate material. 134

Figure III. 41: Cooling conduct generation on hot stamping dies. 135

Figure III. 42: Visual inspection using penetrating liquids. 135

Figure III. 43: 3 axis blade (left) and a 5-axis LMD manufactured Blisk (right). 136

Figure III. 44: Generation of coatings using various filler materials. 137

Figure III. 45: Generation of copper electrodes using LMD. 137

Figure IV. 1: Flowchart of the deployed methodology. 142

Figure IV. 2: Applied boundary conditions for modeling the melt pool under a static laser beam. 145

Figure IV. 3: Surface forces and the buoyancy force. 147

Figure IV. 4: Powder particle heating before they reach the melt pool. 148

Figure IV. 5: 3D simulation of a LMD test considering fluid-dynamic phenomena inside the melt pool. Process parameters: P=800 W, vf=500 mm·min^{-1}, m=4 g·min^{-1}. 150

Figure IV. 6: Melt pool temperature measurements by means of a two-color pyrometer. 153

Figure IV. 7: Different topographies of the generated craters after the melt pool solidification. a) P=500 W, t=0.6 s; b) P=750 W, t=1 s. 153

Figure IV. 8: Comparison between simulated and experimental melt pool cross sections. a) Test 1: P=500W, t=1s; b) Test 2: P=750W, t=0.6W. 154

Figure IV. 9: Comparison between the cross sections of the test 1, where material displacement is allowed (left), and the test 1', where no material movement is allowed (right). 155

Figure IV. 10: a) Comparison between the maximum temperatures reached in tests 1 and 1'; b) Temperature field in test 1 (P=500 W, t=1 s) after 1 s of interaction time. 155

Figure IV. 11: Comparison between the simulated and experimental cross sections of a) Line 3 and b) Line 6. 157

Figure IV. 12: Relevance of the fluid-dynamic phenomena consideration in the LMD process. 159

Figure IV. 13: Comparison between the cooling rates for lines 3 and 4 (*Line 3*: *P*=800 W, vf=500 mm·min^{-1}, m=4 g·min^{-1}; *Line 4*: *P*=800 W, vf=1000 mm·min^{-1}, m=4 g·min^{-1}). 160

Figure V. 1: Heat fluxes on a differential element. 167

Figure V. 2: Heat transmission mechanisms: Conduction, convection and radiation. The number inside the elements indicates the amount of free faces and corresponds to the value of "*n*" in equation (Eq. V. 14). 169

Figure V. 3: Central finite differences 170

Figure V. 4: Scheme of the material addition model. 172

Figure V. 5: Scheme of the generated melt pool on the surface of the substrate. 175

Figure V. 6: Machines used for the validation of the model. Kondia Aktinos 500 LMD center (left), Rofin FL010 laser generator (center) and a Sulzer Metco Twin 10C powder feeder (right). 176

Figure V. 7: Spiral test. Photo of the deposition process (left) and final shape of the generated geometry (center and right). 177

Figure V. 8: Boundary conditions of the modeled geometry for the spiral test. 177

Figure V. 9: Scheme (left) and real (right) setup used for measuring the temperature during the deposition of the spiral shaped geometry. 178

Figure V. 10: Photo of the corner test (left) and the boundary conditions of the modeled geometry (right). 179

Figure V. 11: Comparison between the modeled and real part for the spiral test. 181

Figure V. 12: Comparison between the cross sections of the deposited spiral for the modeled (red line) and real part. 181

Figure V. 13: Comparison between the modeled and real layers after the deposition of the 8 turns of the spiral. 182

Figure V. 14: The modeled thermal field during the deposition of the eighth lap (left) and a comparison between the real and simulated temperatures during the deposition of the whole spiral (right). 183

Figure V. 15: Cross section of the modeled spiral where the elements are colored according to the solidification time (left). The cooling rate is defined as the inverse of the solidifying time (right). 183

Figure V. 16: Comparison between the real DAS and the modeled DAS, which is obtained based on the cooling rate predicted by the model. 184

Figure V. 17: Microhardness measurements plotted over the modeled cross section of the part, where the elements are colored according to the amount of time each element is between the 560 and the 760 °C. 185

Figure V. 18: Pore apparition prediction according to the molten time (left) and the Shrinking Cavity Probability (center) and the analysis of the real cross section (right) where the detected pores are highlighted. 186

Figure V. 19: Comparison between the melt pool and the temperature field during the deposition of the first turn of the spiral and the eighth turn. 187

Figure V. 20: Longitudinal cross section of the melt pool during different stages of the deposition process (left) and the cross section of the spiral colored according to the solidifying front angle (right). 187

Figure V. 21: Geometry of the deposited material during the generation of the first layer after 5.7 seconds from the start of the deposition process. 188

Figure V. 22: Geometry (left) and temperature field (right) of the deposited material during the generation of the third layer. Screenshots are taken after 5.7 seconds from the start of the third layer. 188

Figure V. 23: Final geometry of the part after the deposition of the ten layers. 188

Figure V. 24: a) Leica DCM 3D confocal microscope; b) Topography of the deposited material; c) Comparison between the simulated and real cross sections of the deposited material. 189

Figure V. 25: Top view of the topographies of the corners: a) Real part without powder flux control; b) Modeled part without powder flux control; c) Real part with powder flux control; d) Modeled part with powder flux control. 190

Figure V. 26: Comparison between the modeled and real part for the corner test. 191

Tables Index

Table II. 1 Industrial laser types for laser material processing according to the active medium. 12

Table II. 2 Process parameters involved in the laser processes 16

Table II. 3 Industrial laser revenue in million US$ [Belforte, 2016]. 17

Table II. 4 Comparison between the SLM and the LMD technologies. 22

Table II. 5 Main patents focused on LMD nozzles until 2011. 41

Table II. 6 Main patents focused on LMD nozzles from 2011 until the date. 42

Table II. 7: Main input and output LMD parameters 48

Table III. 1: Nozzle design specifications. 98

Table III. 2: Process parameters. 101

Table III. 3: Protective and drag gas flows. 104

Table III. 4: Powder captured inside the container for the different covers. 115

Table III. 5: Process parameters for the nozzle efficiency determination. 117

Table III. 6: Calculation of the nozzle efficiency. 118

Table III. 7: Boundary conditions used in the simulations. 123

Table III. 8: Conditions for the straight line deposition. 127

Table III. 9: Average height (H) and width (W) of the deposited lines. 129

Table III. 10: Correlation between the average velocity error vector and the generated PWM signal. 130

Table III. 11: DIN 1.2379 chemical composition in weight percentage [AZOM, 2017]. 134

Table III. 12: Inconel 718 chemical composition in weight percentage [Oerlikon, 2017]. 134

Table III. 13: DIN 1.2344 chemical composition in weight percentage [Uddeholm, 2017]. 135

Table III. 14: Hastelloy X chemical composition in weight percentage [Haynes, 2017]. 136

Table IV. 1: AISI 304 properties [Pang, 2016]. 151

Table IV. 2: Chemical composition of the AISI 304 [ASM, 2017]. 152

Table IV. 3: Conditions of the different stationary tests and the diameter of the generated crater. 153

Table IV. 4: Dimensions of a crater generated under a stationary laser beam. 154

Table IV. 5: Influence of the material movement in the melt pool geometry. 154

Table IV. 6: Values of the input variables for the powder particle-heating model. 156

Table IV. 7: Validation of the inflight particle-heating model. 156

Table IV. 8: LMD conditions for validating the developed model. 157

Table IV. 9: Comparison between the experimental and simulated geometries of the deposited material. 157

Table IV. 10: Influence of the material displacement in the final geometry of the deposited lines.......... 158

Table IV. 11: Influence of the material displacement in the final geometry of the deposited line. 159

Table V. 1: Process parameters for the spiral test 178

Table V. 2: Process parameters for the corner test 179

Table V. 3: MP parameter value for the corner and spiral tests.......... 180

Table V. 4: Comparison between the real and modeled dimensions of the deposited material in the spiral tests. 182

Table V. 5: Comparison between the real and modeled dimensions of the deposited material in the corner tests. 190

Nomenclature

AM	Additive Manufacturing
BPP	Beam Parameter Product
CAD	Computer Aided Design
CAE	Computer Aided Engineering
CAM	Computer Aided Manufacturing
CFD	Computational Fluid Dynamic
CNC	Computer Numerical Control
DAS	Dendrite Arm Spacing
DC	Duty Cycle
DPM	Discrete Phase Model
DRIFT	Do It Right The First Time
EC	European Commission
EU	European Union
FAC	Fast axis collimation
FGM	Functionally Graded Materials
FP	Framework Programs
fpp	focal plane position
GDP	Gross Domestic Product
HAZ	Heat Affected Zone
ILT	Fraunhofer Institute for Laser Technology
IPR	Intellectual Property Rights
IPR	Intellectual Rroperty Rights

IPT	Fraunhofer Institute for Production Technology
IWS	Fraunhofer-Institut für Werkstoff-und Strahltechnik
LENS	Laser Engineered Net Shaping
LMD	Laser Metal Deposition
NAMII	National Additive Manufacturing Innovation Institute
NNMI	National Network for Manufacturing Innovation
PBF	Powder Bed Fusion
SAC	Slow axis collimation
SLM	Selective Laser Melting
TIG	Tungsten Inert Gas
UPV/EHU	University of the Basque Country
VOF	Volume of Fluid

Symbols

Symbol	*Units*	*Description*
Δt	[s]	Time step.
Δt_{max}	[s]	Maximum time step to guarantee the convergence.
Δx	[m]	Element size in the X axis direction.
Δy	[m]	Element size in the Y axis direction.
Δz	[m]	Element size in the Z axis direction.
μ	$[kg \cdot m^{-1} \cdot s^{-1}]$	Material viscosity.
a	$[m^{2} \cdot s^{-1}]$	Thermal diffusivity.
A	[-]	Global losses coefficient.
c	$[J \cdot kg^{-1} \cdot K^{-1}]$	Specific energy.
DAS	[µm]	Dendrite Arm Spacing.
dV	[m]	Differential volume of an element.
$\hat{e}$	[-]	Z+ direction unitary vector.
F	[K]	Source vector.
fpp	[mm]	Focal plane position.
g	$[m \cdot s^{-2}]$	Gravitational acceleration constant.
h	$[W \cdot m^{-2} \cdot K^{-1}]$	Convection coefficient.
I	$[W \cdot mm^{-2}]$	Laser beam average intensity.
k	$[W \cdot m^{-1} \cdot K^{-1}]$	Heat conductivity.
K_{att}	[-]	Dimensionless attenuation factor.
L	$[J \cdot kg^{-1}]$	Latent heat of fusion.
$L_{average}$	[m]	Average distance traveled by powder particles.

M	[-]	Transference matrix.
$\dot{m}$	$[\mathrm{g \cdot min^{-1}}]$	Powder mass rate.
m_p	[kg]	Powder particle average mass.
MP	[-]	Melt Pool fluid-dynamic relevance coefficient.
n	[-]	Number of free faces of each element.
$\check{n}$	[-]	Vector normal to the surface (solid/liquid – gas interface).
P	[W]	Laser power.
q	$[\mathrm{W \cdot m^{-3}}]$	Energy generation term.
q_L	$[\mathrm{W \cdot m^{-3}}]$	Latent heat energy exchange term.
q_{laser}	$[\mathrm{W \cdot m^{-2}}]$	Laser beam intensity.
q_{losses}	$[\mathrm{W \cdot m^{-2}}]$	Energy losses due to radiation and convection.
q_S	$[\mathrm{W \cdot m^{-3}}]$	Heat exchange at the surface.
r_l	[m]	Laser beam radius in the focal plane.
r_{pm}	[m]	Powder particle average radius.
S_b	$[\mathrm{kg \cdot m \cdot s^{-2}}]$	Buoyancy force
SCP	[-]	Shrinking Cavity Probability.
S_d	$[\mathrm{kg \cdot m \cdot s^{-2}}]$	Velocity reduction term
S_m	$[\mathrm{kg \cdot m \cdot s^{-2}}]$	Momentum generation term
S_p	$[\mathrm{m^2}]$	Powder particle projected area.
t	[s]	Time.
T	[K]	Temperature.
T_∞	[K]	Room temperature.
$T_{initial}$	[K]	Powder particle-preheating temperature.

t_{int}	[s]	Interaction time between laser beam and powder particles.
$T_{liquidus}$	[K]	Liquidus temperature.
T_p	[K]	Temperature of the particles when they reach the melt pool
$T_{solidus}$	[K]	Solidus temperature.
u	[m·s^{-1}]	Fluid velocity in the X axis direction.
U	[m·s^{-1}]	Absolute fluid velocity
v	[m·s^{-1}]	Fluid velocity in the Y axis direction.
v_f	[m·s^{-1}]	LMD machine feed rate.
v_p	[m·s^{-1}]	Powder particle average velocity at the nozzle exit.
w	[m·s^{-1}]	Fluid velocity in the Z axis direction.
α	[-]	Absorptivity.
β	[K^{-1}]	Thermal expansion coefficient.
γ	[-]	Volume fraction (solid/liquid).
δ	[°]	Angle between the horizontal and the free surface.
ε	[-]	Emissivity.
θ	[-]	Laser beam semi-angle.
κ	[m^{-1}]	Surface curvature.
ρ	[kg·m^{-3}]	Material density.
σ	[N·m^{-1}]	Material surface stress.
σ_b	[W·m^{-2}·K^{-4}]	Stefan-Bolzmann coefficient.
Φ	[m·s^{-1}]	Relevant velocity component.

Chapter I. Introduction

Chapter I. Introduction

I.1. Background and motivation

The present document exposes the obtained results after the realization of a research work focused on the development of a holistic model for the enhancement of the Laser Metal Deposition (LMD) process. The work has been carried out at the Department of Mechanical Engineering of the University of the Basque Country (UPV/EHU) in collaboration with the Fraunhofer Institute for Production Technology IPT (Aachen, Germany) and intends to establish a methodology in the LMD modeling and facilitate the industrial integration of this process. The final aim of the project is to help in the inclusion of the LMD in CAD/CAM/CAE tools and the application of this technology for the 5-axis manufacturing of high added value components.

Laser technology is a rising sector that has experienced a continuous growth during the last years. For example, in the year 2015 the laser manufactures income grew by a 6.9%, especially dragged by the continued growth of the fiber lasers for industrial macroprocessing applications, which grew 22% during the same period. The Trumpf group, which is one of the laser manufacturer leaders, obtained a 2717 M€ revenue in sales in the year 2014/15, with an increase of a 5% regarding the previous year [Trumpf, 2015].

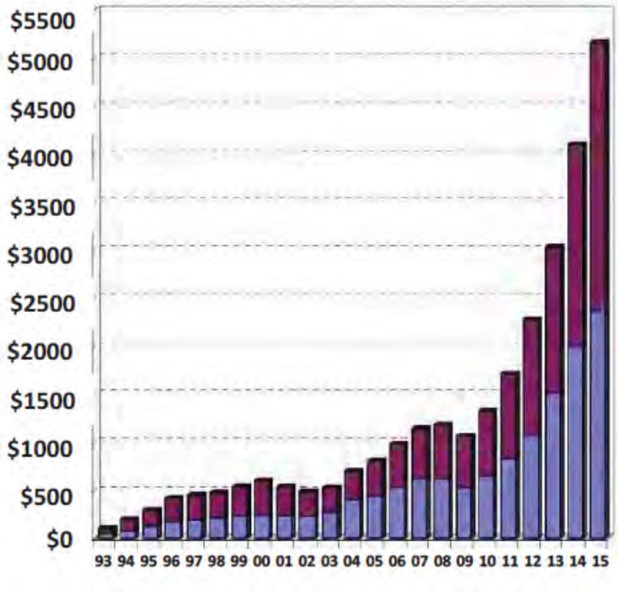

Figure I. 1: Additive manufacturing revenue (in millions of dollars) for AM products and services worldwide. The lower (blue) represent the products revenue, whereas the upper (garnet) represents the services revenue [Wohlers, 2016].

In Figure I. 1 the evolution of the Additive Manufacturing revenue in million dollars is shown [Wohlers, 2016]. As it can be seen, despite the world financial crisis, the additive manufacturing (AM) market is increasing and in the last six years the AM revenues have multiplied by five.

Among the additive manufacturing technologies, the Laser Metal Deposition (LMD) is a growing technology. The process is based on the generation of a melt pool on the surface of the substrate thanks to the high density energy of a laser beam, while simultaneously filler material is injected into it. As the LMD nozzle moves, filler material solidifies and a clad is generated. With the overlap of the subsequent clads, the desired final geometry is obtained. The main characteristic of the LMD is the high quality of the deposited material and the minimum heat affected zone (HAZ) generated in the nearby region [Toyserkani, 2005]. Thanks to these advantages, LMD is becoming a relevant technology for the repair of high value components [Costa, 2009] and many companies and research centers have focused their efforts on the development of this laser based additive technology.

As a result of this economical effort, the number of published books, articles and patents that are related with lasers and especially laser additive processes has experimented an increase during the last years. Over 3500 patents focused on laser based AM methods have been published between the 1975 and the 2011 [Weber, 2013].

The high number of patents and developments related with the AM, results in a wide nomenclature for referring to the process: such as Laser Material Deposition (LMD), nomenclature developed by the Fraunhofer ILT; Laser Engineered Net Shaping (LENS) developed by the Sandia National Laboratories; Laser Cladding; etc. In the following graph, the evolution of the published works since the year 2000 related with the laser based additive processes are shown.

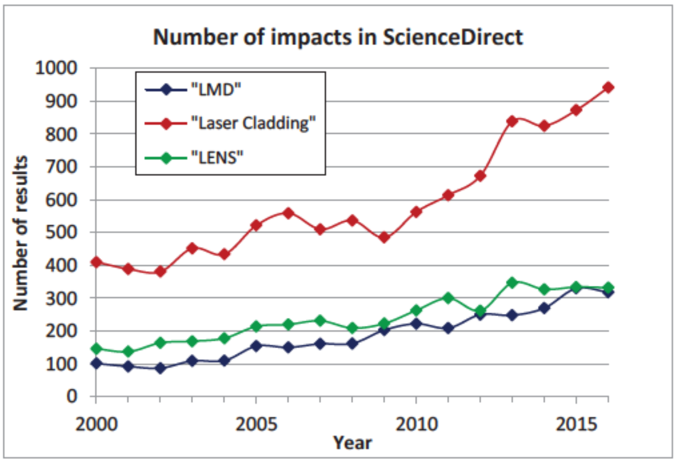

Figure I. 2: Evolution of the number of publications related with the additive manufacturing [Sciencedirect, 2016].

The main drawback of the LMD process is its complex nature and the fact that many interrelated physical phenomena occur during the process. Usually, the LMD operations are critical operations, since they are applied to high added value components. Therefore, an error in the process would entail big losses. Moreover, parts to be manufactured are frequently unique and there is only one chance to process them correctly. In order to implement the LMD process in the modern industry, the *DRIFT (Do It Right The First Time)* manufacturing philosophy must be applied and the machine operator needs to be sure that the process will work correctly.

Consequently, the setup of the process is a critical task and, with the aim of easing it, many authors have worked in the development of numerical models to predict the geometry and mechanical properties of the final part after the LMD process. However, due to the complex nature of the process, it is not easy to determine which factors should be simplified in order to obtain a reliable model with a low computational cost. In the present work, the main effort is focused on the proper modeling and the enhancement of the whole LMD process: starting from the LMD nozzle, to the fluid-dynamic phenomena that occur inside the melt pool and the deposition of the filler material.

I.2. Objectives

The main objective of the present work is the development of a holistic Laser Metal Deposition model that simulates the entire process: from the nozzle, to the melt pool dynamics and the material deposition. The developed model pretends to provide a better understanding of the LMD process. Moreover, the methodology is focused on the prediction of an optimum parameter window for the LMD process, resulting in a reduction of the experimental tests required for the setup of the process.

Once the general objective of the thesis is stated, the following specific objectives can be formulated:

- ✓ Development and manufacture of a new coaxial LMD nozzle based on CFD simulations. The nozzle is designed to optimize the distribution of the powder particles at the working plane and therefore, increase the efficiency of the process.
- ✓ Validation of the nozzle for different real cases, involving different materials, powder sizes and process parameters.

- ✓ Development of an instantaneous powder flux regulation system. The powder flux regulation enables the enhancing of the stability of the process and also increases the efficiency of the powder usage.
- ✓ Determination of the influence of considering or neglecting the melt pool fluid dynamics for the LMD process. The consideration of the melt pool dynamics that generate the movement of the molten material increases considerably the computational cost of the model. Therefore, the importance of the consideration of the melt pool dynamics in the accuracy of the model is quantified.
- ✓ Generation of a 3D thermal model of the LMD process that estimates the geometry of the deposited material. Moreover, the model should predict the mechanical properties of the deposited material on the basis of the process thermal history.

I.3. Memory organization

The present work is organized in a series of chapters that are described as it follows:

Chapter I shows a brief description of the motivation of the work and the actual situation of the additive manufacturing in the industry. Furthermore, the objectives of the thesis work are stated and its organization is also presented.

In **Chapter II** a review work is carried out and the state of the art of the Laser Metal Deposition technology is detailed. First of all, an introduction to the industrial lasers is presented. The different lasers used in the industry for LMD operations are described and the parameters involved in the process are explained. Secondly, the LMD process is explained in depth, focusing especially on the existing nozzles and filler material delivery systems. Besides, the latest commercial LMD machines and global market numbers are also presented with the aim of providing a global view of the current market.

With regard to the different applications of the LMD technology, real application examples of aeronautical, die & mold and naval industry are detailed. Lastly, an analysis of the latest and more relevant publications in the field of the LMD process modeling are presented. Especial attention is paid to the models related with the powder particle tracking, melt pool modeling, filler material addition and clad generation.

In **Chapter III** the development of a new LMD nozzle based on CFD simulations is presented. Firstly, the design, manufacturing and validation processes of a continuous coaxial nozzle are detailed. On a second step, with the aim of enhancing the stability and efficiency of the process, a powder flux regulation system is developed and installed in the nozzle. Besides explaining the operation of the system, different examples of the validation tests are presented. Lastly, different components manufactured using the developed nozzle are shown.

Chapter IV is focused on the evaluation of the fluid-dynamics phenomena inside the melt pool in the LMD process. The relevance of considering or neglecting the melt pool dynamics on the accuracy of the model is quantified. It is concluded that the influence of the fluid-dynamics phenomena is almost negligible for most of the LMD process application cases.

Taking into account the results obtained in the previous chapter, in **Chapter V** a 3D thermal model that simulates the deposition of the filler material during the LMD process is presented. In addition to the geometry of the deposited material and thermal field, the model is also able to predict the mechanical properties of the deposited material on the basis of the thermal cycles that the different zones of the component go through during the LMD process.

Lastly, in **Chapter VI** the main contributions of the present work are highlighted. Besides, the possible future working lines that have come out after the realization of this work are detailed and their importance is explained.

Chapter II. State of the art of the Laser Metal Deposition process and the latest developments

Chapter II. State of the art of the Laser Metal Deposition process and the latest developments

In this second chapter a summary of the state of the art of the Laser Metal Deposition process is presented. On the one hand, the basics of the LMD process are explained. On the other hand, the latest LMD machines and especially the new hybrid machines that combine the additive and subtractive processes are addressed and some figures of the laser market are shown. Additionally, the latest advances in process monitoring and control systems are detailed. Lastly, a deep review of the most relevant models published until the date for the LMD process modeling is presented. Models related with powder particle trajectories tracking, the melt pool dynamics and the filler material addition are discussed.

II.1. Introduction to the lasers

The LASER was discovered in the 1960, when Dr. Theodore H. Maiman invented the first Ruby Laser [Maiman, 1960]. However, the laser cannot be defined as a simple invention, because when it was discovered there was no application or use for it. As Irnee D'Haenens stated when he was reflecting upon the ruby laser that he had helped to create together with Dr. Maiman, the laser was "*a solution looking for a problem*" [Hecht, 2005].

The name LASER is an acronym that stands for "*Light Amplification by Stimulated Emission of Radiation*" and it should be understood as a high quality light with certain properties that enable its transport in long distances and concentrate its energy in a small area. More rigorously, a LASER is a high intensity radiation energy formed by same wavelength and coherent electromagnetic waves.

II.1.1. Laser generation principles

Laser systems are based on an active medium that is pumped using an external energy source until most of the molecules of the active medium are in an exited state. This situation is called population inversion. At this situation, the active medium starts to emit light with the specific properties above mentioned. Among the industrial lasers used for laser material processing, the following laser types can be distinguished according to the active medium that generates the radiation.

Table II. 1 Industrial laser types for laser material processing according to the active medium.

INDUSTRIAL LASER TYPES FOR LASER MATERIAL PROCESSING		
CO_2 LASERS	SOLID STATE LASERS	DIODE LASERS
• Slab • Sealed • Flux	• Rod Disk • Disk • Fiber • Slab	• Diode stacks

Fiber lasers (Solid-state lasers)

In solid state lasers, Neodymium (Nd) or ytterbium (Yb) ions are used as dopants of the active medium, which are excited using radiation from an external source, typically another laser. The wavelength of the laser beam varies depending on the dopants: 1.064 nm wavelength for neodymium and 1.030 nm for ytterbium ions.

Fiber lasers emerged as a variation of the rod solid-state lasers, where instead of using a Nd:YAG rod, the active medium is a coiled fiber. The main advantage of the fiber lasers is their high ratio surface/volume, what improves the heat distribution and the cooling efficiency of the active medium, which increases the laser generation performance. Thanks to this, a high quality beam is produced and Beam Parameter Product factor (BPP) values under 4 mm·mrad are obtained at average powers as high as 3kW [Propawe, 2011].

The active core of the active-fiber is usually several meters length and has a typical diameter of 10 µm. The surrounding coating, named as cladding, has a lower refraction index than the active core in order to achieve a total internal reflection. Thanks to this configuration, the ratio surface to volume of the fiber is increased and heat is easily removed. When high output laser power is required, power scaling is achieved by coupling several active fibers before they all are connected to a passive transport fiber. Laser powers up to 500 kW can be obtained [IPG, 2017].

In Figure II. 1 a scheme of a fiber laser generator is shown [Heston, 2010]. Multiple diode lasers are used to pump light through optical fibers until a coupler, which simultaneously feeds into a coiled active fiber. This pumped light excites the doped medium and leads to the population inversion of the active medium. Consequently, the active medium emits light, which goes amplifying through the active-fiber. Then, the laser beam exits the active-fiber, which is coupled to a passive transport optical fiber and directs the energy towards the processing area.

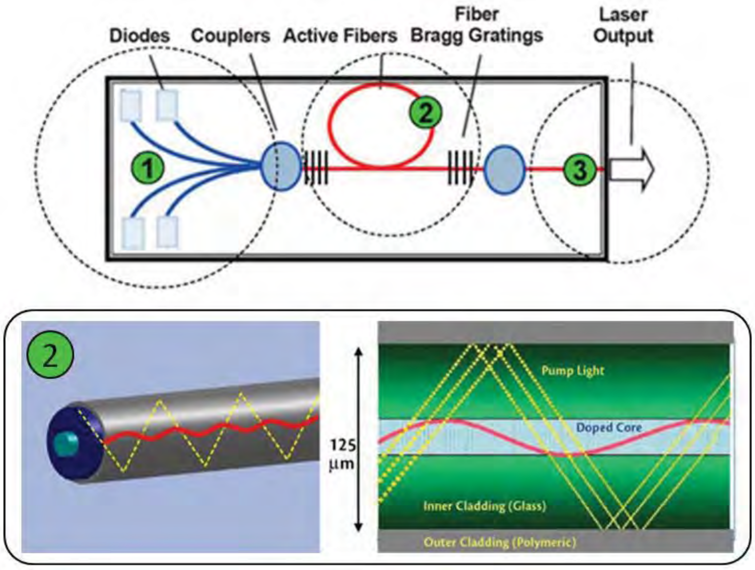
Diodes
Couplers
Active Fibers
Fiber Bragg Gratings
Laser Output
1
2
3
2
125 µm
Pump Light
Doped Core
Inner Cladding (Glass)
Outer Cladding (Polymeric)

Figure II. 1: Scheme of a fiber laser generator [Heston, 2010].

The main advantage of this type of laser is the wavelength of the laser itself, which is around 1 µm and shows a higher absorptivity in metals compared with the CO_2 lasers. Furthermore, laser light with this wavelength can be transported through flexible glass fibers, what increases the flexibility of the process [Koechner, 2006].

Diode lasers

Diode lasers are formed by semiconductors that emit light when they are plugged to an electrical current. In order to achieve the desired output power, these semiconductors are coupled in bars, which are stacked forming a diode stack. In Figure II. 2 a scheme of a diode bar is shown.

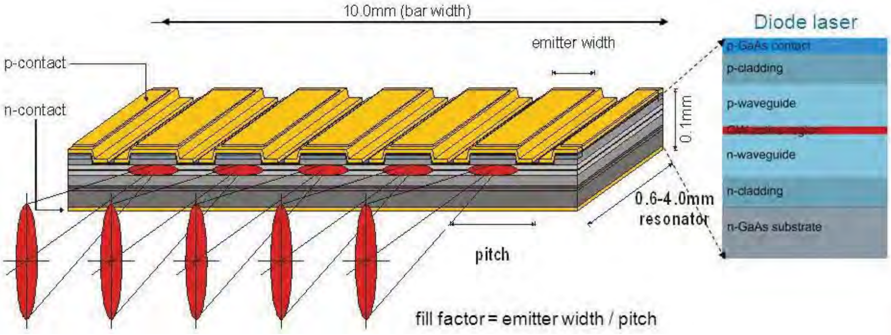
10.0mm (bar width)
emitter width
p-contact
n-contact
0.1mm
0.6-4.0mm resonator
pitch
fill factor = emitter width / pitch
Diode laser
p-GaAs contact
p-cladding
p-waveguide
n-waveguide
n-cladding
n-GaAs substrate

Figure II. 2: Scheme of a diode bar.

A diode bar consists of several emitters arranged in parallel and, therefore, the output beam properties differ considerably from other types of laser. Once the laser beam is generated, it needs to be collimated in order to obtain a high intensity laser beam with an acceptable quality, see Figure II. 3. The collimation is necessary because of the high divergence of the beam and the necessity to improve the beam parameter product (BPP) of the laser.

In the vertical direction, diode lasers achieve a high quality beam, whereas in the horizontal direction, a multimode beam is obtained, with a poor beam quality. BPP values below 20 mm·mrad are obtained in 3 kW diode lasers and BPP values below 200 mm·mrad in 20 kW lasers [Laserline, 2017]. Furthermore, diode lasers emit radiation in a wider wavelength than fiber lasers and therefore, the quality of the beam is lower.

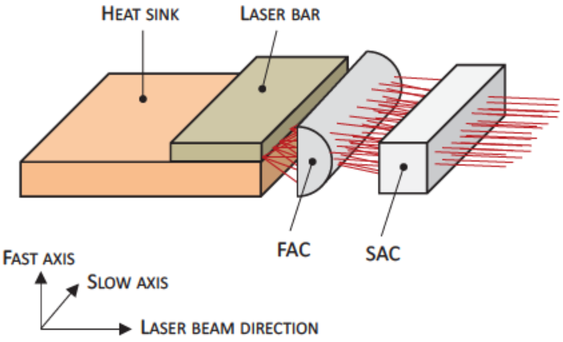

Figure II. 3: Fast axis (FAC) and Slow axis collimation (SAC) of the diode laser.

For low laser powers, until 100 W, the diodes can be directly coupled to the transporting fiber. Nevertheless, for higher output powers, individual diode lasers are multiplexed by installing diode lasers on top of each other or arranging them in parallel [Bachmann, 2007]. The most common arrangements are the spatial multiplexing, where individual laser beams are simply set one next to the other in a 1D or 2D arrays and therefore, the power output is increased. Another alternative is the polarization multiplexing. Lastly, a very common setup is the usage of a wavelength multiplexing system to combine four laser modules with different wavelengths into the same optical path.

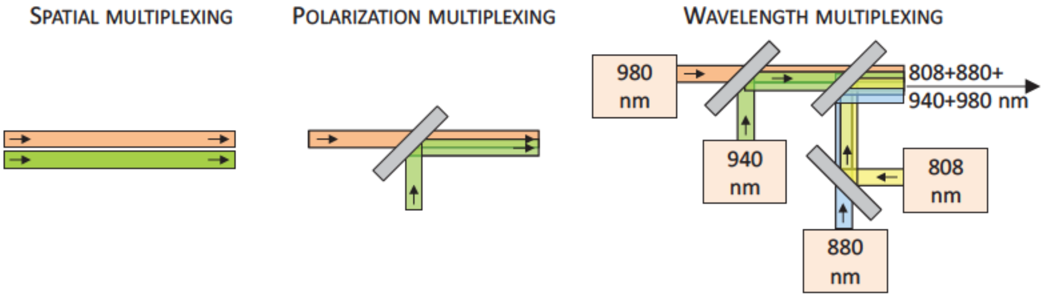

Figure II. 4: Different alternatives for multiplexing the diode lasers.

The main advantage of these lasers is their high efficiency, electrical/optical efficiencies up to 45% are achieved [Laserline, 2017]. Consequently, high power lasers can be obtained from small volumes of active material. In the Figure II. 5 a comparison between the efficiencies of the different laser types is shown. The equipment efficiency is influenced by the maximum laser power, and therefore, lasers of the same power are compared [Trumpf, 2015].

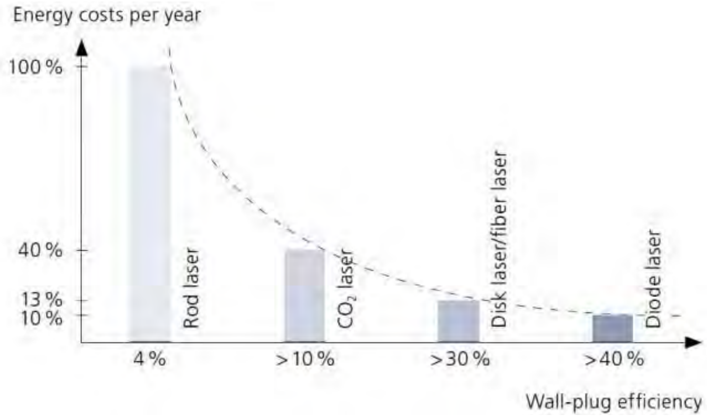

Figure II. 5: Comparison of the efficiency of different lasers [Trumpf, 2015].

II.1.2. Main parameters of the laser based processes

In the laser-material interaction process, high amounts of parameters are involved and in many cases, their complete understanding is a complex task to achieve [Tagliaferri, 2013]. Consequently, the laser technology remains a challenge and provides an added value to the manufactured parts. Some of the main laser material processing parameters are defined below:

- Laser Power: Represents the total power of the laser beam and it is usually limited by the laser source or the process optimum parameters. It is usually measured in watts (W) or kilowatts (kW).
- Energy density: The energy density measures the amount of radiated energy per surface unit by the laser beam. It is usually measured in J·cm^{-2} and combines the laser power, the time of interaction between the laser and the part and the size of the laser beam diameter.
- Laser beam diameter: The laser beam diameter "w" in a perpendicular plane to the laser beam is defined according to equation (Eq. II. 1). The variable "z_0" is the beam waist position and "w_0" is the beam waist diameter.

$$w^2(z) = {w_0}^2 + \left(\frac{\lambda}{\pi \cdot w_0}\right)^2 \cdot (z - z_0)^2 \qquad \textbf{(Eq. II. 1)}$$

- Laser beam quality: According to the norm UNE-EN ISO 1146/1999, the laser beam quality is described by means of the Beam Parameter Product (BPP) and it is defined as the product between the radius of the waist of the laser beam "$w_0/2$" and the divergence of the beam in the far field "$\theta/2$".

$$BPP = \frac{w_0}{2} \cdot \frac{\theta}{2} \qquad \textbf{(Eq. II. 2)}$$

- Mode order: The transversal energy distribution inside the laser beam depends on the active medium and the structure of the resonator. The different modes are named by the initials TEM (Transverse Emission Mode). The TEM_{XY} refers to the distribution of the electric and magnetic fields in a perpendicular plane to the laser beam and the subscripts indicate to the number of zero intensity regions in the horizontal (X) and vertical (Y) directions.

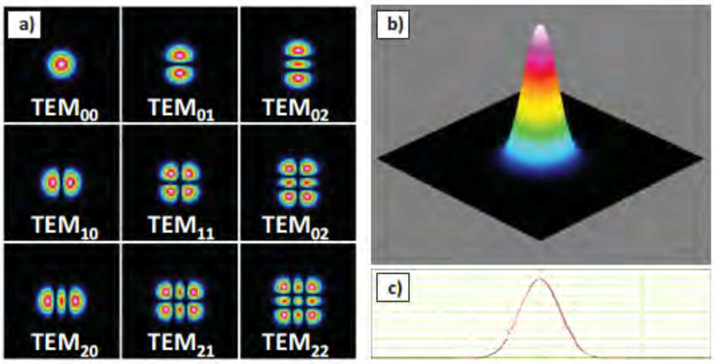

Figure II. 6: a) An array of subplots containing the various Hermite-Gaussian modes; b) 3D view of multi-mode Hermite-Gaussian beam consisting of 80% TEM_{00}, 10% TEM_{10}, and 10% TEM_{01}; c) Profile and Gaussian fit of the multi-mode Hermite-Gaussian beam in b) [DataRay, 2017].

In Table II. 2 the parameters involved in laser based processes are detailed.

Table II. 2 Process parameters involved in the laser processes

PROCESS PARAMETERS		
LASER BEAM	OPTICS	MATERIAL PROPERTIES
• Laser type - Wavelength - Mode order - Beam quality - Polarization - Pulse quality • Laser power • Energy density • Pulse duration / CW • Switch technology	• Focal distance • Focus depth • Beam waist / spot size • Mirrors and transporting fiber - % absorption - Heating	• Absorptivity / reflectivity • Heat conductivity • Fusion latent heat • Phase changes • Molten material - Viscosity - Surface tension • Geometry of the part • Surface condition and roughness • Plasma generation

II.1.3. Industrial laser market and revenue numbers

Since the development of the first laser in the year 1960 [Maiman, 1960], lasers have widespread in different industrial sectors and nowadays they have uncountable applications. The consulting firm MarketsandMarkets (M&M) presents an annual report where the global future of the laser technology is analyzed, both from a technical and a market point of view [M&M, 2017]. In Figure II. 7 (left) the laser sales revenue evolution during the last years and the future prospects are shown. Laser sales are expected to generate a total of 17.06 billion dollars by the 2020. Among the different market segments, in the year 2016 the laser revenues in the Material Processing industry have become the most important for the first time [Overton, 2016].

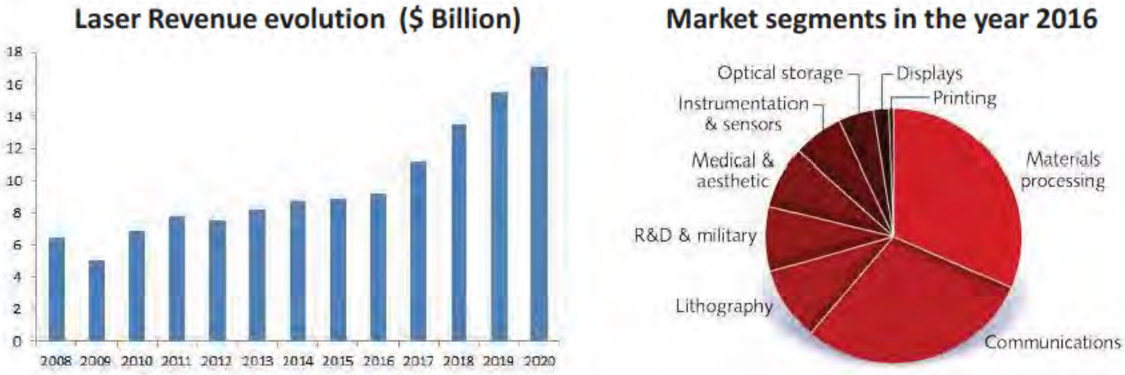
Laser Revenue evolution ($ Billion)

Market segments in the year 2016

Figure II. 7: Laser revenue evolution and future expectations [M&M, 2017] (left) and market segments in the year 2016 [Overton, 2016] (right).

In Table II. 3 the revenue numbers of the different kW lasers types are shown. Results are provided by Strategies Unlimited and they are based on the several leading laser supplier results from the fourth quarter of the year 2015. Laser total revenues are expected to grow a 4.4% in the year 2016 [Belforte, 2016].

Table II. 3 Industrial laser revenue in million US$ [Belforte, 2016].

	2014	2015	2016
CO2	$ 694.5	$ 656.7 (-5%)	$ 587.3 (-11%)
Fiber	$ 1483.6	$ 1713.7 (+16%)	$ 1902.6 (+11%)
Solid state	$ 463.9	$ 463.4 (+0%)	$ 461.0 (-1%)
Other	$ 331.6	$ 346.3 (+4%)	$ 367.8 (+4%)
Total	$ 2973.6	$ 3180.1 (+6.9%)	$ 3318.7 (+4.4%)

Due to the improvement of the fiber and disk lasers, CO_2 lasers have shown the largest decline and in the year 2016 their revenue suffered an 11% decrease. Other laser types include diode and excimer laser. As an example, IPG is the worldwide high power diode laser manufacturer leader [IPG, 2017] and its outstanding numbers justify on its own the 4% total increase of "Other" lasers in Table II. 3. The laser type that presents the highest increase is the fiber laser. In 2014, 75% of the major worldwide companies that manufacture laser cutting machines powered their systems with fiber lasers. And the tendency goes on increase. Regarding the LMD process, most machine manufactures install fiber and diode lasers, which are explained in the section "*II.1.1. Laser generation principles*".

II.2. Introduction to the Laser Metal Deposition process

Laser Metal Deposition (LMD) is an Additive Manufacturing (AM) technique based on the generation of new geometry by adding filler material over a substrate [Thompson, 2015]. The ASTM (American Society for Testing and Materials) defines the additive manufacturing as "*the process of joining materials to make objects from 3D model data, usually layer upon layer, as opposed to subtractive manufacturing technologies*" [ASTM, 2012]. During the last decades, since the beginning of the additive manufacturing, the process has evolved drastically and the generated parts are almost 100% dense and functional, what opens new challenges and opportunities to the LMD process.

With the aim of comparing the LMD process with other additive alternatives, such as the thermal spaying or arc based processes, and highlighting its advantages, Michael Breitsameter, Director of Sales & Marketing at F.W. Gartner Thermal Spraying Ltd stated the following: "*The Thermal spray is a low cost method for recovering the original part dimensions, but the resulting part does not recover the original mechanical properties. On the contrary, the LMD process gives an excellent integrity and, in some cases, the mechanical properties of the resulting repaired part may exceed the original´s*" [Riedelsberger, 2013].

II.2.1. LMD and SLM comparison

In the present section the different laser based AM processes are addressed and a comparison between them is presented. Nevertheless, the PhD concentrates on the LMD process in the following chapters.

Two main branches can be distinguished within the laser based AM processes: the Selective Laser Melting (SLM) or the "Powder bed" based processes and the Laser Metal Deposition (LMD) or the "Direct Material Deposition" processes. It is necessary to make a difference between them, since the process principles are completely different. Both processes are laser based AM processes that use powder as filler material, but the deposition process and the type of objective parts are completely different.

In general terms, powder bed processes are addressed to the manufacture of whole parts starting from zero. On the contrary, in direct material deposition methods filler material is added to a previously existing part. They are mainly used for the repair of damaged parts, the addition of some geometrical details or the enhancement of the surface properties by the addition of a coating layer. Moreover, they can also be used for the generation of whole parts starting from zero.

The **Selective Laser Melting (SLM)** process was developed initially by the Fraunhofer ILT. This type of additive process is also named as Powder Bed Fusion (PBF) or metal 3D printing. It was patented in 1979 and fully commercialized in the 1990s. The desired geometry is manufactured layer by layer based on a CAD geometry, which is previously sliced using an appropriate program that generates the required trajectories to be followed by a laser scanner. The SLM machines can process a wide range of metals, including industrial polymers, titanium alloys, cobalt, chromium, stainless steels, nickel alloys and aluminum alloys [EOS, 2017; Renishaw, 2017].

The process is divided into two differentiate steps. In a first step, a layer of a determined thickness of powder material is placed on the surface of the base material. Afterwards, in a second step the preplaced material is melted and added to the substrate using a laser beam. The SLM enables to manufacture functional and geometrically complex parts, with almost no geometrical restriction. Moreover, almost 100% dense parts can be manufactured and good dimensional accuracy is obtained. In Figure II. 8 the main steps of SLM processes are shown, from the CAD design to the final part.

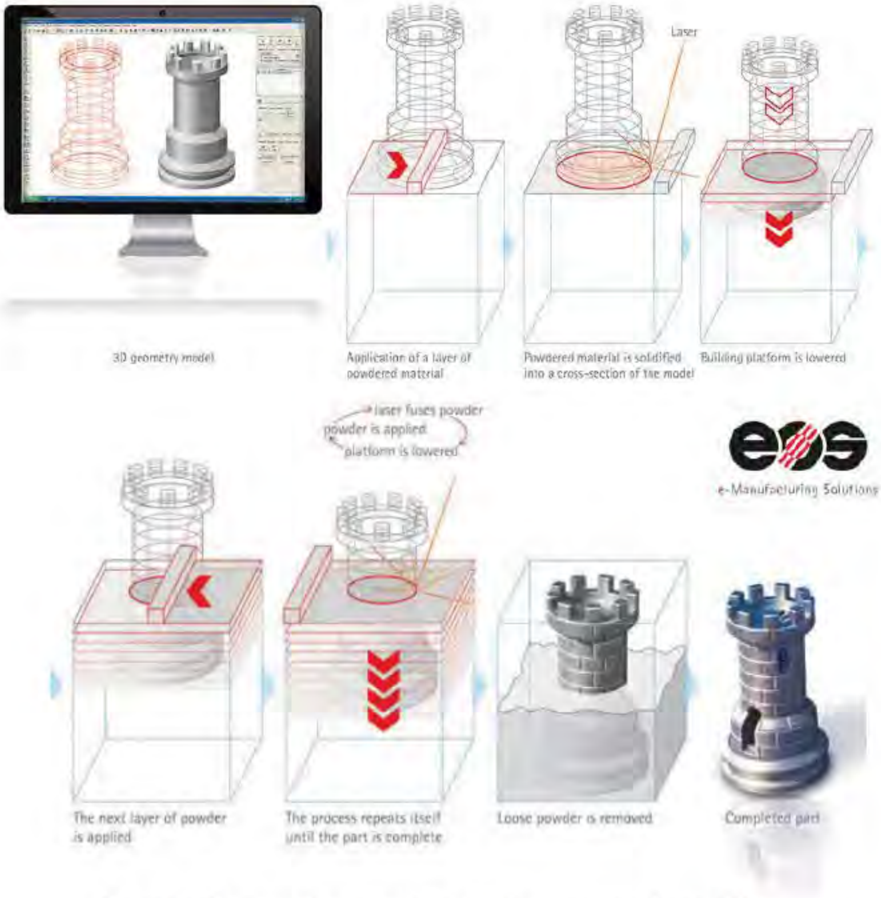
Laser
3D geometry model
Application of a layer of powdered material
Powdered material is solidified into a cross-section of the model
Building platform is lowered
laser fuses powder
powder is applied
platform is lowered
e-Manufacturing Solutions
The next layer of powder is applied
The process repeats itself until the part is complete
Loose powder is removed
Completed part

Figure II. 8: General function principle of laser sintering [EOS, 2017].

The laser movement over the powder bed is achieved thanks to a galvanometric scanner that moves the laser beam with velocities up to 15 m·s^{-1} without losing positioning accuracy. Thanks to these high velocities, the HAZ is reduced to almost zero and current finished parts show a microstructure with high mechanical properties. One of the main limitations of the Powder Bed based processes is the size of the part. Since the process is carried out in a closed chamber full of inert gas, the size of the part is limited to the chamber size. Currently, SLM machines are becoming larger, but are still limited to parts smaller than 800x800x800 mm in metal applications.

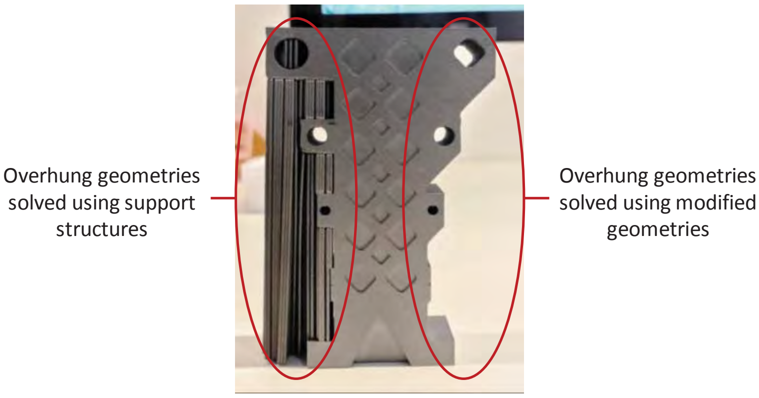
Overhung geometries solved using support structures
Overhung geometries solved using modified geometries

Figure II. 9: Different alternatives to generate overhung geometries [Renishaw, 2017].

In addition, contrary to what is stated in many publications, SLM process presents some design restrictions, which are usually solved by using support structured during the layer-by-layer building process. Consequently, when the deposition process is finished, these support structures must be removed by conventional methods using machining, EDM or even manual tools. Finally, finishing operations are required to achieve the desired surface roughness and dimensional accuracy.

The SLM has wide applications, such as: automotive, aerospace and consumer goods. All these applications show the common denominator of a complex geometry. The first industrial serial production using SLM machines was focused on dental restoration, see Figure II. 10. Furthermore, the capability to use lightweight materials such as titanium and create parts with internal hollow structures, gives the possibility to generate ultra-lightweight and functionally optimized parts.

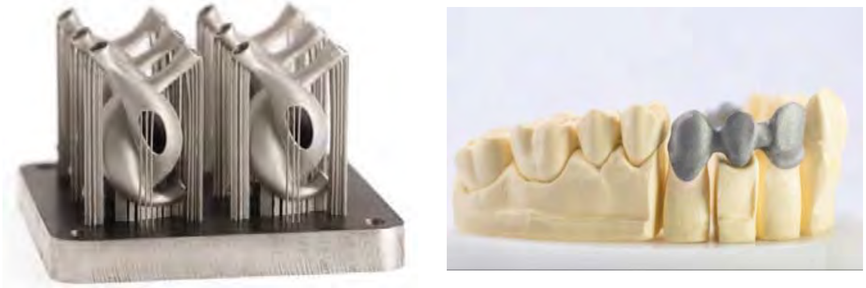

Figure II. 10: An Aorta pendant on small build plate with supports (left) and an image of a SLM manufactured bridge model (right) [Renishaw, 2017].

Thanks to these characteristics, a relevant number of companies have paid special attention to this process. In this context, General Electric is becoming one of the most relevant players in the PBF processes with the recent acquisition of Concept Laser [GE Aviation, 2016] and ARCAM [Arcam, 2016] companies. Likewise, EOS [EOS, 2017] and Renishaw [Renishaw, 2017] are the current worldwide leading SLM machine manufacturers and their benefits are increasing every year thanks to the widespread of the SLM technology. Besides, many companies like Mizar in Spain are betting directly on this technology [Mizar, 2017].

In the **Laser Metal Deposition (LMD)** process, the filler material is directly injected through a nozzle into the melt pool. The resulting part is a near-net-shape component with an almost 100% density and properties comparable to those of the wrought or cast material.

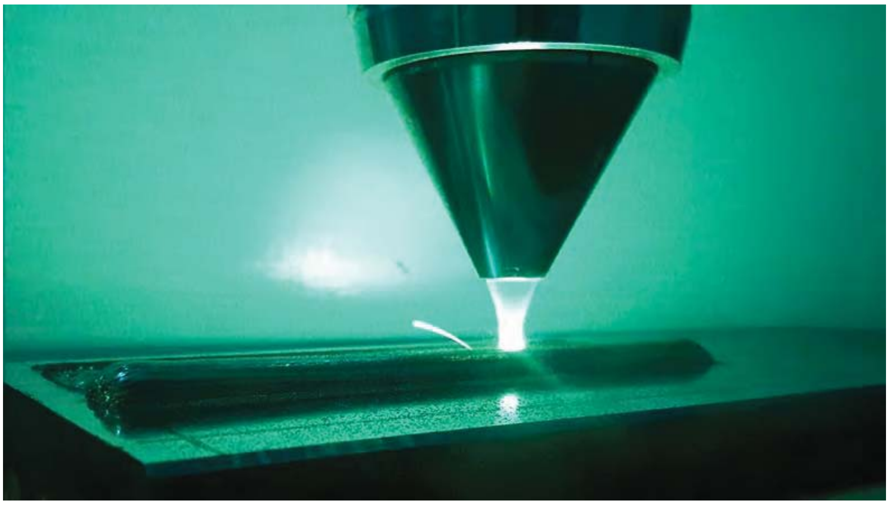

Figure II. 11: LMD process using a coaxial continuous nozzle.

LMD can be used for the generation of entire parts starting from zero, but it is more likely used for the addition of some substructures or details. The LMD process offers the possibility to repair damaged parts or even increase the wear or corrosion resistance properties of the bulk material by adding a coating layer with specific properties. Moreover, various materials can be fed simultaneously, what enables to adjust the chemical composition and consequently modify the mechanical properties of each layer according to the final utility of the part.

The LMD process can be carried out in a Cartesian machine, similar to a milling center or even in an anthropomorphic robot, see Figure II. 12. The manufactured part size is only limited by the size of the LMD nozzle handling system. Nevertheless, the dimensional accuracy of this process is comparatively lower than that of the SLM and bigger allowances are required for the subsequent finishing operations.

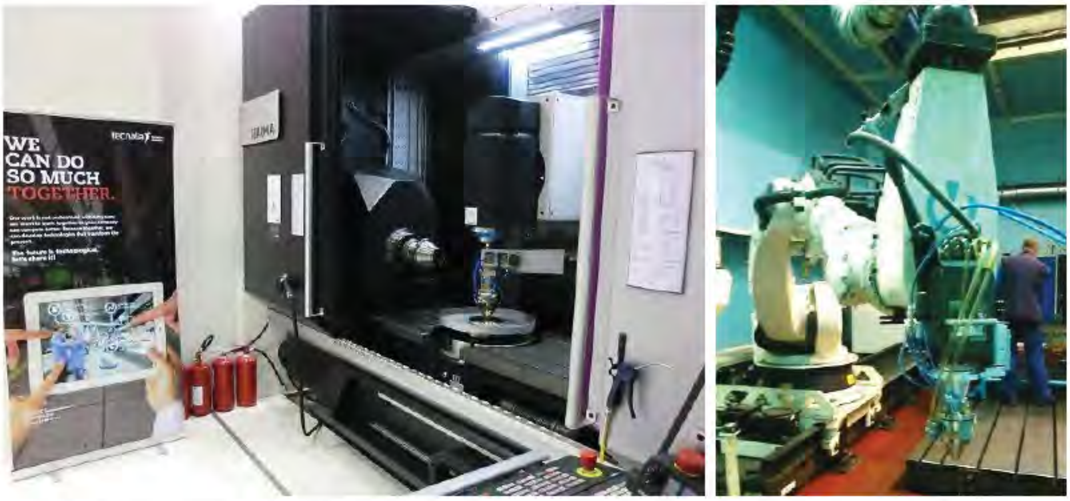

Figure II. 12: Different alternatives for LMD systems, a Cartesian hybrid machine from Ibarmia (left) [Ibarmia, 2017] and an anthropomorphic robot (right).

If LMD and SLM process are compared, the LMD has a higher deposition rate. In LMD typical values of 5-30 $g\cdot min^{-1}$ are obtained, whereas the SLM process presents typical values of 2-3 $g\cdot min^{-1}$ [Sciaky, 2017]. On the contrary, the SLM manufactured parts have a higher dimensional accuracy and the LMD parts need to be manufactured afterwards in order to achieve the desired tolerances and dimensional accuracy. In Table II. 4 a comparison between both processes is shown:

Table II. 4 Comparison between the SLM and the LMD technologies.

	SLM (Powder bed)	LMD (Direct injection)
Accuracy	High (±20 µm)	Medium (±0.2 mm)
Roughness	>2.5 µm Ra	>10 µm Ra
Particle size	10 - 50 µm	45 - 200 µm
Structural integrity	High integrity. Void chamber/protected atmosphere chamber is used.	High integrity. A protective atmosphere is used.
Part size	Small. Part size limited to the chamber size (*usually smaller than 800x800x800 mm*).	Variable. Able to manufacture big parts.
Industrial application	• Direct part manufacture	• Repair of damaged parts • Coating • Complex geometry manufacture over a substrate • Entire part manufacture

II.2.2. Laser Metal Deposition process basics

In LMD process, the laser beam is used as an energy source to generate a melt pool on the surface of the substrate. The reasons for using a laser are the technical advantages which offers in comparison with other heat sources like electric arcs or plasma. Thanks to the properties of the laser beam mentioned in the section *"II.1. Introduction to the lasers"*, the laser beam can be concentrated in a small area (0.1-2 mm diameter) on the surface of the substrate and the size of the HAZ is reduced.

As it can be seen in Figure II. 13, the process is based on the melting of a substrate by a laser beam. Part of the energy is absorbed by the substrate, whereas the rest is reflected and therefore lost. The heat absorbed by the substrate is transmitted towards its interior by means of conduction and a melt pool is generated. Filler material is added into the melt pool in powder particle shape and they are also melted by the laser beam. During the inflight time, powder particles or wire interact with the laser beam and they get heated as well as the laser beam is attenuated. Consequently the power of the laser that reaches the surface is lower than the programmed. Laser beam attenuation values up to the 20% of the nominal laser power are obtained in the LMD process [Tabernero, 2012_1].

Once the laser beam moves, the solidification of the deposited material occurs. Due to the relatively small total amount of energy introduced into the part and the fact that it is localized in a very small area, the cooling process is very fast and molten material solidifies almost instantly. In LMD typical cooling rates up to 10^3-10^5 K·s^{-1} are obtained, what leads to dendritic structures [Dinda, 2009]. After the solidification of the filler material, a single track of deposited material is generated. By the overlap of different tracks, a single layer is obtained. Finally, whole parts can be built using a common layer-by-layer method as in other AM processes.

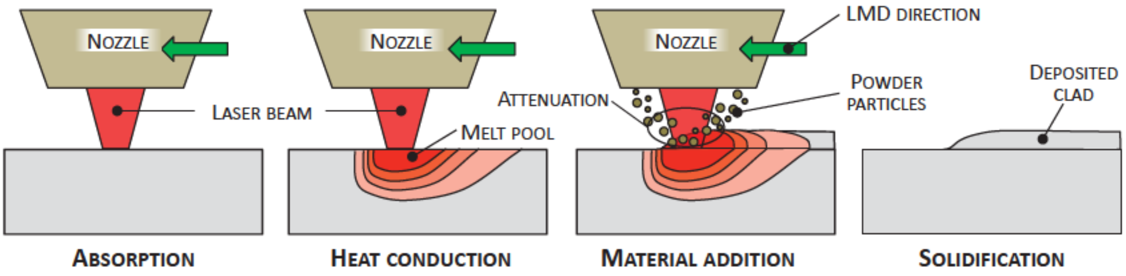

Figure II. 13: LMD process step by step.

Filler material can be addressed in two different forms (wire or powder) and the process differs significantly. Inside the realization of the present research work, a comparison between powder and wire LMD processes is carried out and the results obtained are shown in the section "*II.2.4. Different filler systems: wire and powder*".

Furthermore, as the introduced total amount of energy is very low (compared with other additive techniques such as plasma), the geometrical distortions resulting in the finished part are also minimal. Consequently, the apparition of cracks is reduced, what enables to deposit a wider range of materials.

II.2.3. Nozzle design for the Laser Metal Deposition process

In order to obtain a stable process, simultaneously to the generation of the melt pool on the surface of the substrate, filler material needs to be addressed and injected using a specific nozzle. There are different types of nozzles for the LMD process and based on their geometry and depending on the powder injection system, three nozzle types can be distinguished, see Figure II. 14.

Depending on the design of the nozzle, the powder mass distribution into the melt pool can change. Since powder particles that are injected outside the melt pool bounce away and are lost, the main objective of a nozzle for the LMD process is to focus the maximum amount of powder into the melt pool. The efficiency of the nozzle can be defined as the ratio between the trapped powder into the melt pool and the total amount of injected powder.

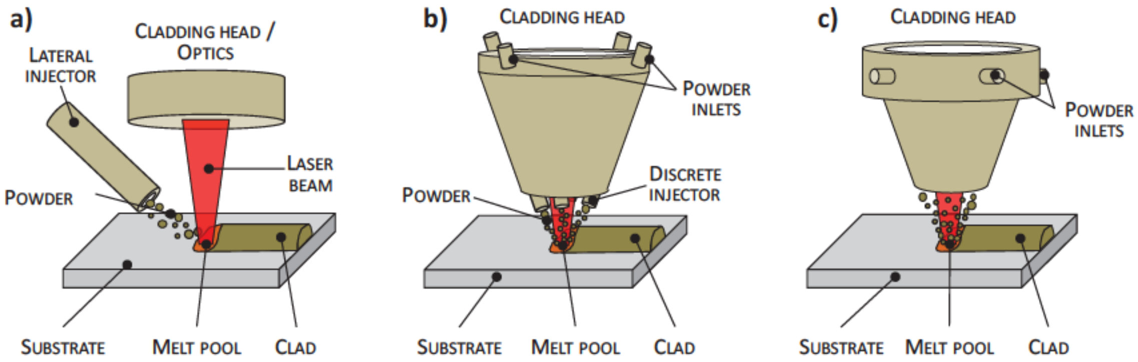

Figure II. 14: Different types of nozzles used in the LMD, a) Lateral; b) Discrete coaxial; c) Continuous coaxial nozzle.

Lateral nozzles present the simplest and more economical alternative for the LMD process. However, this simplicity results to be a drawback itself, because the process turns to be unidirectional and its efficiency is rather low. These types of nozzles are usually used for rotatory part coatings, where the deposition strategy is unidirectional.

As an evolution of lateral nozzles, coaxial discrete nozzles have been developed. The coaxial discrete nozzle principle is based on a number of discrete injectors that are positioned around the rotatory axis of the nozzle. Depending on the design, three or four injectors may be positioned in order to cover the complete range of directions. Their main characteristics are the capability to add material in all directions and their intermediate price. The major advantage of the coaxial discrete nozzles is that they enable to tilt the cladding head without influencing the powder flow at the nozzle exit due to the gravity forces. This characteristic enables to use this type of nozzle in 5-axis operations where the laser processing head includes tilting movements [Zekovic, 2007].

Lastly, the coaxial continuous nozzles have been also developed and their main characteristic is the fact that they distribute uniformly the powder among the whole periphery of the nozzle. Coaxial continuous nozzles achieve the highest focalization of the powder particles, resulting also in the highest efficiencies. Coaxial continuous nozzles have gained a wide acceptance because of their higher efficiency and capability to deposit material in all directions with a high quality [Weisheit, 2001]. However, their main disadvantage is the comparatively higher price due to their more complex geometry.

Later on, in section "*II.5.3. Review of the evolution of designs and patents of industrial* LMD nozzles" the latest developments and patents with regard to the nozzle design are described, focusing particularly on coaxial continuous nozzles.

II.2.4. Different filler systems: wire and powder

In the present research work, when referring to the LMD process, powder is applied as the filler material. However, there are two alternatives for delivering the filler material into the melt pool in the Laser Metal Deposition process. Therefore, two different processes should be distinguished: Wire or Powder LMD.

The present work includes a 7 month stay in the IPT Fraunhofer research center in Aachen, Germany [IPT, 2017]. During that stay a comparison between both processes has been carried out with the aim of generating the sufficient knowledge to determine which process is more adequate in different situations [Arrizubieta, 2016].

Powder and Wire LMD processes are based on the same principle, but even both processes may look similar, there are some relevant differences between powder and wire LMD. In powder LMD, the laser beam is attenuated as a result of the powder cloud generated above the working plane, see Figure II. 15. As a consequence of this attenuation, powder particles are heated, but the laser power that reaches the surface of the substrate is lower than the programmed value. In wire LMD this phenomenon does not occur, nonetheless, a percentage of the heat introduced to the process is lost through the wire itself due to conductivity. In Figure II. 15 the schemes of powder and wire LMD processes are shown and the main physical phenomena that are involved are detailed.

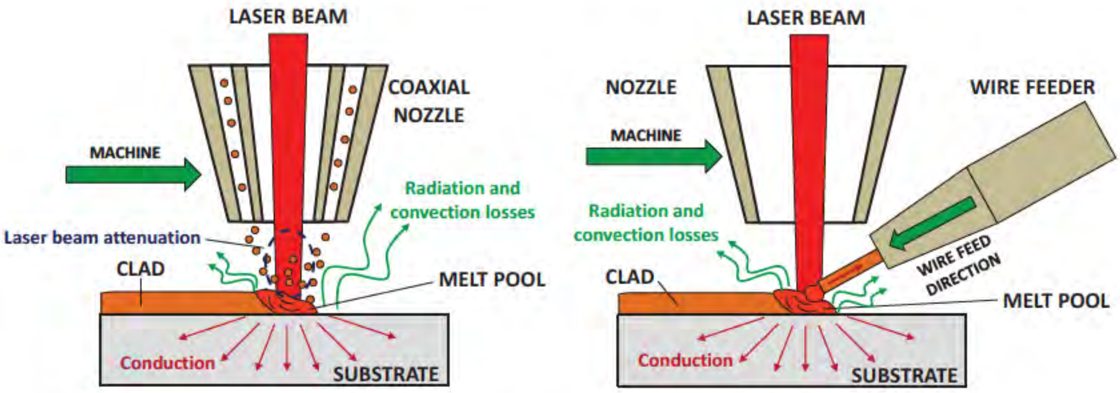
LASER BEAM
COAXIAL NOZZLE
MACHINE
Radiation and convection losses
Laser beam attenuation
CLAD
MELT POOL
Conduction
SUBSTRATE
LASER BEAM
NOZZLE
WIRE FEEDER
MACHINE
Radiation and convection losses
CLAD
WIRE FEED DIRECTION
MELT POOL
Conduction
SUBSTRATE

Figure II. 15: Schemes of powder and wire LMD processes including the physical phenomena involved.

In wire LMD, usually a lateral wire feeder is used, where the position of the wire and the incidence angle are key factors of the process [Mok, 2008]. On the contrary, in powder LMD usually coaxial nozzles are used and since powder is distributed coaxially among the laser beam, material can be deposited in any direction [Kaierle, 2012].

Regarding the productivity of both processes, wire LMD deposition rate is much higher than the powder LMD, since material deposition rate is higher and the deposition efficiency is 100%. Consequently, when high productivity is required and the geometry to be generated is rather simple (especially rotatory parts), wire LMD is a more competitive process.

On the one hand, powder LMD is a more robust technology, since there is no direct contact between the nozzle and the melt pool. Moreover, the process is partially auto-regulated, because if the powder stream is slightly out of focus, the material deposition is reduced but the process continues.

On the other hand, in the case of wire LMD, if the wire contacts the surface of the substrate outside the melt pool, the process becomes unstable and must be stopped. Moreover, the wire LMD process is very sensitive to the positioning of the wire. This lack of stability mentioned in the wire feeding mechanism, needs to be solved in order to obtain good quality clads [Pavlov, 2011], and the wire end has to be positioned correctly inside the melt pool. Besides, the wire feeding rate plays a key role in ensuring the quality of the deposited material.

With the aim of comparing the mechanical properties of the parts produced by wire and powder LMD, tensile test parts are built using the same equipment. For this purpose, a 5-axis CNC machine (Alzmetall GX 1000/5-T-LOB), coupled with a 4.5 kW diode laser is used. The machine is prepared for both wire and powder LMD processes. In all cases a longitudinal ZIG strategy was used, this strategy ensures the best mechanical properties for the tensile tests [Tabernero, 2011].

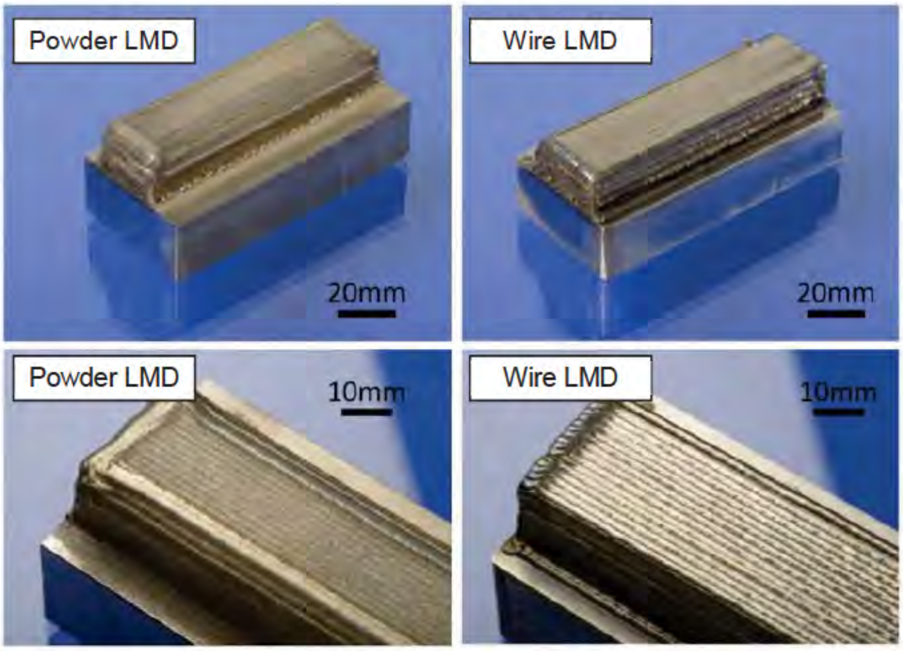

Figure II. 16: Final shape of powder (left) and wire (right) LMD manufactured parts.

Tensile test are carried out according to the DIN EN ISO 6892-1 standard. The result analysis shows that the wire LMD parts present a higher deformation and necking at their breakage. Thus, it is concluded that powder parts show a slightly more brittle nature compared with the wire ones, see Figure II. 17.

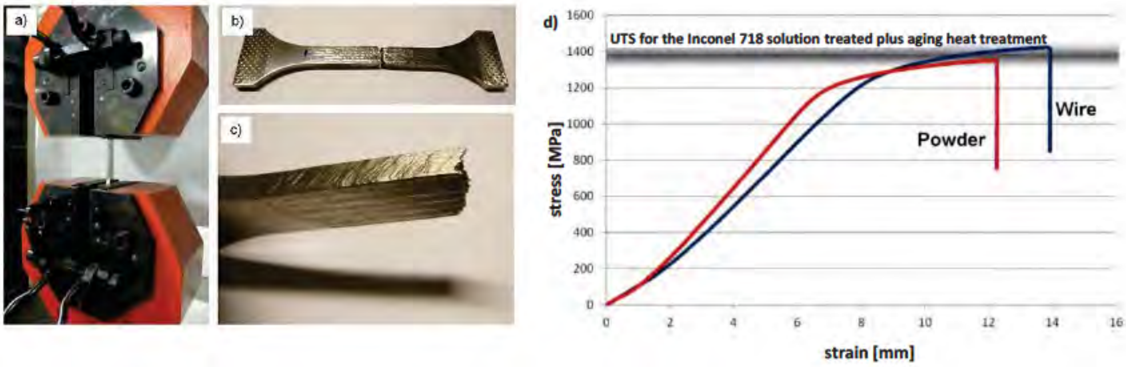

Figure II. 17: a) Tensile test of a powder LMD manufactured part. b) The same part after the breakage. c) Detail of the tested. d) Average results of the tensile tests for Wire and Powder LMD test probes.

In conclusion, both processes are suitable for building high quality parts regarding material integrity and mechanical properties. However, powder LMD is a more appropriate process when complex geometries or all-directional clads are to be generated. On the contrary, wire LMD results to be advantageous when simple geometries combined with higher deposition rates are required for the repair or entire manufacture of bigger parts.

On the basis of the knowledge obtained during the stay in the IPT Fraunhofer, a nozzle for wire LMD is designed and manufactured at the University of the Basque Country (UPV/EHU) in cooperation with Tecnalia. The nozzle works properly and enables a stable deposition process. In Figure II. 18 an example of a flange built in AISI 316L is shown. The part is faced in order to obtain a smooth surface.

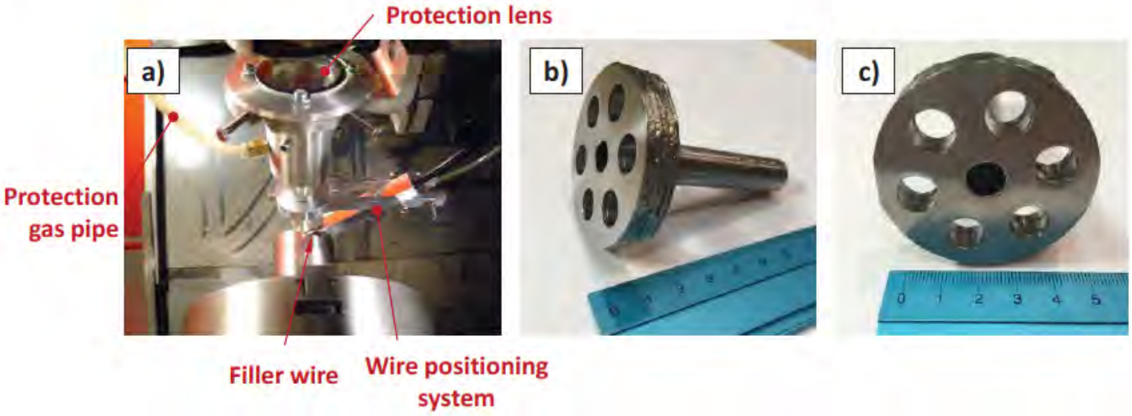

Figure II. 18: a) Designed wire-LMD nozzle; b) Flange built in AISI 316L; c) Front view of a flange built in AISI 316L.

II.3. Latest machines for the LMD and hybrid processes

As a consequence of the widespread of the additive manufacturing processes, an increasing number of machine tool manufacturers are investing heavily in laser technology and especially in LMD. In the present section the latest developments and hybrid machines launched to the market by some of the most recognized worldwide machine tool manufacturers are presented.

The German-Japanese company DMG Mori has strongly invested in the LMD technology. As they stated in the last EMO that took place in Milan in the year 2015, the reason for investing in the LMD technology rather than in the SLM, is the much higher deposition rate it offers. Moreover, thanks to the capability to deposit material while the five axes of the LMD machine are simultaneously interpolated, complex geometries can be generated without using support structures.

The latest hybrid machine launched by DMG Mori is the LASERTEC 65 3D, see Figure II. 19 [DMG Mori, 2017]. This machine includes a tilting table and enables to generate a part by LMD technology and afterwards mill it in 5-axis without losing the part. Moreover, they put special emphasis on the fact that they offer assistance during the whole additive process: CAD/CAM software and deposition strategy design, material documentation and process control. Additionally, The LASERTEC 65 3D includes various control and monitoring systems, such as laser power control based on an artificial vision that measures the size of the melt pool.

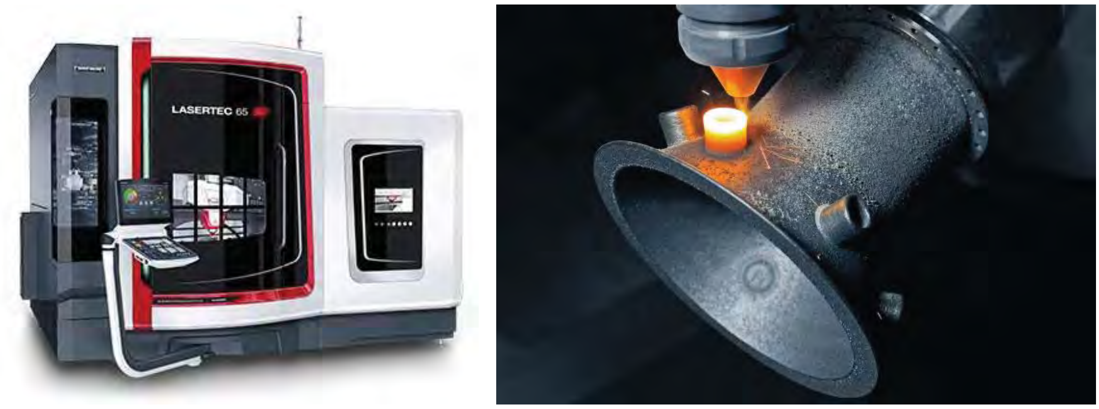

Figure II. 19: The hybrid machine LASERTEC 65 3D developed by DMG-Mori (left) and an additive operation (right) [DMG Mori, 2017].

Almost simultaneously, the Japanese company Mazak launched the 5-axis hybrid machine Integrex i-*400AM* that combines milling and LMD processes [Mazak, 2017]. This is the first additive machine manufactured by the Yamazaki Mazak Corporation and it is developed in collaboration with Hybrid Manufacturing Technologies. The machine uses the Ambit™ range of tool-changeable cladding heads and offers the possibility to switch between different LMD nozzles: high speed nozzle, fine nozzle, etc. what enables to adjust the height and width of the deposited line depending on the process requirements.

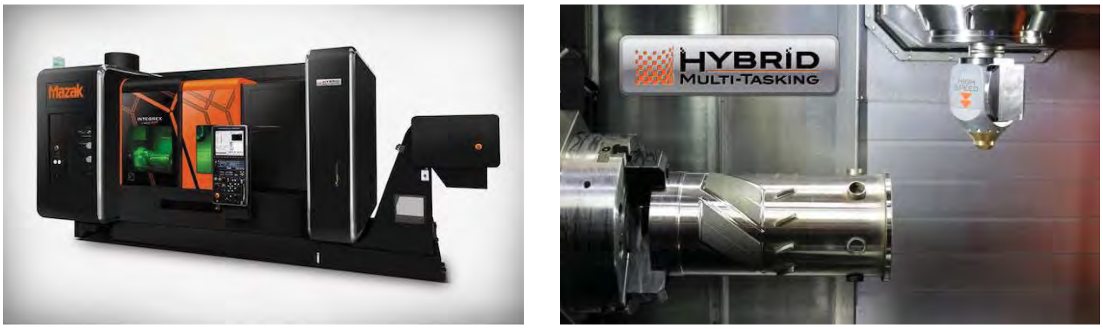

Figure II. 20: The hybrid machine Integrex i-400AM developed by Mazak (left) and a demonstration part (right) [Mazak, 2017].

The Austrian company WFL Millturn Technologies launched its latest machine M80 Millturn that combines LMD and milling/turning processes [WFL, 2017]. It includes a 6 kW diode laser, what enables to deposit high amount of materials.

In view of the large investment that worldwide machine tool manufacturer leaders are performing in the field of the LMD and hybrid machines, smaller companies have also invested in the field of hybrid machines. An example of it is the ZVH 45/L1600 ADD+PROCESS machine developed by the Basque company Ibarmia [Ibarmia, 2017].

Traditionally, the hybrid-manufacturing has been related to milling and turning operations, but also new hybrid manufacturing alternatives have arisen. In the Paris Air Show that took place in 2015, the first hybrid machine that combines LMD and grinding technologies was presented [Hybrid, 2017]. The machine was developed by the Elb-Schliff WZM GmbH ("ELB") and equipped with Ambit™ laser cladding heads [ELB, 2017]. The main advantage of the machine is that it offers a new standard for precision by integrating grinding and LMD in a single setup.

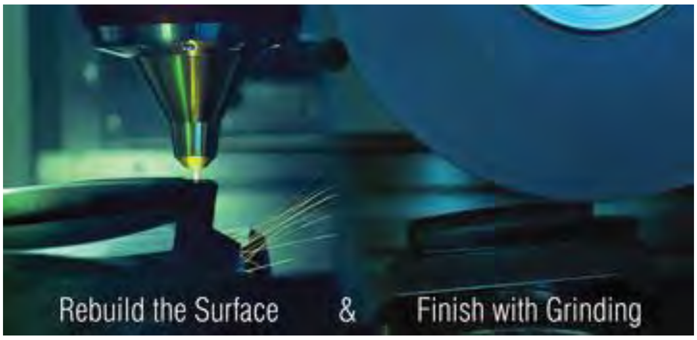

Figure II. 21: Rebuilding the surface using AMBIT™ laser cladding head (left) and in-process finishing via grinding (right) [Hybrid, 2017].

II.4. Laser manufactures and market numbers

In the present section the market numbers related with the laser technology and the laser manufacturers are detailed. Especial attention is paid to the AM numbers.

The growth of the laser industrial applications led to an increase in the number of sold lasers and so have done the incomes of the laser manufacturers. Since the world economy started to slow down, especially in Europe, the global numbers of the manufacturing companies have also suffered. However, industrial laser sales have remained strong, particularly high power fiber laser sales. In Figure II. 22 the evolution of the laser manufacturer companies revenue during the last years is shown. The figure includes all types of lasers used in material processing: Lasers for welding, cutting, drilling, additive, marking and other material processing operations.

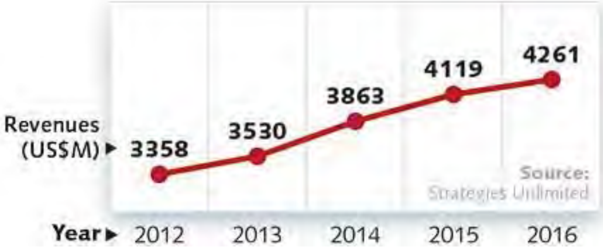

Figure II. 22: Revenue of the laser manufacturer companies.

In order to give some numbers to illustrate this laser boom period, Trumpf (the world's largest industrial laser equipment and system manufacturer and supplier) reported a 3% increase in sales during the year 2015/2016 that finished on June 30, 2016. During this period, sales reached a value of 2800 million Euros [Trumpf, 2015].

Challenging Trumpf for market leadership is the fiber laser manufacturer IPG Photonics, which sales have increased exponentially during the last years. In the year 2015, it reported an outstanding growth of the 22%, reaching the amount of 243.5 million Euros growth. At the end of the year 2015 they reached the value of 901.3 million Euros net sales. This increase of the revenue consolidates the astonishing growth of the 17% that has experienced during the last 4 years [IPG, 2015]. Following this two companies are Coherent and Rofin-Sinar, which reached revenue values of 760 and 492 million Euros respectively during the year 2015 [Belforte, 2016], values obtained according to the exchange rate USD/EUR at the 11/12/2016.

This continuous increase of the laser technology is due to the ambitious projects launched by various governments with the aim of promoting the additive manufacturing. A global view of the most important projects and programs to support the additive manufacturing is given in the following paragraphs.

The United States of America founded in the National Additive Manufacturing Innovation Institute (NAMII) in the 2012 and since then, they have funded over 20 projects with a $13.5 million public investment and $15 million industry cost share [Martin, 2013]. Furthermore, in March 2014 it was announced that Obama's government would increase the funding to $50 million [Wholers, 2014]. Furthermore, the US government designed the National Network for Manufacturing Innovation (NNMI) to coordinate private and public investment with the aim of bringing together industry, academia and government partners and accelerating commercialization.

On this side of the Atlantic, the European Commission (EC) is strongly supporting the goal of achieving the 20% of the total European Union (EU) Gross Domestic Product (GDP) from the manufacturing industry, a 5% increase compared with the current 15%. During the last years, the funding from different Framework Programs (FP) has increased significantly to support the Additive Manufacturing, especially during the last years of the FP7, from 2011-2013. Only with the FP7, the EC funded more than 60 successful projects in AM. The EU made a contribution of over 160 million Euros and the program had a total budget of 225 million Euros [FP7, 2014].

The trend continues with the Horizon 2020 program that the EU launched with an 85 billion Euros in funding available from 2014 to 2020 (in addition to private investments). The aim of the Horizon 2020 program is to generate breakthroughs between science and industry and ease the path of new ideas and projects form the laboratory to the marketplace [FP7, 2014].

An example of the readiness level of the additive manufacturing is the ACAM (Aachen Center for Additive Manufacturing). The ACAM was founded in September 2015 and is a strategic partnership between Fraunhofer IPT and ILT and many partners from science. The ACAM is directed by Dr. Kristian Arntz from Fraunhofer IPT and Dr. Johannes Witzel from Fraunhofer ILT and its objective is to explore new opportunities for the additive technologies towards the Industry 4.0, as well as to enable manufacturing companies to take advantage of the AM technology in a profitable way for their production processes. Moreover, the center promotes the exchange of information and offers training seminars to expertise the future workers in the AM sector.

In the same direction, the Chinese government has presented an ambitious project named "*Made in China 2025*" based on the German initiative "*Industry 4.0*" for the creation of a smart factory. In Figure II. 23 the roadmap of the project is shown.The aim of this project is China to become the world leader manufacturer country within the next years [HKTDC, 2016].

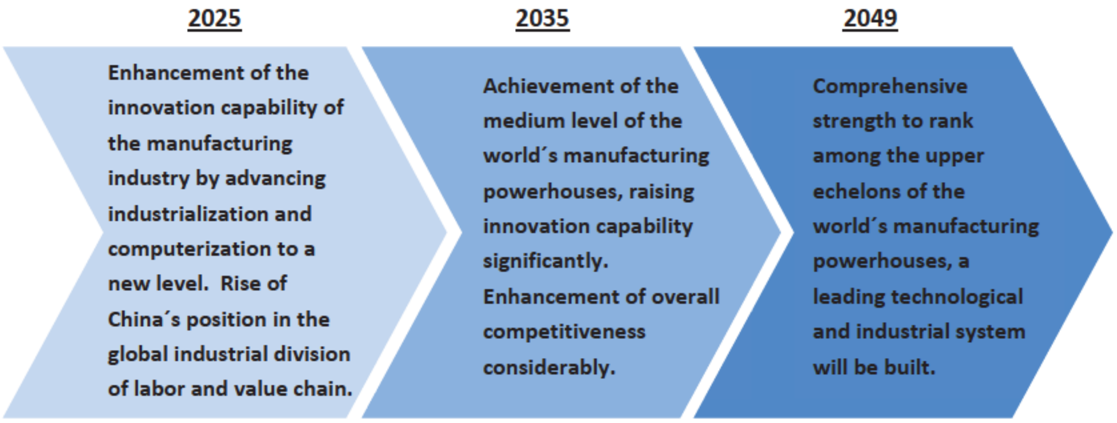

2025

Enhancement of the innovation capability of the manufacturing industry by advancing industrialization and computerization to a new level. Rise of China´s position in the global industrial division of labor and value chain.

2035

Achievement of the medium level of the world´s manufacturing powerhouses, raising innovation capability significantly. Enhancement of overall competitiveness considerably.

2049

Comprehensive strength to rank among the upper echelons of the world´s manufacturing powerhouses, a leading technological and industrial system will be built.

Figure II. 23: Made in China 2025 Roadmap for Building China into a Manufacturing Powerhouse [HKTDC, 2016].

II.5. Characteristics of the filler material and different delivery systems

II.5.1. Powder characteristics

As it has been previously mentioned, filler material for the LMD process is usually supplied in powder form. Powder particles used in the LMD process have typically a spherical morphology and their diameters range between 20 and 200 µm. The powder is obtained by gas atomization or water atomization (which is less common) [Zekovic, 2007]. The sphericity of the particles is very important for the correct powder flow inside the feeder and the nozzle and the proper concentration of the powder particles at the focal plane.

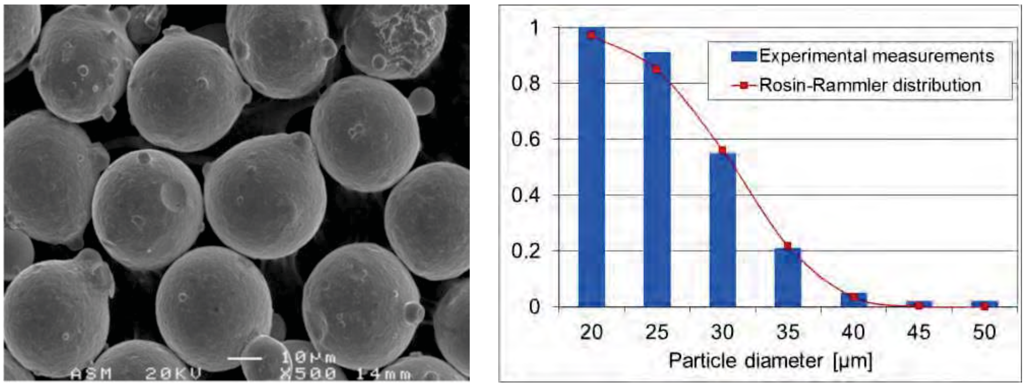

Figure II. 24: Inconel 718 powder: SEM image and particle size distribution.

The usage of different powder materials enables to build tailored parts and the development of Functionally Graded Materials (FGM) [Udupa, 2014]. Functionally Graded Materials are very important in engineering and other applications but their production cost makes their use prohibitive in some applications [Rahamood, 2012]. Nevertheless, the LMD offers a high manufacturing flexibility together with an acceptable cost in the generation of FGM.

The main characteristic of these advanced materials is the possibility to change the properties gradually within the part. The overall properties of FGM are unique and different from any of the individual material that forms it [Naebe, 2016].

Moreover, the existence of sharp interfaces, where failure initiates, between the different materials that conform the part is avoided. Instead of that, smooth interface gradients between adjacent materials are obtained [Kievack, 2003]. Thanks to it, FGMs offer the possibility to withstand very high thermal gradients without failure, what makes these materials appropriate for applications in aerospace, automobile, medicine, sport, energy and sensors [KMM, 2017].

There are three alternatives for obtaining the desired composition of the deposited material:

1. Layers of different materials can be deposited. Each layer has different properties, such as high resistance to corrosion, wear, etc. As it can be seen in Figure II. 25, an Inconel 718 layer is added between the AISI D2 (DIN 1.2379) tool steel substrate and the AISI D2 filler material with the aim of avoiding cracking problems.

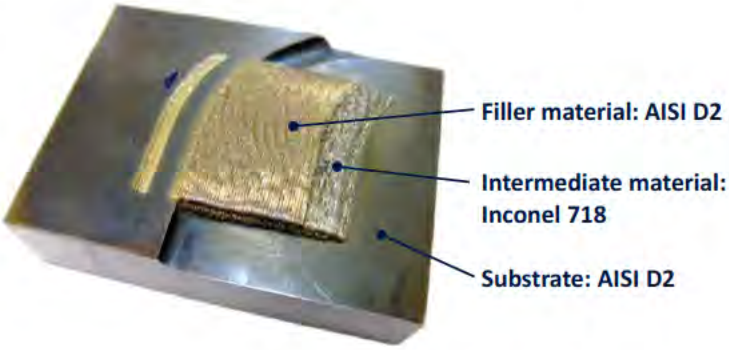

Figure II. 25: AISI D2 material deposition over an AISI D2 substrate using an Inconel 718 intermediate material.

2. Powder particles can be mixed before injecting them into the melt pool. The simplest way to mix the powders is to generate the desired mixture before introducing it to the powder feeder hopper. Depending on the mixing percentage of the materials, the deposited layer will have different properties. This way specific material layers can be generated.

   Some authors, like Xu et al., analyzed the enhancement of the wear resistance properties by using a mixture of Co-based powder alloy (Stellite 6) and tungsten carbide (WC) particles [Xu, 2006]. Another example would be adding a small amount of WC into an AISI 316 matrix in order to improve the wear resistance of this second material [Iglesias, 2014].

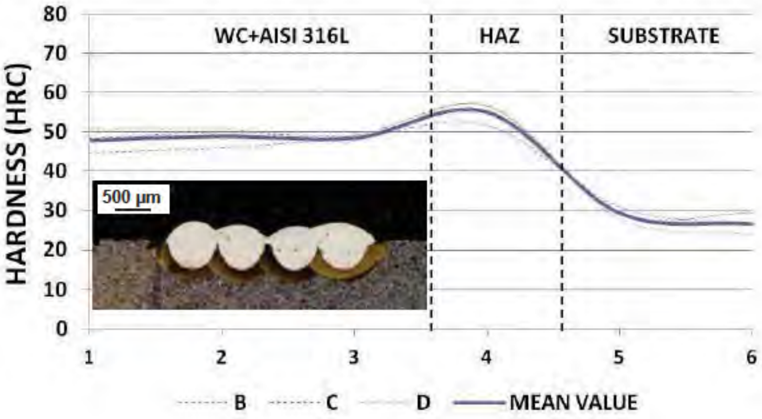

Figure II. 26: Microhardness vs depth measurement for a 30% WC and 70% AISI 316L (400W laser power and 2050mm·min^{-1} machine feed rate) [Iglesias, 2014].

However, if powder particles with different size and density are mixed, the resulting mixture may not be homogeneous. Consequently, the properties of the deposited material would differ from the expected ones.

3. The third alternative for obtaining the desired composition of the deposited material is by mixing the different powders directly at the nozzle. Instead of feeding the nozzle with one drag gas inlet and only one type of powder, two or more different powders are fed from different powder feeders and they are directly mixed at the exit of the nozzle. The programmed powder mixture proportion is determined as the feeding ratio between the two powder feeders. In this way, homogeneity problems mentioned in the previous alternatives can be completely avoided.

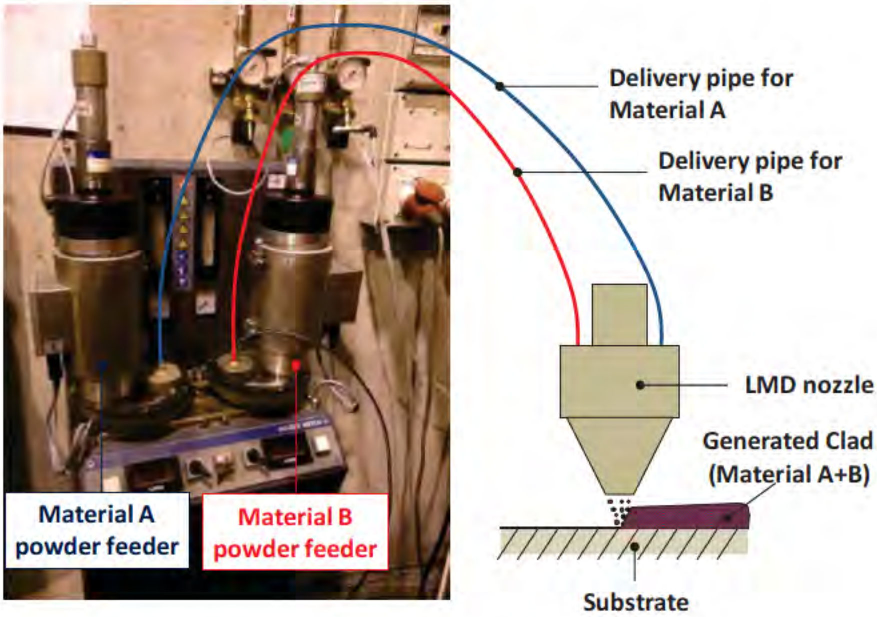
Delivery pipe for Material A
Delivery pipe for Material B
LMD nozzle
Generated Clad (Material A+B)
Material A powder feeder
Material B powder feeder
Substrate

Figure II. 27: Mixture of filler materials directly in the LMD nozzle.

Before choosing the right powder feeding system, the proper powder must be selected. There are basically two critical factors that influence the right feeding of the powders: On the one hand, the size of the particles and, on the other hand, the capacity to flow.

- ✓ If powder particles are too big, the drag gas would not be able to drag them properly, but if the grain size is decreased, the fluidity of the powder particles is also decreased. This is the reason why the size of the powder particles usually ranges between 20 and 200 µm in the LMD process. Other processes, such as the PBF process, use finer powder particles in order to obtain higher quality parts. However, the powder is preplaced in a previous step and not injected directly into the melt pool through a nozzle, so the fluidity of the particles is not a critical factor.

- ✓ If powder particles are not spherical, the drag forces that actuate on them would not be uniform and the particles would not be injected properly. Consequently, the LMD nozzle would not be able to concentrate the powder particles correctly. Similar problems are encountered if the powder particles have a sticky or cohesive behavior, like the copper particles. Same effects could be present if the powder is not preheated and the moisture is not properly eliminated.

  In Figure II. 28 (left) a deficient concentration of the powder at the nozzle exit is shown. In this case, this effect is due to the humidity of the powder particles, that are stuck to the nozzle walls and do not flow properly. In the limit case, the nozzle output can get blocked. In Figure II. 28 (right) the functioning of the same nozzle with the same Inconel 718 powder is shown. In this case, the moisture of the powder is removed by preheating it up to a temperature of 60 °C before starting the process. As it can be observed, the powder flow presents a conical shape and powder concentration is significantly improved.

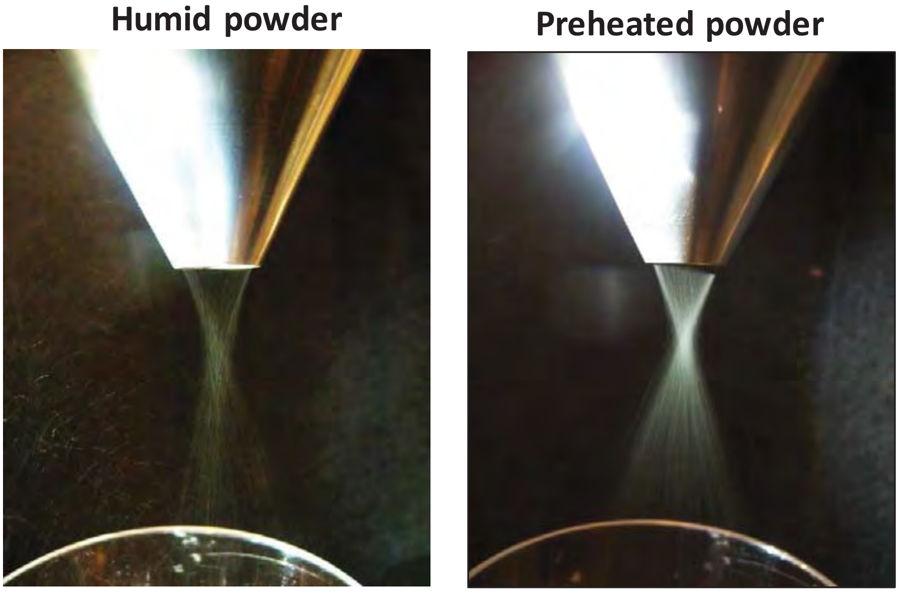

Figure II. 28: Comparison between the nozzle functioning with humid (left) and preheated (right) powder.

II.5.2. Powder feeder types used in Laser Metal Deposition

One of the most important variables in the LMD process is the powder mass flow, which determines the amount of powder per time unit. The powder flow does not only have a direct impact on the height of the generated clad [Ocelík, 2007], but it also affects the stability of the process [Arrizubieta, 2016]. Therefore, the achievement of a constant powder flow is a key factor in the LMD process.

Because of the huge variety of powders used in the LMD process (different size, shape, properties, etc.) it is almost impossible to feed all of them using a unique powder feeder. The selection of a suitable powder feeder is a key element for achieving a stable powder flow. Powder feeders may be categorized based on their operation principle and the following types can be distinguished in industry [Toyserkani, 2005].

1. Gravity-based powder feeders.
2. Mechanical wheel powder feeders.
3. Fluidized-bed powder feeders.
4. Vibratory powder feeders.

1) Gravity based powder feeders

Gravity based powder feeders are probably the most extended powder feeder types thanks to their simplicity and reliability. Different systems can be found in the market, but those with a rotating wheel for metering are normally employed in the LMD application. In Figure II. 29 a scheme of a gravity based powder feeder with a rotating wheel is shown. Due to the gravitational force, powder falls from the hopper into an annular slot manufactured in the metering disk. The hopper may include some stirrers inside in order to prevent the powder from caking and ensure a smooth feeding. Afterwards, the powder is lifted in a suction unit thanks to an overpressure generated inside the powder feeder by the drag gas and it is transported through a pipe to the nozzle.

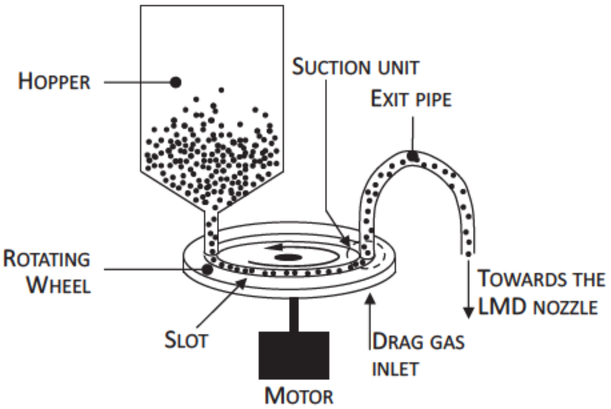

Figure II. 29: Scheme of a gravity based powder feeder with a rotating wheel.

The powder mass flow of the system is controlled by the dimensions of the slot and the rotation speed of the disk. With the aim of adapting to the process requirements and keeping the rotation speed of the disk within the admissible range proposed by the manufacturer, the size of the slot in the rotating wheel may be changed. In Figure II. 30 the relationship between the rotation speed of the powder feeder and the real powder mass flow for different materials is presented.

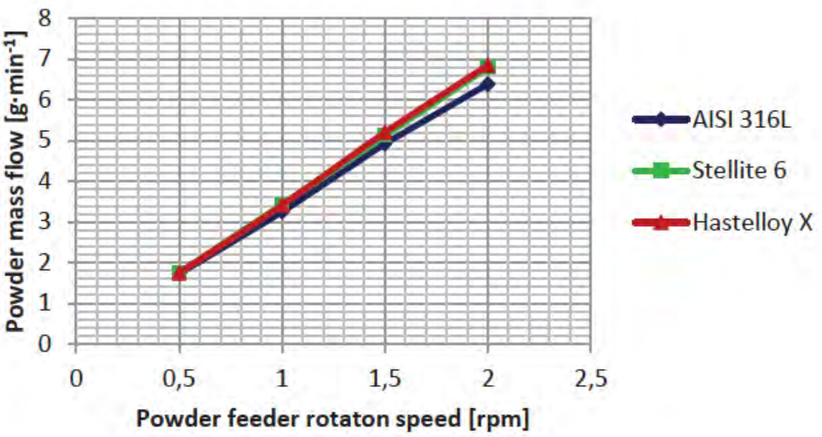

Figure II. 30: Relation between the powder feeder rotation speed and the measured powder mass flow.

2) Mechanical wheel powder feeders

These feeders are based on a rotating screw that pushes the metallic powder from the hopper situated in an upper position. There are different rod configurations that enable to obtain a steady powder flow. However, this kind of system is not very used in LMD applications due to the high friction they present and the wear generated in the screw after long time working periods.

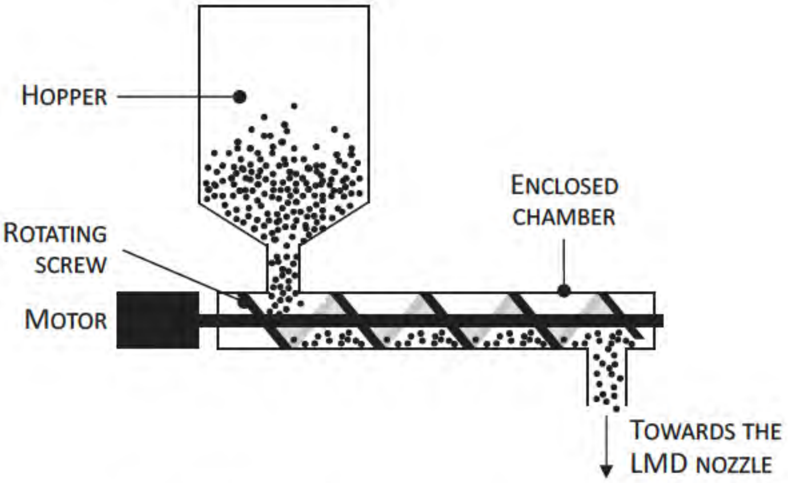

Figure II. 31: Scheme of a mechanical wheel powder feeder.

As it can be seen in Figure II. 31, powder comes from a hopper situated in an upper position and falls into a enclosed chamber. Inside the chamber a rotating screw pushes the powder towards the exits. The feed rate of the system is proportional to its rotation speed, so the mass flow can be controlled by means of the rotation speed of the motor. These systems are able to regulate the rotation speed of the screw within a range of 1-15 rpm and a speed tolerance of the 0.05% with regard to the maximum speed value [Bay, 2017].

3) Fluidized-bed powder feeders

They are based on the principle of fluidizing the powder particles and their subsequent transport using the same gas stream that lifted the powder particles. Fluidized-bed powder feeders offer the advantage of an aerated feeding of the particles, a simple construction and a stable flow rate for small and medium scale operations [Pugsley, 1996].

The feeding system is designed in the following way: a gas flow is delivered to a closed hopper that contains the powder. The gas flow passes through a filter located at the bottom of the unit, becoming diffused and catching the stored powder, which is fluidized. Once the powder is fluidized, the gas flow passes over an obstacle in order to control the amount of powder that goes to the LMD nozzle.

Various configurations have emerged over the last decades. Each design offers a series of advantages and disadvantages and is appropriate for a certain material. Different existing configurations have been collected and summarized by Suri and Horio [Suri, 2009].

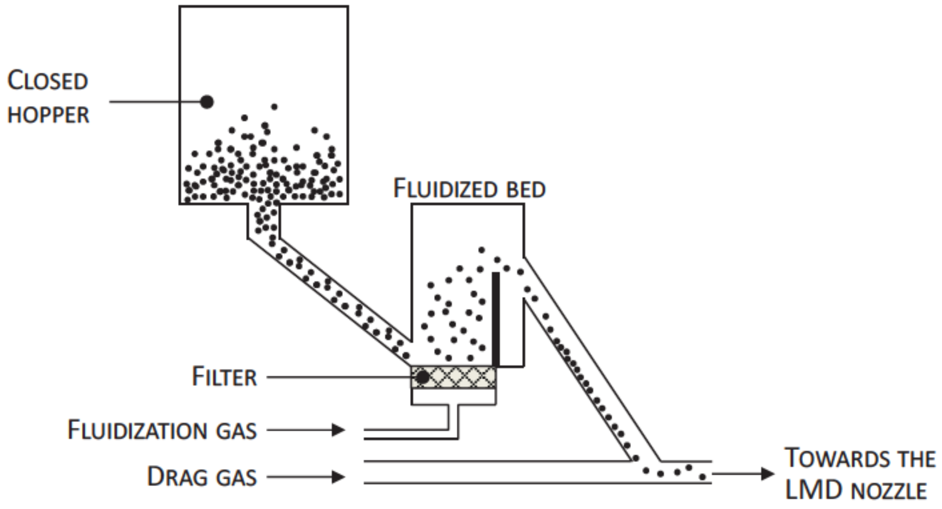

Figure II. 32: Scheme of a fluidized-bed powder feeder.

4) Vibratory powder feeders

Vibratory powder feeders have also a simple design and are based on angled trays that are excited using an external vibratory device. Powder particles that exit the hopper bounce along the tray until they reach the outlet [Tolochko, 2004]. A vibratory based powder feeder can feed materials with mass flow rates between 8 and 2000 g·min^{-1} with a ±1% precision [Toyserkani, 2005]. In the following figure a scheme and a real photo of this type of powder feeder are shown.

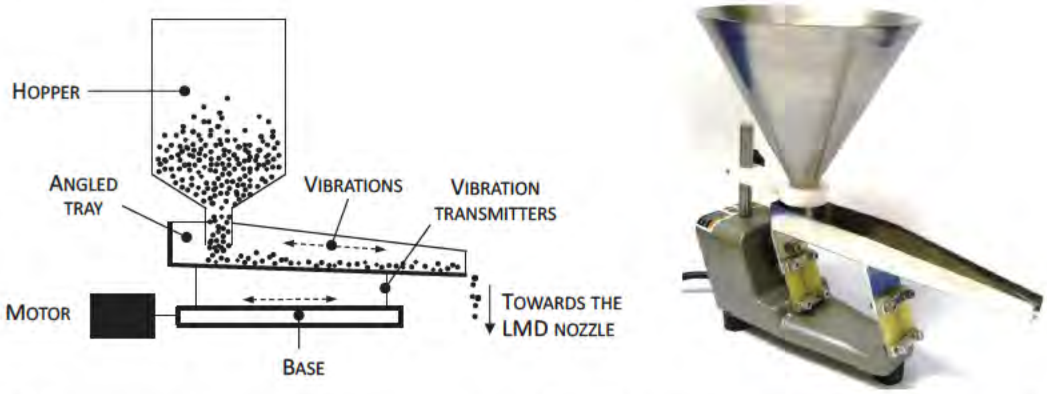

Figure II. 33: Hosokawa Mikro® Vibratory Feeders, Model PF 7.5/1-U. Rates from 20 grams per hour to 5 kg per hour [Hosokawa, 2017]

The Swiss company Medicoat commercializes powder feeders based on an oscillating conveyor that determines the powder mass flow as a function of the amplitude of the oscillations. In Figure II. 34 a scheme of the powder feeder is shown. Moreover, they include a volumetric powder flow control sensor named "Flow Watch" that enables to measure the powder flow permanently [Medicoat, 2017].

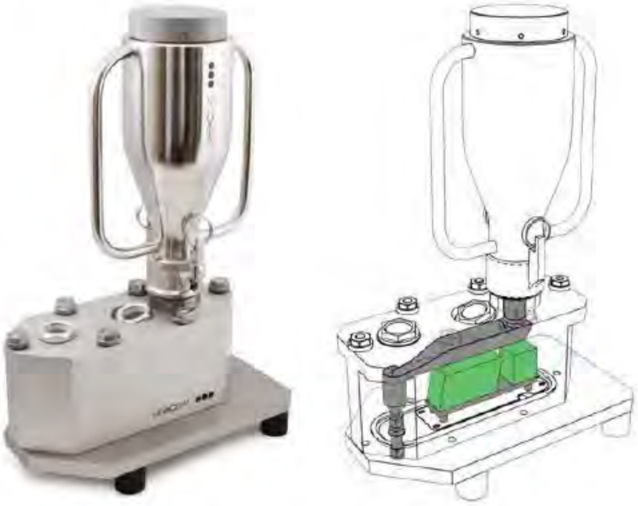

Figure II. 34: Flowmotion powdef feeder from Medicoat [Medicoat, 2017].

On the basis of the idea of vibratory powder feeders, Wang and Li developed a gas-free powder LMD nozzle that delivers the powder using a vibration delivery system. Authors state that a 100% powder efficiency is achieved using this vibration based delivery system [Wang, 2011].

II.5.3. Review of the evolution of designs and patents of industrial LMD nozzles

The state of the art of the design of the LMD nozzles has been also reviewed in order to design a completely new nozzle. With this aim, the present section describes the latest patents and developments related with the design of the powder LMD nozzles.

Lamikiz et al. carried out a study of the more relevant patents published until the year 2011 [Lamikiz, 2011]. In Table II. 5 an overview of the patents studied in that work is shown.

Table II. 5 Main patents focused on LMD nozzles until 2011.

Patent	Authors	Company	Country	Year	Characteristics
US4724299	Hammeke, A. W., Pennsauken, N. J.	QUANTUM LASER Corp.	USA	1988	Two cooling stages
WO93013871	Freneaux, O., Poulet, J. B., Lepre, O., Montavon, G.	ELECRICITE DE STRASBOURG (S.A.)	France	1993	Coaxial and tangential powder inlets
QO9300171	Krause, A., Uelze, A., Becker, R.	SULZER AG	Germany	1993	Optimized nozzle for inclined substrates
US5477026	Buongiorno, A.	CHROMALLOY GAS TURBINE Corp.	USA	1995	Modular design
WO9721515	Lewis, G., Less, R.	UNIV. OF CALIFORNIA	USA	1997	Discrete nozzle with three protective windows.
WO03066272	Baker, M., Winchester, G., Renteria, F., Papotto, V.	HONEYWELL INTERNATIONAL Inc.	USA	2003	Manual discrete nozzle
WO2005028151	Hu, Y.	HONEYWELL INTERNATIONAL Inc.	USA	2005	Optimized protective gas distributor
US7259353	Guo, W.	HONEYWELL INTERNATIONAL Inc.	USA	2007	Optimized Powder distributor
US7626136	Sato, A. Yoshinori, I. Steffen, N., Siegfried, S.	TOYOTA HIDOSHA KABUSHIKI KAIESHA	Japan	2009	Optimized Powder distributor
WO2009077870	Whitfield, R.P.	Whithfield, R.P.	USA	2009	Vacuum channel to optimize powder flow

Therefore, taking this study as the starting point, the most important patents and developments related with the design of the nozzles from that year onwards are studied.

Table II. 6 Main patents focused on LMD nozzles from 2011 until the date.

Patent	Reference	Authors	Company	Country	Year	Characteristics
US0089151 A1	[Miyagi, 2011]	Miyagi, M., Tsukamoto, T., Kawanaka, H.	HITACHI, Ltd.	Japan	2011	Laser processing head and laser cladding method
US8129657 B2	[Nowotny, 2012]	Nowotny, S., Schmidt, A., Scharek, S., Naumann ,T., Kempe, F.	FRAUNHOFER-GESELLSCHAFT ZUR FOERDERUNG DER ANGEWANDTEN FORSCHUNG E. V.	Germany	2012	Machining head with integrated powder supply for deposition welding using laser radiation.
EP3012060A1	[Iwatani, 2014]	Iwatani, S., Sato, A., Ishikawa, Y.	TOYOTA JIDOSHA KABUSHIKI KAISHA	Japan	2014	The present application claims priority from Japanese patent application JP 2014-207490 filed on October 8, 2014
US8901453B2	[Miyagi, 2014]	Miyagi, M., Tsukamoto, T., Kawanaka, H.	HITACHI, Ltd	Japan	2014	Laser processing system and overlay welding method
US0021379A1	[Albrecht, 2015]	Bruce Patrick Albrecht, B.P., Hsu, C.	ILLINOIS TOOL WORKS INC.	USA	2015	Additive manufacturing system for joining and surface overlay.
US9352420B2	[Whitfield, 2016]	Whitfield, R.P., Hageniers, O.L.	Whithfield, R.P.	USA	2016	Laser cladding device with an improved nozzle.

Miyagi et al. [Miyagi, 2011] developed a laser processing head that enables to change the width of the cladding track during the process without stopping it. They proposed two embodiments, one for a coaxial continuous nozzle and another for a coaxial discrete one. In both cases the nozzle has two positioning mechanisms, with their corresponding control systems.

On the one hand, the distance between the laser emitting unit and the substrate can be adjusted by means of the positioning mechanism of the nozzle, see Figure II. 35. On the other hand, a powder angle adjustment unit is included, what allows to vary the angle of the powder stream at the nozzle outlet and focus correctly on the workpiece. Therefore, combining both positioning mechanisms, the developed laser processing head enables to change the width of the deposited track without interrupting the process.

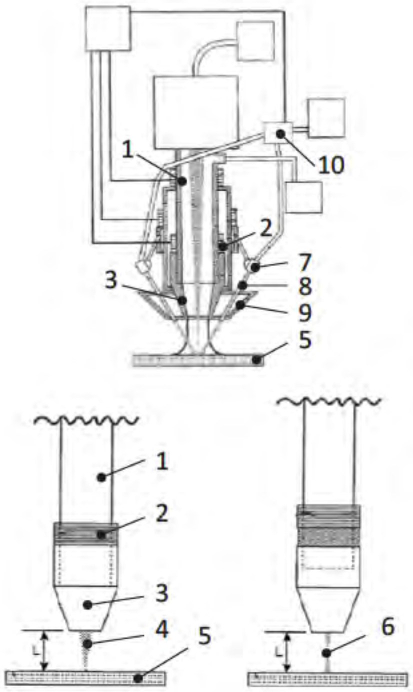

1) Laser emitting unit
2) Nozzle positioning mechanism
3) Shield gas nozzle
4) Powder stream
5) Workpiece
6) Focal position
7) Angle adjustment unit
8) Powder feeder
9) Holder
10) Powder switch adjustment mechanism

Figure II. 35: Design of the nozzle patented by Miyagi et al. [Miyagi, 2011].

Nowotny et al. developed a nozzle that enables to achieve a high deposition rate in the LMD process with an improved homogeneity of the powder flow at the exit of the nozzle and, therefore, a higher homogeneity in the deposited material [Nowotny, 2012]. The nozzle is prepared for its application with a square laser beam, typically generated by a high power diode laser. The nozzle enables to achieve widths of the clad over 20 mm, see Figure II. 36. Furthermore, it enables the mixture of different powders inside the nozzle and the achievement of the corresponding alloys. Using this invention, deposition rates over 5 kg per hour can be achieved and functionally graded material (FGM) depositions can be also performed.

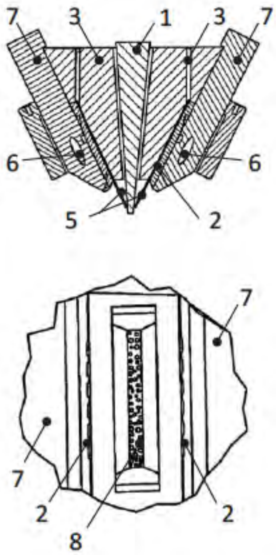

1) Rectangular focal spot
2) Inserts
3) Powder channels
4) Laser radiation
5) Powder
6) Cooling channel
7) Holders
8) Opening

Figure II. 36: Design patented by Nowotny et al. [Nowotny, 2012].

In the same way, Iwatany et al. [Iwatani, 2014] patented a nozzle that enables to maintain the quality of the deposited material even when high areas are to be coated. The patent EP3012060A1 claims priority from a previous Japanese patent application JP207490 filed on the 8th of October 2014 and it is also applied in the US patent US0101484A1 presented in the 2016 and titled "Power cladding nozzle".

Authors claim that the nozzle has a powder passage (4) between the outer (3) and inner (1) cones that increases its width (named as "X" in Figure II. 37) towards the nozzle tip. Thanks to this widening passage, powder is dispersed at the nozzle exit and distributes in a homogeneous way in a wider area to be machined. As authors highlighted, this fact increases the productivity of the nozzle.

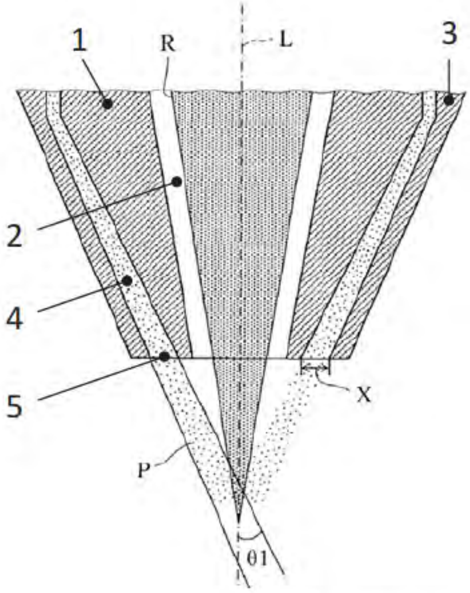

1) Inner nozzle member
2) Laser passage
3) Outer nozzle member
4) Discharge passage
5) Discharge outlet
θ1) Tilt angle of the outer circumferential plane
R) Laser beam
L) Center axis
P) Metallic powder
X) Passage width

Figure II. 37: Design patented by Iwatany et al. [Iwatani, 2014].

In addition, patents related to the powder regulation have been found. Miyagi et al. [Miyagi, 2014] developed a LMD head that includes a system that controls the powder mass flow supplied to the LMD nozzle, see Figure II. 38. The powder supply mechanism controls the amount of powder that is directed towards the nozzle by distributing the powder mass flow at the main branch valve (1). A percentage of the powder mass flow is directed to the nozzle through the pipe (7) and the rest of the powder goes to a recycling container through the return pipe (8).

Each pipe, (7) and (8), includes an additional gas supply mechanism controlled by the supplementary branch valve (2), which introduces a gas stream and maintains the gas flow constant for every working position of the main branch valve (1).

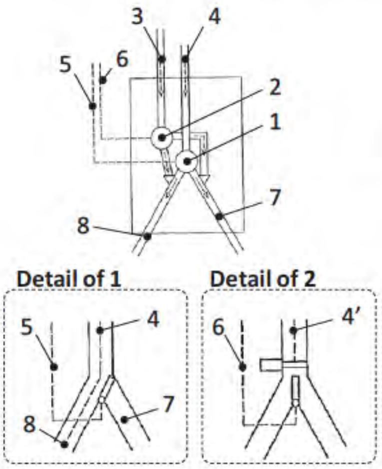

1) Main branch valve
2) Supplementary branch valve
3) Supplementary gas flow
4) Drag gas and powder inlet
5) Signal line
6) Supplementary signal line
7) Pipe toward the nozzle
8) Return pipe

Figure II. 38: Powder flux control system patented by Miyagi et al. [Miyagi, 2014].

Whitfield et al. patented a laser cladding device with an improved nozzle [Whitfield, 2016]. The aim of the nozzle is to increase the mass efficiency by increasing the amount of powder particles trapped into the melt pool. The developed nozzle comprises three different gas circuits (see Figure II. 39): a central flow for the protective gas (6), a circuit for the drag gas (4) and a last circuit for the shaping gas (3). With the aim of increasing the efficiency of the nozzle and optimizing the focalization of the filler material into the deposition zone, the nozzle has a vacuum mechanism (2). Additionally, the vacuum mechanism enables to adjust the direction of the coating flow (7).

Furthermore, Whitfield et al. claim that the developed nozzle allows varying the size of the laser spot and the laser focusing distance. This is achieved by means of a gear system situated above the LMD nozzle (12), similar to that used in zoom lenses for laser welding processes.

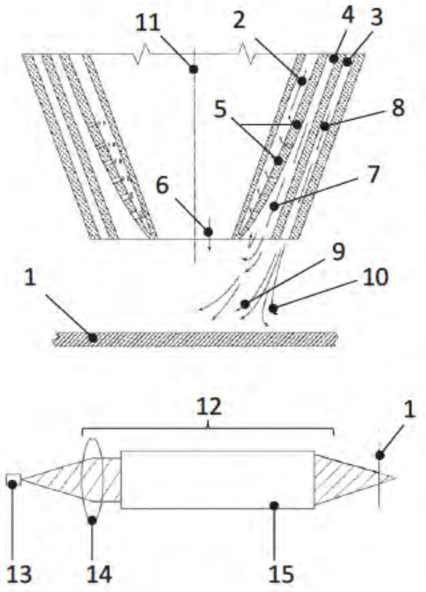

1) Surface of the part being clad
2) Flow induced by the vacuum
3) Shaping gas port
4) Powder and drag gas port
5) Side holes through the outer wall
6) Inert gas flow
7) Powder flow
8) Shaping gas flow
9) Shaping gas that provides additional pressure
10) Shaping gas that goes away
11) Nozzle centerline
12) Zoom lens assembly
13) Light source
14) Collimating lens
15) Zoom mechanism (that alters the laser light focus)

Figure II. 39: LMD nozzle and laser focusing variation system patented by Whitfield et al. [Whitfield, 2016].

Besides the patents described above, many companies have gone one step beyond and they manufacture and commercialize LMD nozzles. In the following paragraphs, some of the most important LMD nozzle manufacturers and their products are described.

The Fraunhofer Institute for Laser Technology (ILT) together with the Reis Lasertec GmbH has developed the LMD processing head VarioClad. For this purpose, both companies have joined forces and have taken advantage of the ILT knowledge on LMD nozzle design [ILT, 2017] and the Reis Lasertec expertise on beam guiding and monitoring systems [Reis, 2017]. The VarioClad has a compact design and includes a motorized optic that permits to vary the diameter of the laser beam during the process. The diameter of the laser spot can vary from 0.7 mm to 4 mm. As it can be seen in Figure II. 40 (right), the VarioClad includes its own control system that eases the usage.

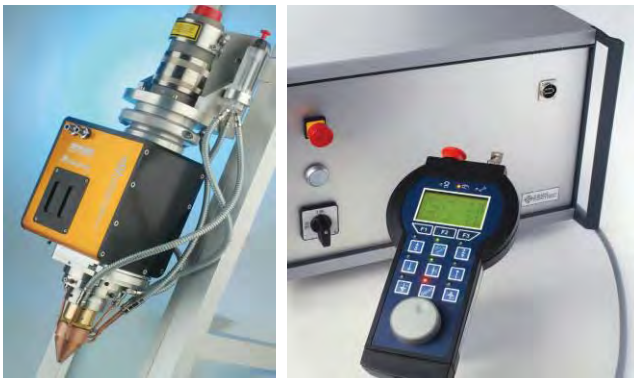

Figure II. 40: LMD processing head VarioClad (left) and the control unit (right) [Reis, 2017].

The German company Precitec has a big expertise in the design and manufacture of all type of welding and cutting heads and they have also entered into the LMD field [Precitec, 2017]. They offer two cladding heads, the discrete nozzle YC30, with a 2 mm minimum powder focus diameter, and the continuous coaxial nozzle YC52, with a 0.7 mm minimum powder focus diameter. The main reason for choosing one or other cladding head is usually the kinematic of the machine. If the LMD head has tilting movements, the discrete nozzle is required in order to ensure the correct feeding of the powder. On the contrary, if the LMD head has no tilting movements, both nozzles would work properly and the decision would be based on economic or process efficiency reasons.

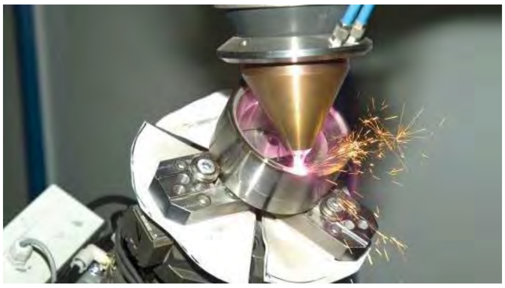

Figure II. 41: The continuous coaxial nozzle YC52 from Precitec [Precitec, 2017].

The company Hybrid Manufacturing Technologies developed the LMD head Ambit^{TM} [Ambit, 2017]. The main advantage of this LMD nozzle is that it uses a traditional clamping system based on ISO or HSK tooling. This system enables the automatic change of the nozzle and its use in any CNC machine for hybrid manufacturing operations. This nozzle was launched to the market in the 2014 and since then it has received many international awards [Hybrid, 2017]. Moreover, the company Hybrid Manufacturing Technologies is working closely with companies like Mazak and ELB in the development of hybrid machines that incorporate the Ambit^{TM} LMD head. In section "*II.3. Latest machines for the LMD and hybrid processes*" further details about these hybrid machines are explained.

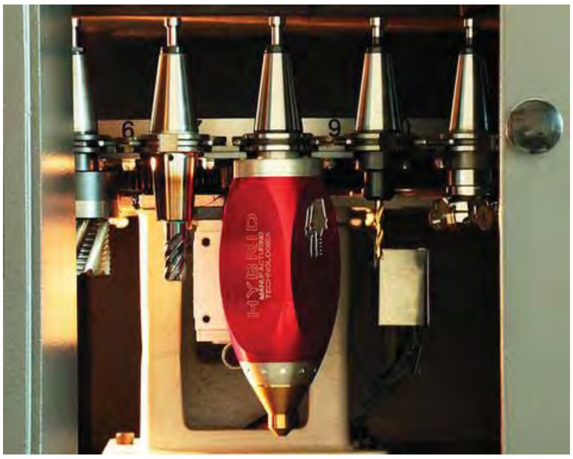

Figure II. 42: The LMD nozzle Ambit^{TM} from Hybrid Manufacturing Technologies [Ambit, 2017].

Another relevant reference regarding the LMD nozzles is the Fraunhofer IWS (*Fraunhofer-Institut für Werkstoff-und Strahltechnik*), located in Dresden, Germany [IWS, 2017]. They have developed a whole line of coaxial nozzles, offering a suitable solution for each application. Examples of the different nozzles are the COAX8, which has a round powder spot, and the COAX12, which has a square powder spot.

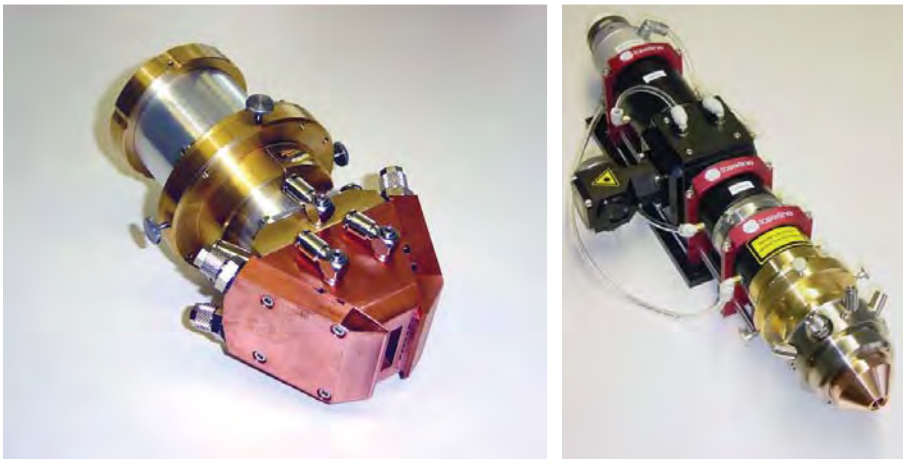

Figure II. 43: LMD nozzles COAX12 (left) and COAX8 (right) developed by the IWS [IWS, 2017].

II.6. Latest developments for predicting the geometry of the deposited material and process monitoring

The LMD process is based on overlapping material layers for achieving the desired geometry. Therefore, the process stability is of great relevance when obtaining a constant height and, thus, the desired final geometry. However, multiple parameters are involved in the LMD process, in which several physical phenomena are interrelated and they have a direct influence on the resulting geometry of the deposited material.

With the aim of controlling the process and obtaining a stable growth, the first objective when depositing material is the determination of the relation between the process input parameters (laser power, feed rate, powder flow rate, gas flows, etc.) and the output parameters (geometry of the clad, mechanical properties and the generated microstructure) [Peng, 2007; Tan, 2010]. In Table II. 7 the main LMD parameters are detailed, where those input parameters that can be controlled during the process are underlined and highlighted in bold.

Table II. 7: Main input and output LMD parameters

LMD parameters		
INPUT		**OUTPUT**
✓ **Laser power** ✓ **Machine feed rate** ✓ **Powder flow rate** ✓ **Preheating temperature** ✓ **DC of the laser** ✓ Deposition strategy ✓ Gas flows	✓ Geometry of the substrate ✓ Absorptivity of the substrate ✓ Laser beam radius ✓ LMD head position ✓ Powder size	✓ Clad geometry ✓ Mechanical properties ✓ Microstructure ✓ Process efficiency

Several authors have worked on the experimental determination of the optimal process parameters for different materials, such as tool steels [Navas, 2005], stainless steels [Pinkerton, 2004], nickel alloys [Richter, 2004] and titanium alloys [Kong, 2010]. Therefore, it could be concluded that for easy geometries and 3-axis material deposition, the LMD process is almost solved. Nevertheless, in 5-axis deposition and complex geometries generation, new variables, such as the kinematic of the machine and non-uniform feed rates, are introduced into the deposition process and the problem is not solved yet.

A typical problem in LMD manufactured parts is the generation of porosity. Pores are generated because gas is trapped inside the deposited material during the LMD process and molten material solidifies before the trapped gas can exit. Their existence reduces the mechanical properties of the generated part and contributes to the generation of future cracks during the usage of the part.

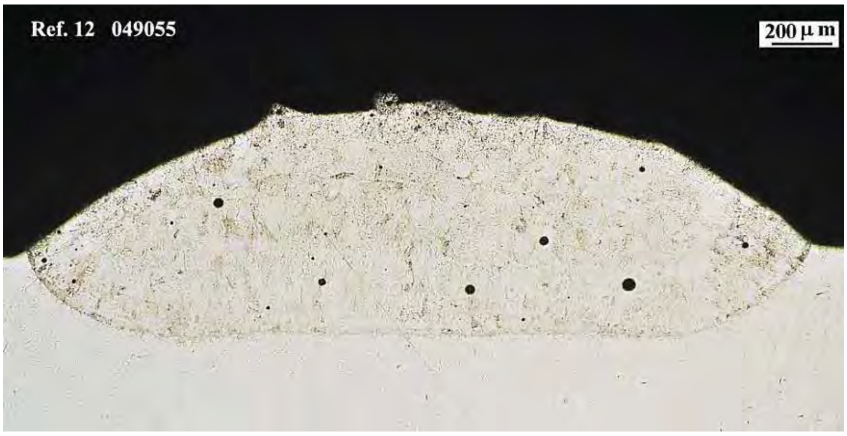

Figure II. 44: Appearance of pores in an AISI 316L clad.

The generation of pores in the LMD process is related with the moisture of the powder, used laser power, size and shape of the particles and the gas flows (both protective and drag). Zhong et al. analyzed the generated porosity in single tracks deposited by high deposition rate LMD and they concluded that the porosity can be reduced by applying the following actions [Zhong, 2015]:

- ✓ Drying the powder by preheating it before using.
- ✓ Using a finer powder to reduce the amount of gas that is introduced inside the melt pool.
- ✓ Using a more homogeneous powder particle size.
- ✓ Increasing the laser power. If the laser power is increased, the energy introduced in the part is higher and the solidification process is slower. Therefore, the gas trapped inside the deposited material has more time to escape.

II.6.1. Latest CAM developments

The LMD process is focused on the generation of coatings and the repair of high added value components. However, these parts may have complex geometries and the LMD process optimum orientation is normal to substrate, what obliges to interpolate the five axes of the LMD machine simultaneously in order to obtain the desired part. As it is previously mentioned, the 3-axis LMD is almost solved and usually presents no difficulties. However, this knowledge cannot be transferred directly to 5-axis manufacturing and many research projects orientate their resources towards this objective.

With the aim of obtaining a methodology for studying the optimal parameters for the continuous 5-axis LMD process, Calleja et al. considered the process optimization using a weighted function that includes the different process parameters [Calleja, 2014]. In that work, an empirical formula that determines how optimum the process is was stated. The formula was defined as a function of different process variables, (Eq. II. 3). Where "DR" represents the deposition rate, "θ" is the wetting angle and "h" and "w" are the height and width of the clad, respectively.

$$WV = 0.7 \cdot \overline{DR} + 0.3 \cdot \bar{\theta} - 0.2 \cdot \overline{\Delta h} - 0.1 \cdot \overline{\Delta w} \qquad \textbf{(Eq. II. 3)}$$

In 5-axis LMD, besides determining the process parameters, the optimal deposition strategy must be defined in order to obtain high quality parts. The Fraunhofer Institute for Laser Technology (ILT) has developed a tool called LaCam3D that enables both programmers and end-users to generate tool paths and translate them into the machine code. Furthermore, it allows to simulate the process and look for possible collisions [ILT, 2013].

Siemens NX is working together with DMG Mori [DMG Mori, 2017] in the development of the PLM software "*NX Hybrid Additive Manufacturing*". Despite this software is not commercially available yet, further details can be found in their webpage [Siemens, 2017]. This is the first commercial solution that allows CAD/CAM additive operations and was presented in Milan at the Machine Tool World Exposition (EMO) in the 2015. NX Hybrid Additive Manufacturing is currently specifically configured for the Lasertec 65 3D from DMG Mori and the Siemens Sinumerik 840D CNC control system. As it can be seen in Figure II. 45, the in-process workpiece designed in the NX CAD module can undergo both additive and subtractive operation in any order.

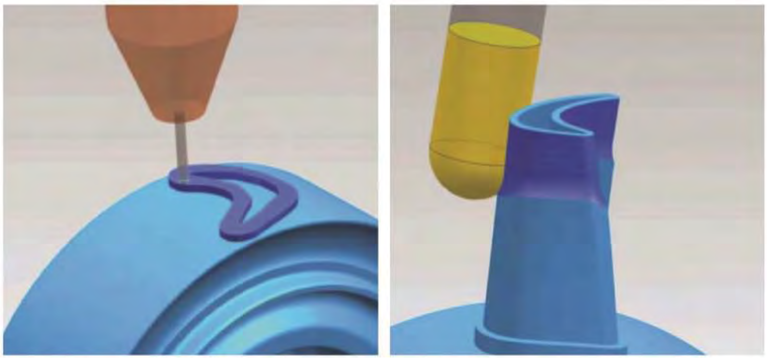

Figure II. 45: In-process workpiece and verification works for both additive and subtractive modes [Siemens, 2017].

However, before determining the LMD strategies for the additive process, the geometry of the substrate must be accurately defined. For this purpose, a 3D laser scanning process is used by some authors, because it allows digitalizing the surface of the substrate without contact

[Liu, 2015]. Liu et al. developed a set of algorithms and numerical methods to generate the most suitable tool paths and enable the LMD process automation.

II.6.2. Process monitoring

The LMD parameters can be optimized for a determined working situation. Nevertheless, as a consequence of the LMD conditions variability, the process parameters need to be re-adapted according to their instantaneous values. Therefore, process parameters need to be controlled instantaneously depending on external variables. Many authors have focused their efforts on monitoring the process during the last decade and the most relevant works are collected by Purtonen et al. [Purtonen, 2014].

The main objective of monitoring the LMD process is the enhancement of the reliability and reproducibility of the process and the improvement of the quality of the deposited material. All this can be directly translated into economic savings and an increase of the competitiveness of the process [Pavlov, 2010]. The LMD process can be monitored focusing on different variables. Up to now, the most promising methods are those based on measuring the size or the maximum temperature of the melt pool and acting instantaneously on the laser power in order to keep the measured signals within a desired range. The control is based on a conventional PID algorithm that adapts the laser power to the new conditions of the process.

Hofman et al. presented a feedback controller system for the LMD process that measures the width of the melt pool in real time and adjusts the laser power in order to keep the measured width at a nominal value [Hofman, 2012]. The melt pool length results a more sensitive variable on the processing parameters than the melt pool width and consequently, when monitoring the melt pool geometry most authors measure the width value [Liu, 2014]. Furthermore, due to the directionality of the process, the plasma that may be generated could interfere to a larger extent in the measurement of the melt pool length than in the width.

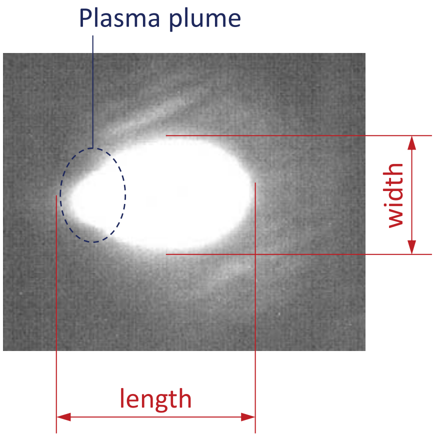

Figure II. 46: Coaxial photo of the melt pool.

Ocylok et al. recorded the length and width of the melt pool during the deposition of straight single lines. As it can be seen in Figure II. 47, the length is a more unstable dimension due to the feed motion. They concluded that the total area of the melt pool is less affected by the disturbances generated during the process than the single values of the length and width of the melt pool. Moreover, Ocylok et al. determined the relation between the laser power and the melt pool size [Ocylok, 2014].

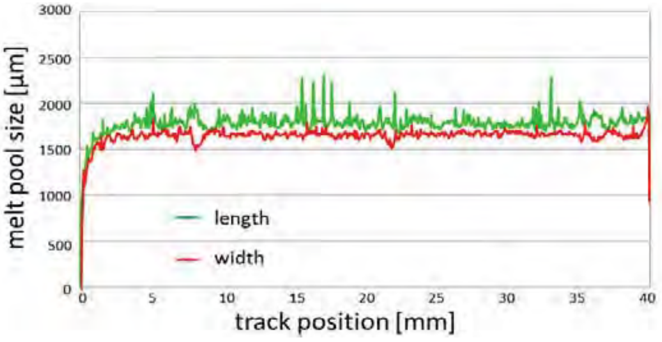

Figure II. 47: Melt pool length and width size measurement during straight line deposition [Ocylok, 2014].

An instantaneous image of the melt pool can be obtained using a CCD coaxial camera. However, in order to measure the geometry of the melt pool, the obtained image needs to be treated and binarized based on a threshold value defined experimentally. The threshold value is the brightness value for which a determined point is considered part of the melt pool or not. In Figure II. 48 the importance of the melt pool size measuring method is shown and the differences between the measured size of a melt pool with a high threshold value in “b” and a low threshold value in “d” are shown.

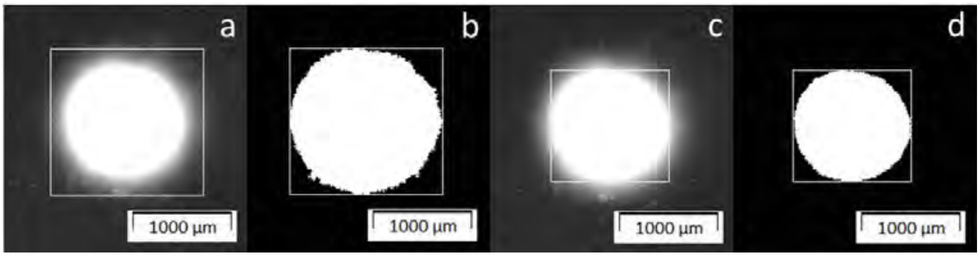

Figure II. 48: Variations of the measured melt pool size due to the differences in the fixed threshold value [Ocylok, 2014].

The measurement of the maximum temperature of the melt pool is a direct and easy method for controlling the stability of the LMD process. In this direction, Bi et al. developed a monitoring system based on the infrared temperature signal of the melt pool. Thanks to this close loop control, instability problems found in building thin walls were overcome [Bi, 2006_1]. Additionally, other authors have carried out similar works in order to analyze the relationship between the quality of the deposited material and the measured infrared (IR) signal [Bi, 2007], [Peng, 2007].

In Figure II. 49 the close-loop control system developed by Bi et al. is shown [Bi, 2006_1]. A Ge-photodiode receives the IR-temperature radiant signal from the melt pool and generates a current value that is compared with a set-value. Afterwards, based on the result of that comparison, the PID-controller actuates on the laser power in order to maintain the temperature of the melt pool within a desired range.

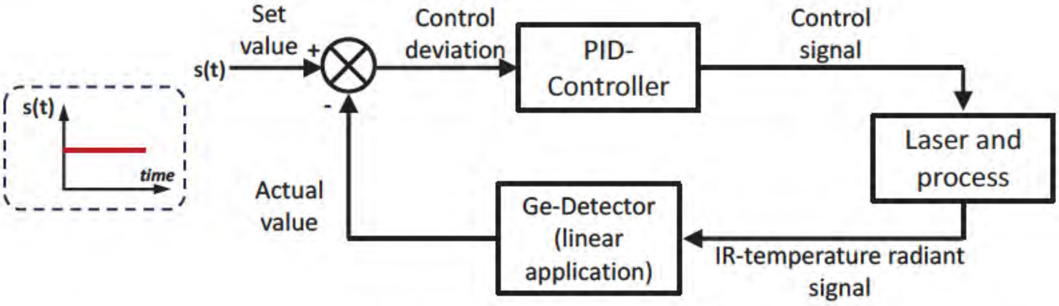

Figure II. 49: Schema of the closed-loop process control based on the IR signal measurement [Bi, 2006_1].

During the stay in the Frauhofer IPT, the thermal stability of the LMD process when depositing thin walls was analyzed, see Figure II. 50. A zig-zag strategy was used and the maximum temperature reached during the deposition process was measured using a coaxial two-color pyrometer. As it can be appreciated, at the edges where the deposition direction is changed, a higher temperature is reached and more material is deposited. Consequently, the height of the part differs from the expected one and the process is out of focus in those regions.

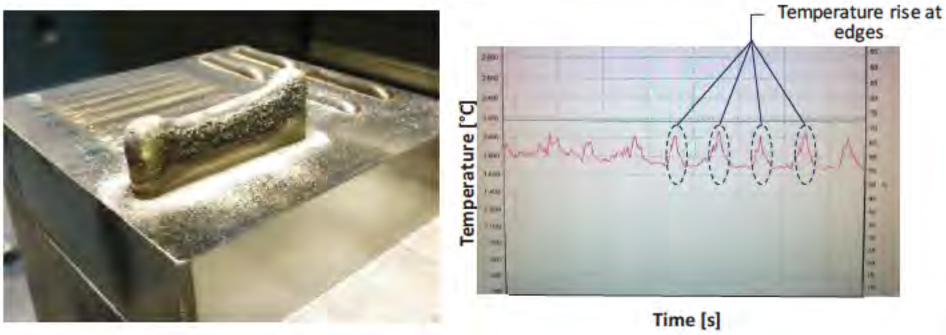

Figure II. 50: Process destabilization when building thin walls using LMD. Both base material and filler material are Inconel 718.

Apart from obtaining an instantaneous control of the process, the monitoring is important for the improvement of the understanding and the analysis of the different interrelated phenomena that take place during the LMD. Smurov et al. presented a study based on monitoring the LMD process using a pyrometer and an infrared camera in order to control the temperature and size of the melt pool [Smurov, 2013]. A CCD camera was employed for measuring the real in-flight velocity of the particles. Because of the image acquisition time, powder particles are seen as straight lines, see Figure II. 51. They calculate the velocity of the particles based on the initial and final points of the detected particle tracks. However, the main drawback of this method is that the measured velocity is not the real one but a projection of it and, consequently, this method is not valid for obtaining the real velocity of the particles.

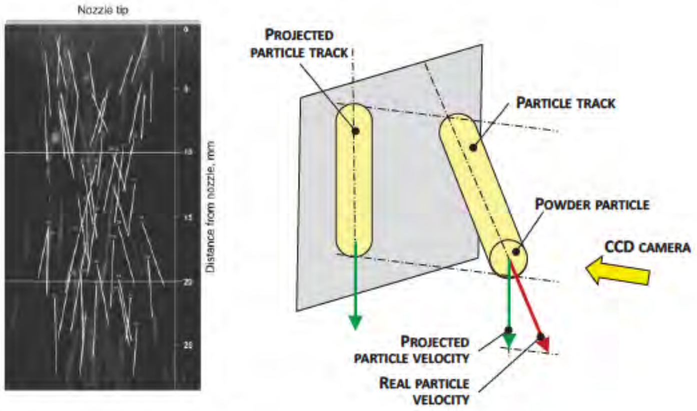

Figure II. 51: Retained particles for velocity calculation, source [Smurov, 2013] (left) and projected velocity due to viewing the particles in 2D (right).

An important parameter in the LMD process is the determination of the Z reference value before depositing the new layer (supposing that the nozzle rotation axis matches the Z axis, which is defined as perpendicular to the surface of the substrate). If the programmed Z increment matches the real growth of the deposited layer, the powder focus would be located exactly in the melt pool generated by the laser beam. However, if this value is not determined correctly, both the laser and the powder stream would be out of focus and the geometry of the deposited material would differ from the expected one. Consequently, the process would destabilize [Bi, 2006_2]. In conclusion, all authors agree in the fact that a constant layer height must be achieved for guaranteeing the stability of the process and enabling its automation.

Depending on the final shape of the desired geometry, the CNC machine or robotic arm that controls the position of the LMD nozzle may need to follow complex trajectories. Therefore, the machine needs to accelerate and decelerate where changes of direction are required or sharp edges are to be manufactured. As a consequence of these variations in the feed rate of the machine, clad height variations may appear in the process.

In conventional manufacturing processes, like milling or turning, when the feed rate in a determined point of the trajectory of the cutting tool is lowered, the material removal rate is also decreased. In the worst case, a higher roughness would be generated in that zone because of the change in the cutting conditions. However, in the LMD process, if the relative velocity between the nozzle and the workpiece is reduced, the amount of deposited material is increased and an over-deposition of material is generated, resulting in an unstable process. Therefore, the LMD process requires constant operating conditions and the deposition rate needs to be kept as constant as possible for guaranteeing the quality of the deposited material. With this objective, Boisselier et al. developed an algorithm that ensures smooth trajectories with stable processing conditions [Boisselier, 2014].

Nenadl et al. studied the geometry of the generated clads depending on the LMD process parameters. They developed a recursive model employing the following input parameters: the material feed rate, scanning speed and the overlap ratio between two adjacent lines [Nenadl, 2014]. The amount of powder and the total heat input per unit length of the laser track are concluded to be the key factors regarding the geometry of the deposited clad. The article states that the amount of powder provided per unit length of the laser track is directly related with the clad height. Therefore, when the machine feed rate is slowed down, the height of the clad is increased.

In the following figure the empirical dependency between the size of the clad and the process parameters for Ni and Co based filler materials on Fe based substrates is shown. “F/S” is the amount of powder provided per unit length of the laser track and “P/S” is the total heat input per unit length of the laser track.

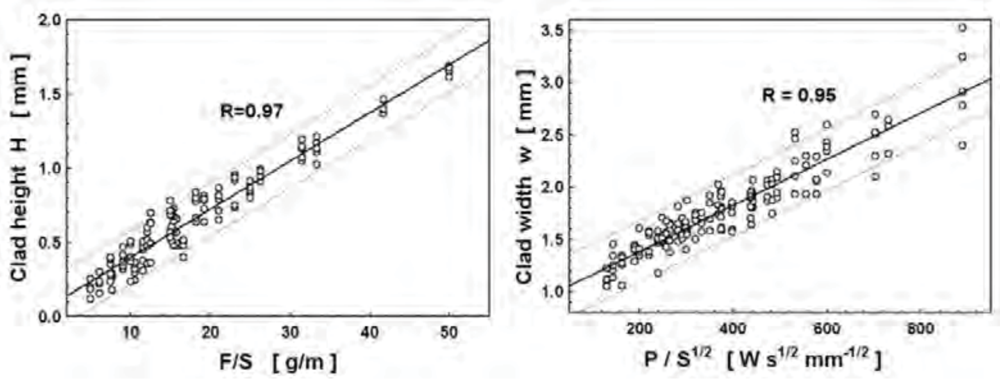

Figure II. 52: Empirical dependence of the laser track height “H” and width “w” on combined processing parameters observed for coaxial and lateral cladding setups for Ni and Co based alloy cladding; from [Ocelík, 2007] (left) and from [de Oliveira, 2005] (right).

More authors have focused their efforts on the powder flow rate in order to obtain a stable LMD process; Ding et al. concluded that measuring the powder flow rate in real time is the key element for achieving an effective control of the powder flux [Ding, 2016]. They developed an optoelectronic sensor that detects the powder flow rate at the outlet of the powder feeder. However, this control of the powder flow is too slow and is useful only for maintaining the powder flow in a constant value (preset value) and not for instantaneous variations.

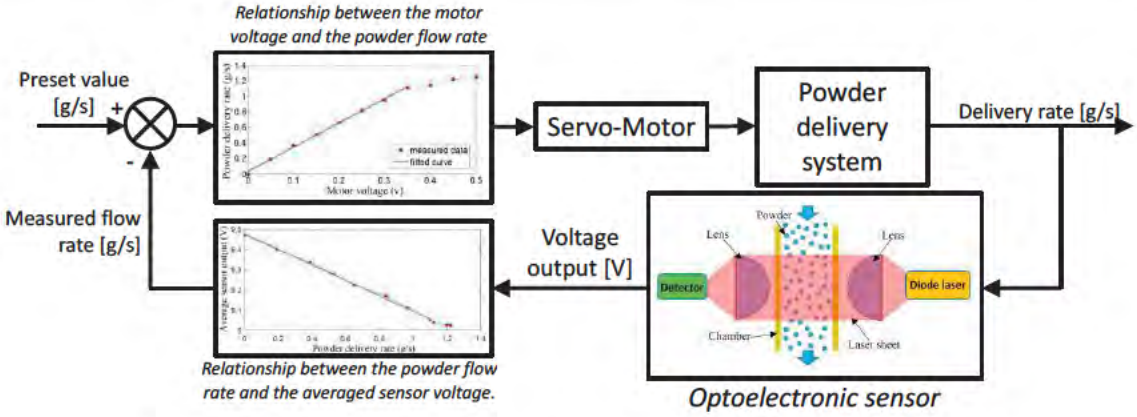
Relationship between the motor voltage and the powder flow rate
Preset value [g/s]
+
-
Measured flow rate [g/s]
Servo-Motor
Powder delivery system
Delivery rate [g/s]
Voltage output [V]
Powder
Lens
Lens
Detector
Diode laser
Chamber
Laser sheet
Optoelectronic sensor
Motor voltage (v)
Powder delivery rate (g/s)
measured data
fitted curve
Average sensor output (V)
Relationship between the powder flow rate and the averaged sensor voltage.

Figure II. 53: Flow chart of the sensing and control of the powder flow rate [Ding, 2016].

With regard to the LMD process, rotatory powder feeders are usually used with the aim of achieving a steady powder flux. They consist of one or two rotating disks and by varying their rotation speed, the mass flow of the powder particles is regulated. All the authors mentioned remark the importance of controlling the powder flow rate, but no references or research regarding this kind of control have been published.

The only powder feeder manufacturer that copes with this problem is Medicoat. As it has been highlighted previously, they offer a flow watch that measures the volumetric flow of the powder particles. Moreover, they have also developed a powder switch, which is able to divert the powder flow to the nozzle or an additional container [Medicoat, 2017]. Therefore, it is able to stop the powder flow when the process requires, but without stopping the powder feeder.

II.6.3. Control systems of the powder feeders

A powder feeder must provide a continuous and uniform powder stream. This fact is evaluated by means of the powder mass flow accuracy (Acc) and the time constant for varying the powder flow (K_T). From the point of view of the control, the delay in the motor control leads to instabilities in the mass flow rate. Furthermore, if powder is introduced inside the motor, this may lead to perturbations and a deficient working of the feeding system [Bitragunta, 2015].

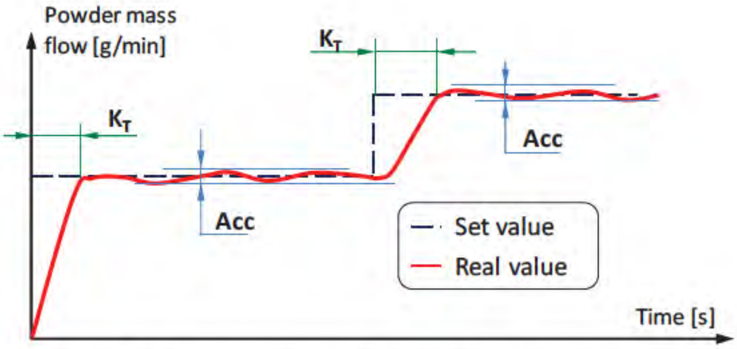

Figure II. 54: Response of a powder feeder for a determined set value.

Once the powder flow exits the powder feeder, it needs to be transported to the processing area. This is usually done by a drag gas, typically Argon, Nitrogen or Helium. The drag gas, apart from dragging the powder particles, helps to generate a protective atmosphere that avoids the oxidation of the powder particles and the processing area.

With the aim of improving the problems described Figure II. 54 in relation with the time delay of the powder flow system, Thayalan and Landers developed a dynamic model of the gravity based powder feeder. Using this model, they minimized the response time of the powder feeder and optimized the feeding system, resulting in a more constant powder flow rate [Thayalan, 2006].

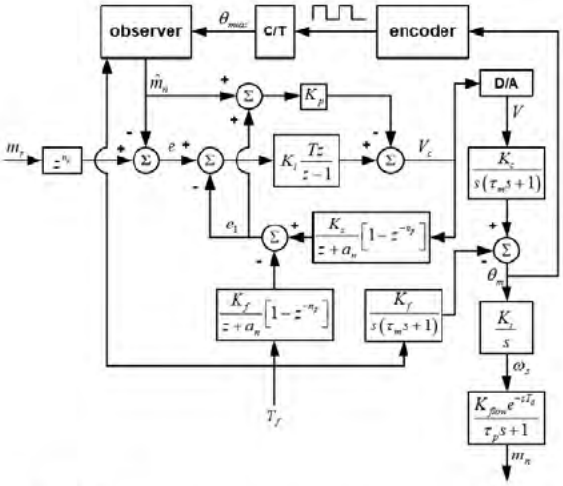
observer
θ_{meas}
C/T
encoder
$\hat{m}_n$
K_p
D/A
V
m_r
z^{-n_p}
e
$K_i \frac{Tz}{z-1}$
V_c
$\frac{K_c}{s(\tau_m s+1)}$
e_1
$\frac{K_c}{z+a_n}[1-z^{-n_p}]$
θ_m
$\frac{K_f}{z+a_n}[1-z^{-n_p}]$
$\frac{K_f}{s(\tau_m s+1)}$
$\frac{K_s}{s}$
ω_s
T_f
$\frac{K_{flow}e^{-sT_d}}{\tau_p s+1}$
m_n

K_f: Screw speed–disturbance torque gain [10 (rad/s)/N·m]
K_C: Screw speed–voltage gain [0.24 (rad/s)/V]
K_P: Controller proportional gain [V/(g/min)]
K_S: Motor internal gear ratio [216.4^{-1}]
K_{flow}: Flow rate–screw velocity gain [15.3 (g/min)/(rad/s)]
m_n: Powder mass flow rate at the nozzle [g/min]
$\hat{m}_n$: Estimated powder mass flow rate at the nozzle [g/min]
m_r: Reference powder mass flow rate at the nozzle [g/min]
n_p: Number of delay samples [171]
s: Laplace variable
T : Sample period [10 ms]
T_d: Powder mass flow rate delay period [1.71 sec]
τ_m: Motor mechanical time constant [0.0092 sec]
θ_m: Motor angular position [rad]
θ_{meas}: Measured motor angular position [rad]
V_c: Control voltage [V]
ω_S: Screw angular speed [rad/s]
z: Discrete time forward shift operator

Figure II. 55: Closed–Loop System Schematic with Modified PI Controller Implemented in a SPCS (Smith Predictor Corrector Structure) [Thayalan, 2006].

In the Figure II. 56 (left) the initial response of the powder feeder when a multiple step reference input voltage is introduced is shown. In Figure II. 56 (right) the response of the system when the developed control is implemented is shown.

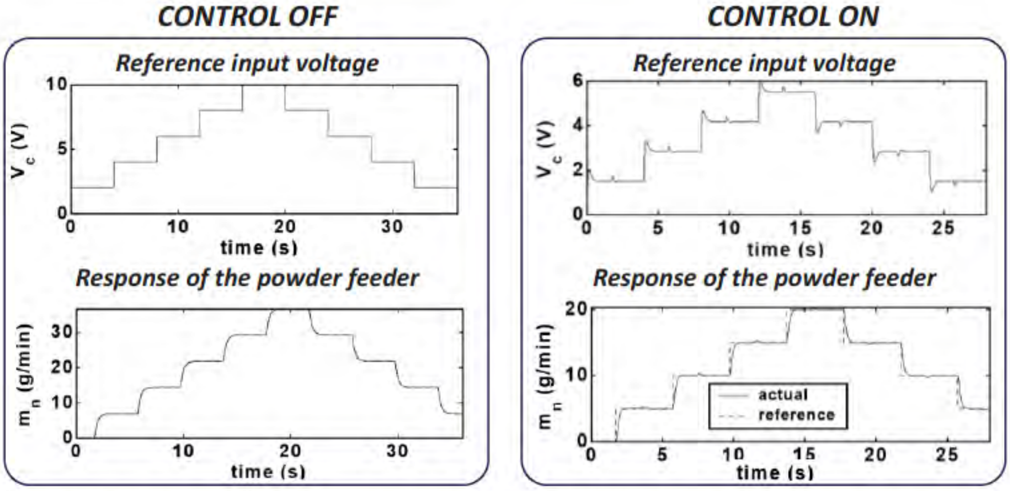

Figure II. 56: Experimental Results for Step Inputs. Experimental Results for Controller Implemented in SPCS (multiple step references) [Thayalan, 2006].

The powder flux variation by means of the powder feeder is too slow for offsetting the machine feed rate variations. Therefore, a fast powder regulation system is required in order to avoid the mentioned powder accumulations.

II.7. Industrial applications

Modern industry is demanding new and sustainable alternatives to reduce production costs. In this direction, the Laser Metal Deposition process has arisen as an alternative to traditional additive processes thanks to the advantages that it provides [Toyserkani, 2005].

One of the LMD industrial applications is the coating of high added value parts. Thus, the LMD process is used for improving the surface properties of existing parts (enhancement of wear, corrosion or heat resistant properties). Other applications are the generation of new parts or the repair of high-value but damaged parts. Therefore, the LMD is mainly employed in those industrial sectors where high added value components are used, such as, the aircraft industry, automotive industry, shipbuilding industry, heavy industry and machine tool industry [IPG, 2017].

In the following sections, some LMD application examples inside the different industrial sectors are detailed. Real applications are explained and special attention is paid to the used materials. In this way, it is important to remark that most of the industrial applications are protected by intellectual property rights (IPR), so it is very difficult to find process parameters or even material specifications used in these cases.

II.7.1. Aeronautical sector

Unlike the traditional manufacturing processes where huge amounts of material are wasted in form of chip, laser based additive processes generate near net shape parts [Urtasun, 2014]. Consequently, the buy-to-flight ratio is considerably reduced. This point is really relevant when expensive material such as nickel based or titanium based alloys are used. Therefore, laser additive processes are becoming more and more relevant in the aeronautical field and they are focused basically in two areas: The manufacture of whole functional parts using the Powder Bed Fusion (PBF) technology and the repair of already existing parts [Sexton, 2002].

PBF processes offer the possibility to develop new designs, with complex geometries and details in inaccessible zones; such as internal cooling channels, which would be impossible to obtain by other manufacturing processes [Richter, 2010]. The first benefit of using the PBF technology is the resulting weight reduction of the final parts, what is crucial in the aeronautical sector.

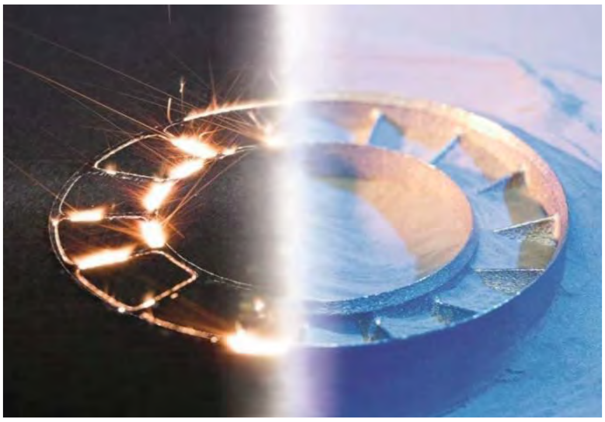

Figure II. 57: Integral NGV manufactured using PBF technology [ILT, 2017].

On the other hand, the LMD process is more focused on the repair of damaged aero engine components and the enhancement of surface properties. For example, it offers the possibility to repair the tips of worn turbine blades [Balazic, 2010]. It can be also used for the additive manufacturing of complex structures onto casted or forged substrates.

With the aim of underlining the readiness of the technology, at the beginning of the 2008 Rolls-Royce installed its first LMD machine and since then, the Fraunhofer ILT and Rolls-Royce have certified the LMD process for the repair of 15 different parts. In Figure II. 58 a repaired case of the BR715 HPT (High Pressure Turbine) is shown [Gasser, 2010].

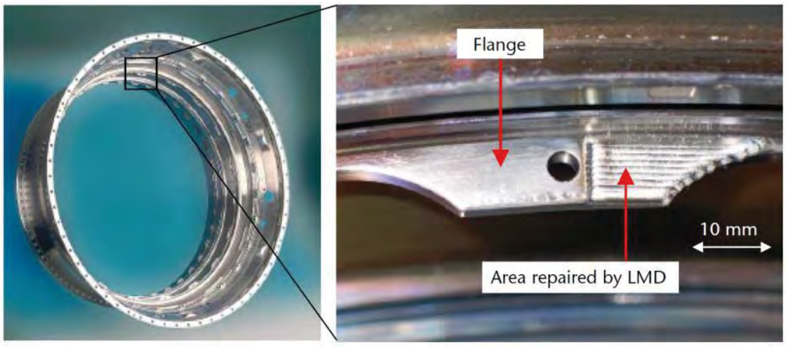

Figure II. 58: BR718 HPT case (left) and a detail of a locally repaired flange using LMD (right) [Gasser, 2010].

In the same direction, Tao et al. presented the whole procedure for the repair of aero engine blades. These parts have to withstand high pressure and temperature working conditions and also external factors, such as bird impacts, during the flight time. Consequently, they are damaged with a higher frequency than the desired. Due to the high cost of the whole part, it is more economical to repair the damaged blades rather than the manufacture of a new part [Tao, 2015].

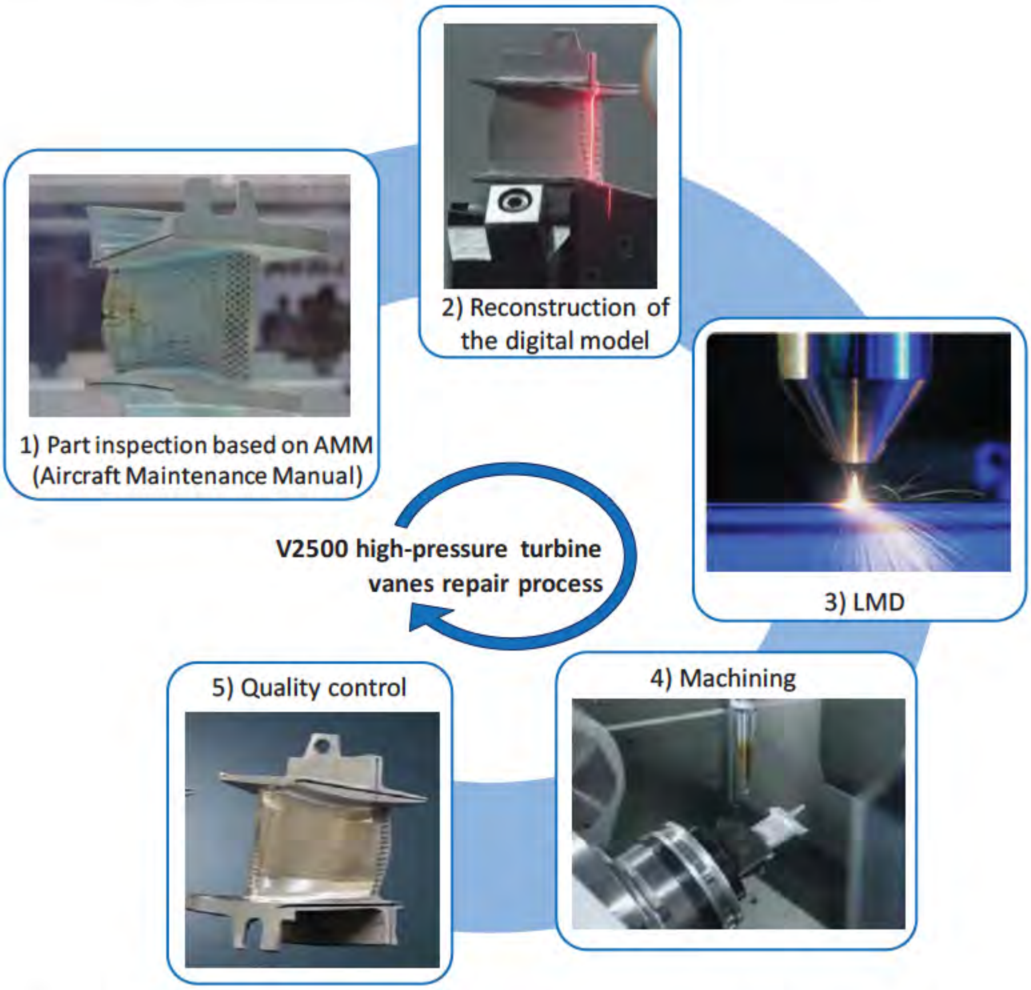
2) Reconstruction of the digital model
1) Part inspection based on AMM (Aircraft Maintenance Manual)
3) LMD
V2500 high-pressure turbine vanes repair process
5) Quality control
4) Machining

Figure II. 59: V2500 high-pressure turbine vane repair process. Photos from MTU [Martens, 2010]

However, as LMD is a multidisciplinary process, it has to be correctly controlled and monitored for obtaining the required quality. Bi and Gasser studied the influence of controlling the process temperature when repairing Ni-based superalloy turbine-blade knife edges in order to avoid the hot-cracking of the material [Bi, 2011].

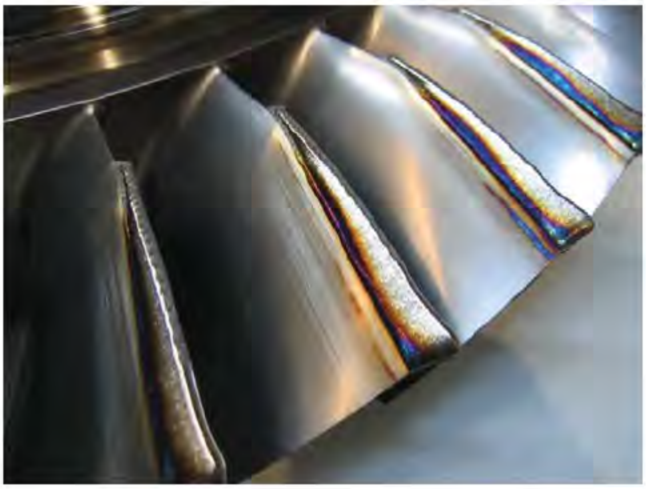

Figure II. 60: Turbine blade edges repair using the LMD technology [IWS, 2017]

Another application of the LMD in the aeronautical sector is the coating of existing parts. For example, it can be used for the generation of wear-resistant coatings on the tips of the turbine engine blades in order to increase their lifetime.

In view of the potential of the LMD technology, many projects have been launched with the aim of improving the LMD process and facilitate its industrialization. In the FLEX-ILAS project, sponsored by the German Federal Ministry of Education and Research, the capability of the LMD technology to generate whole blades of a Blisk starting from the central cylinder was evaluated. The project concluded that the mechanical properties and the in-flight behavior of the LMD generated Blisk blades are comparable to a newly machined part [Richter, 2008].

Other examples of European projects that highlight the importance of the LMD inside the aerospace industry are the RepAIR, the FANTASIA and the TurPro projects. The RepAIR is an ambitious project launched under the European Union Seventh Framework Program (FP7/2007-2013). The main objective of this project is the reduction of aircraft maintenance costs by repairing damaged parts instead of substituting them with new ones. With the same objective, Iberia Maintenance installed a LMD equipment in their Workshop in Madrid for the repair of damaged engine parts. Lufthansa Technik also uses the LMD technology for the repair of high-pressure compressor blades since the beginning of the 2014 [Metzger, 2013]. In general, LMD process is currently being used by many MROs (Maintenance, Repair and Operations) at different airports.

Another relevant project related with the LMD is the FANTASIA, which stands for Flexible and near-net-shape generative manufacturing chain and repair techniques for complex aero-engine parts. This project was launched in the 2016 and its main aim is the reduction of the repair costs of the aero-engine parts over the 40%.

With a similar objective, ILT and IPT Fraunhofer Institutes together with the local government of North Rhine-Westphalia and a consortium of companies from the turbo-engine industry launched the project TurPro. The project seeks the full integration of production technologies for efficient turbo-engine manufacturing, maintenance and repair. Both FANTASIA and TurPro are European and German projects, whose aim is to contribute to the global leadership of European turbo-engine manufacturers.

One of the characteristics of the LMD manufactured parts is their relative low dimensional accuracy. Therefore, the parts need to be machined afterwards in order to achieve the desired surface quality and the final geometrical dimensions [Klocke, 2014]. With this objective, a consortium that integrates additive and subtractive processes is formed since the 2008 in the UK: the RECLAIM (Remanufacture of high value products using a Combined Laser cladding, Inspection and Machining system) [Jones, 2012].

II.7.2. Die & Mold

Production of die & molds is a complex process that requires a final manual polishing and adjustment operation before being able to shape the final part. This adjustment process usually requires the removal of material, but many times the addition of material is also necessary. This additive process has been traditionally carried out by highly skilled workers using TIG or plasma welding equipment. Nevertheless, the results obtained always depend on human factor, what is detrimental for the repeatability of the process. Moreover, due to the tight schedules that die & mold companies work with, especially those associated with the automotive sector, these manufacturing periods are critical.

The main characteristic of the LMD is the capability to produce high added value parts, with high repeatability, good surface quality and relatively low manufacturing costs. Besides, the material deposition process can be fully automated, what minimizes the human factor in the process. Consequently, the LMD has caught the attention of many die & mold manufacturers [Chen, 2014]. Nowadays, the LMD is used for the reparation of die & mold with different filler materials, both in wire and powder form [Jhavar, 2013]. In addition, the introduction of the laser hardening process allows also the application of the LMD process in the same machine with a minimal adaptation. Thus, many die & mold manufacturers that have introduced a laser hardening system are also using LMD process for the repair of the parts.

The main applications of the LMD in the die & mold manufacturing sector are the repair of damaged parts and the generation of coatings that enhance the wear and corrosion resistant properties. Moreover, it offers the possibility to add material on sensitive zones without damaging the substrate where they are deposited. Moreover, various combinations of materials can be deposited, enabling the generation of tailor-made parts. Therefore, the LMD results to be a useful tool when design changes are required once the mold is finished. Besides, it is useful even when the manufacturing process of the mold is not successful and it needs to be repaired. In Figure II. 61 a repaired mold of a car lamp is shown. A 0.15 mm thickness layer is applied.

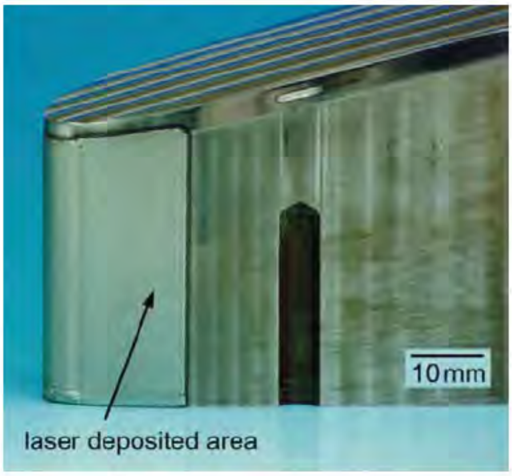

Figure II. 61: Repair of worn-out areas in a car lamp mold [Propawe, 2011].

Due to the brittle nature of the extremely hard materials used for the die & molds (hardness values over 55HRC), sometimes even the deposition of a single line entails a great complexity due to the thermal origin crack formation. If the appropriate process parameters are not used, cracking phenomena may occur during the deposition process or the afterwards cooling due to a combination of the thermal induced stresses and the brittle nature of the materials. With the aim of overcoming these problems, many authors have studied specific cases. For instance, Prakash et al. analyzed the LMD process for repairing AISI H13 (DIN 1.2344) tool steel using CPM 9V as filler material [Prakash, 2015]. Parishram studied the effects of the LMD process parameters on an AISI H13 (DIN 1.2344) tool steel. He concluded that the laser power has a great influence on the process depth [Parishram, 2007]. In the following figure the effect of the laser power on the clad dilution is shown. The first four tracks are deposited with a 1000 W laser power and the subsequent six lines with a 600 W laser power. Two layers are overlapped with the aim of achieving the desired height. As it is appreciated, the dilution of the deposited material is higher as the laser power is increased.

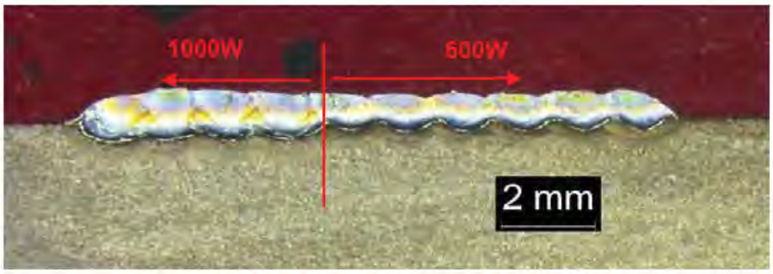

Figure II. 62: Co-based alloy coating using different laser powers.

Song et al. evaluated the fatigue behavior of the AISI H11 (DIN 1.2343) hot work tool steel repaired by LMD. They noticed that the fatigue resistance of the repaired part is lower than the base material. Nevertheless, the properties of the original material could be recovered after the appropriate heat treatment [Song, 2008].

II.7.3. Naval industry and heavy industry

Due to the large size and high manufacturing costs of the components used in the naval industry, their maintenance and repair is a key factor for reducing costs. Consequently, the main application of the LMD process is the repair of damaged parts, such as: hydraulic cylinders, pump shafts, bearing surfaces for propeller shafts, etc.

Besides, the LMD is used for the surface properties enhancement, where it offers a series of advantages compared to traditional alternatives used for coating applications. An example of the LMD coating is the usage of a low cost material such as a low carbon content steel for creating the basic part, and afterwards the generation of a coating using the LMD process, so that the desired wear and heat resistant properties are obtained. Typical materials used in the naval and the heavy industry are the nickel based alloy Inconel 625 for enhancing the corrosion and thermal resistance properties and Tungsten carbides for improving the wear resistance [Riedelsberger, 2013].

In the case of the heavy industry, the main application of the LMD technology is the repair of different rotating parts that suffer from erosion and wear. Due to the high cost that entails the substitution of whole parts, their repair is economically profitable. The shafts belonging to steam or gas turbines that are often damaged at the raceways are examples of this. In Figure II. 63 a scheme and a real photograph of the reparation process of a gas turbine shaft are shown. As detailed by the company GE Oil & Gas, the application is based on:

- ✓ A 2.2kW fiber laser with the corresponding LMD nozzle and the optical tooling.
- ✓ A gravity powder feeder.
- ✓ A 6-axis robotic system as kinematic platform for the LMD system.
- ✓ A first class protection cabin (not shown in the figure).

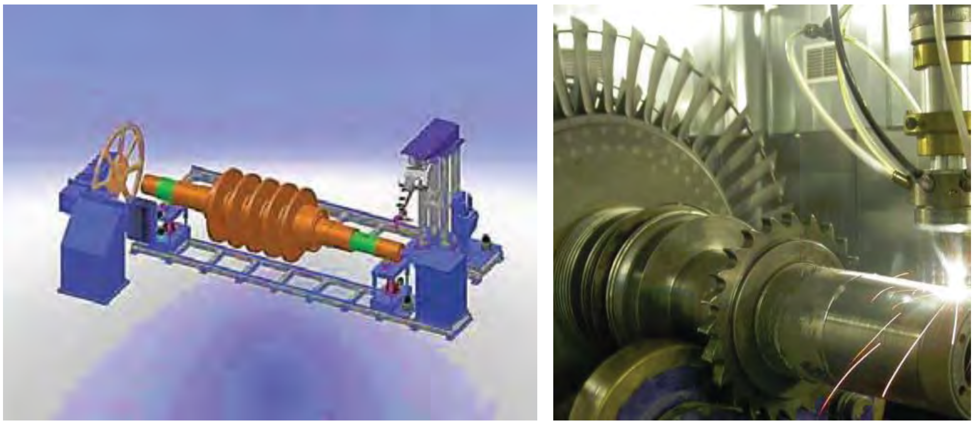

Figure II. 63: A scheme (left) and a real photo (right) of the reparation of a gas turbine shaft using the LMD [Andolfi, 2012]

The following materials are used depending on the application: Nickel based superalloys are used for repairing buckets, steel alloys such as the ASTM A322 type 4340 (DIN 1.6511) for centrifugal compressor shafts, the ASTM A182 F22 (DIN 1.7380) for impellers and stainless steels such as the X22CrMoV12.1 (DIN 1.4923) for steam turbines [Andolfi, 2012]. Depending on the total thickness to be added, more than one layer have to be deposited and once the additive process is finished, the part needs to be re-machined in order to obtain the final geometry and surface finish.

Another example of the LMD process in the naval industry is the repair of marine diesel engine crankshafts. Due to the rough working conditions, crankshafts suffer from severe wear at the friction surfaces. Consequently, their periodical repair is needed in order to keep them working in the right conditions. Koehler et al. studied the repairing process of the crankshafts and obtained promising results when adding a Stellite 21 coating over a 42CrMo4 steel [Koehler, 2010].

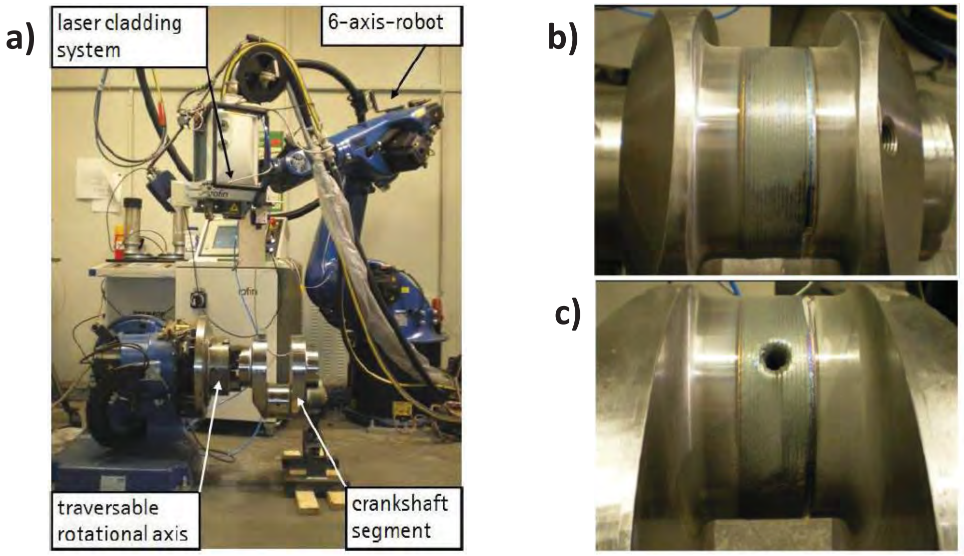

Figure II. 64: a) Laser cladding head attached to a 6 axis robot; b) Bottom side at lower dead center position of a crankshaft; c) Crankshaft segment around oil bore [Koehler, 2010].

Thanks to the developments in the laser technology during the last decade, Nowotny concluded that it is possible to repair the crankshafts directly in the ship instead of dismantling and transporting the heavy parts to the workshop [Nowotny, 2011]. In the same direction, Torims et al. stated that a grinding platform can be extended to its use with the laser cladding technology; what suits perfectly with the requirements of the repairs of shipboard crankshafts and opens a new dimension to the LMD process [Torims, 2012]. This combination results in economic benefits and repair-time reductions, but it is still far from an industrial solution and a much deeper analysis is required to increase the readiness level of the LMD portable solutions.

II.8. LMD process model

The LMD process is being introduced in different industrial sectors and new applications are being constantly developed. Nevertheless, many difficulties need to be faced as a consequence of the elevated number of variables involved in the process, see paragraph "II.2.2. Laser Metal Deposition process basics". Moreover, as it is mentioned in the introduction, parts to be manufactured are frequently unique and there is only one chance to process them correctly. Therefore, the possibility to simulate the LMD process before going to the machine facilitates the determination of the process parameters and reduces the number of initial tests required to optimize the process.

However, due to the complexity of the LMD process and the high amount of involved physical phenomena, it is almost impossible to consider all of them. Authors usually divide the LMD process into different steps. Thus, the work done on the modeling of the LMD process so far is divided into three groups:

a) Powder particle modeling: The trajectories of the powder particles are calculated and the interaction between the powder particles and the laser beam is modeled.
b) Generation of the melt pool and the thermal field developed in the substrate.
c) Filler material addition and material deposition.

II.8.1. Powder particle modeling

The simulation of the powder particle paths is important in order to achieve a LMD model. Not only to simulate the clad geometry, but also to design appropriate and efficient LMD nozzles.

The geometry of the nozzle and the operation conditions are of major importance in the LMD process. Therefore, many authors have focused their efforts on analyzing the powder distribution at the nozzle exit and its influence in the resulting LMD process. Liu and Li studied the influence of the fluctuations on the powder feed rate in the deposited material [Liu, 2005]. They concluded that an increase of the powder concentration results in a higher but narrower clad geometry. Therefore, if powder flux is not uniform at the nozzle exit, instabilities occur.

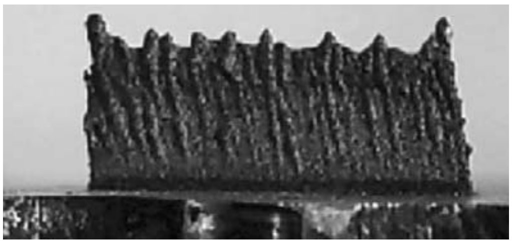

Figure II. 65: Sample produced with an unsteady powder feed rate [Liu, 2005]

In the same way, Zekovic et al. concluded in their work entitled "*Numerical simulation and experimental investigation of gas-powder flow from radially symmetrical nozzles in laser-based direct metal deposition*" that the nozzle is a key element in the powder delivery system. A proper nozzle design increases the quality of the deposited material [Zekovic, 2007]. Moreover, they highlighted that the best feeding properties are obtained with spherical shaped particles, i.e. particles obtained by means of gas atomization.

In 1999, Lin stated that the performance of a coaxial nozzle depends on the different gas flows [Lin, 1999]. Using image analysis and different optical techniques based on the light scattering and attenuation, he studied the powder distribution at the nozzle exit. The powder stream shows a Gaussian shaped transverse distribution at the focal plane. Moreover, the influence of the velocity of the protective gas was studied.

Since then, many authors have focused their work on this field and because of the complexity of the problem; different simplifications have been considered. A typical assumption is the omission of the laser beam and the simulation of just what is called the "cold stream".

Zekovic et al. simulated and studied the powder flow for a LMD nozzle using the commercial software Fluent [Zekovic, 2007]. They used a standard κ-ε turbulent model and a standard wall-function approach to overcome the viscous phenomena that occur near the wall boundaries. Authors concluded that a 3D model is required for the simulation of a LMD nozzle, because the generated turbulence inside the nozzle and especially at the exit is a 3D phenomenon.

A Lagrangian approach was used for the two-phase (gas and powder) flow modeling, where the gas phase is considered to be the continuous medium and the powder particles the discrete phase. The Lagrangian model treats the disperse phase as a continuous stream of powder particles moving through the continuous medium (the drag gas). The following assumptions were considered when developing the model:

- The problem is treated as a steady-state turbulent flow and constant gas velocity is supposed at the inlets.
- The only forces that actuate on the particles are the drag force, gravity and the very own inertia of the particles.
- The amount of powder particles (discrete phase) is very low compared with the gas volume (continuous phase), less than 10%. Consequently, the collisions between the particles are omitted.
- The influence of the gas velocity on the particle trajectory is considered.

- The laser radiation is neglected.
- The size of the particles is assumed to follow a Rosin-Rammler distribution (statement validated by [Tabernero, 2010]).

Rosin-Rammler distribution can be expressed by means of the following equation.

$$Y_d = e^{-(d/\bar{d})^n} \qquad \textbf{(Eq. II. 4)}$$

Where, "Y_d" is the proportion of particle diameter "d" in a unit base. "n" is the dispersion parameter of the distribution and "$\bar{d}$" is the average diameter. The average diameter is defined as the diameter for which the 36.8% of the particles have a bigger diameter.

$$if \quad d = \bar{d} \implies Y_d = e^{-1} \Rightarrow Y_d = 0{,}368 \qquad \textbf{(Eq. II. 5)}$$

With regard to the dispersion parameter "n", it is defined as the average value of the dispersion parameter "n_i" of each couple "$(d_i, Y_{d,i})$" and it is calculated by means of (Eq. II. 6).

$$n_i = \frac{\ln(-\ln Y_{d,i})}{\ln(d_i/\bar{d})} \implies n = \frac{1}{k}\sum_{i=1}^{k} n_i \;\; (k = number\ of\ analyzed\ diameters) \qquad \textbf{(Eq. II. 6)}$$

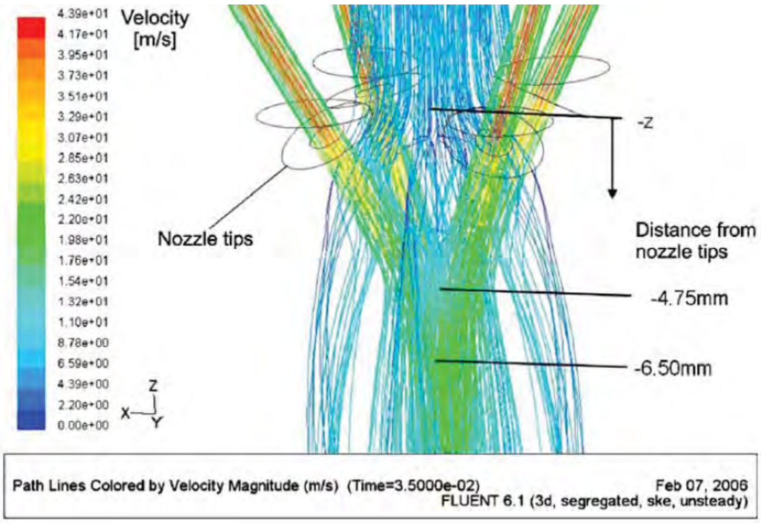
4.39e+01
4.17e+01
3.95e+01
3.73e+01
3.51e+01
3.29e+01
3.07e+01
2.85e+01
2.63e+01
2.42e+01
2.20e+01
1.98e+01
1.76e+01
1.54e+01
1.32e+01
1.10e+01
8.78e+00
6.59e+00
4.39e+00
2.20e+00
0.00e+00
Velocity [m/s]
Nozzle tips
-Z
Distance from nozzle tips
-4.75mm
-6.50mm
Z
X
Y
Path Lines Colored by Velocity Magnitude (m/s) (Time=3.5000e-02)
Feb 07, 2006
FLUENT 6.1 (3d, segregated, ske, unsteady)

Figure II. 66: Powder particle trajectories colored according to their velocity magnitude [Zekovic, 2007].

Zekovic et al. validated the model with the corresponding experimental tests in three different situations regarding the LMD nozzle and the position of the substrate: a) Substrate surface far from the nozzle tip, b) Substrate close to the tip of the nozzle, c) The tip of the nozzle is close to the top of a thin-wall that is being deposited. Results obtained proved that when depositing on a flat surface or thin-wall, the protective gas plays an important role in order to prevent powder particles from getting inside the nozzle and spotting the laser head optics.

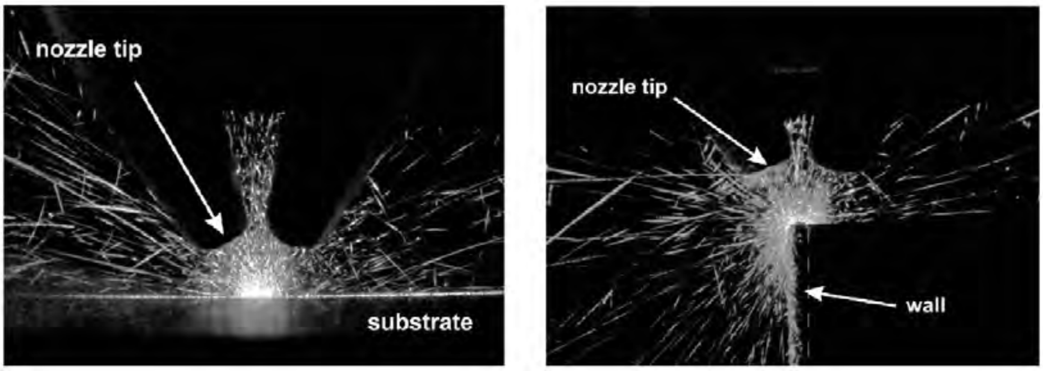
nozzle tip
substrate
nozzle tip
wall

Figure II. 67: Image of the powder particles at the exit of the nozzle when depositing on a flat surface (left) and when depositing on a previously deposited thin wall (right) [Zekovic, 2007].

Yang proposed a model that predicts the maximum powder concentration in a coaxial nozzle for different powders, nozzle geometries and shielding gas flows [Yang, 2009]. They concluded that the smaller the nozzle diameter and the nozzle angle, a more focused powder spot is obtained.

Tabernero et al. presented a model based on the CFD program Fluent to predict the powder flux distribution in a real continuous coaxial nozzle [Tabernero, 2010]. The model solves the continuous phase based on the Navier-Stokes equations together with the standard κ-ε turbulent model. This same assumption was also considered by other authors in their research works [Lin, 2000]. The main contribution of this work is the development of a mechanic method for measuring the powder concentration at the nozzle exit, which is described afterwards.

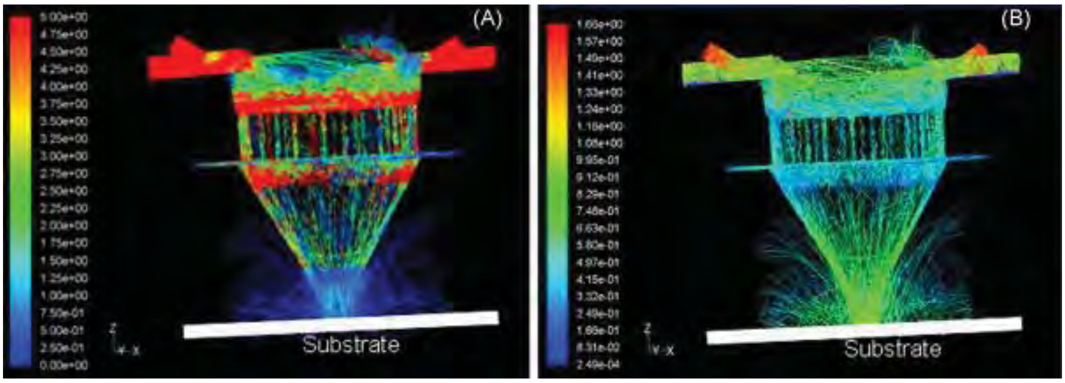
(A)
5.00e+00
4.75e+00
4.50e+00
4.25e+00
4.00e+00
3.75e+00
3.50e+00
3.25e+00
3.00e+00
2.75e+00
2.50e+00
2.25e+00
2.00e+00
1.75e+00
1.50e+00
1.25e+00
1.00e+00
7.50e-01
5.00e-01
2.50e-01
0.00e+00
Z
Y X
Substrate
(B)
1.66e+00
1.57e+00
1.49e+00
1.41e+00
1.33e+00
1.24e+00
1.16e+00
1.08e+00
9.95e-01
9.12e-01
8.29e-01
7.46e-01
6.63e-01
5.80e-01
4.97e-01
4.15e-01
3.32e-01
2.49e-01
1.66e-01
8.31e-02
2.49e-04
Z
Y X
Substrate

Figure II. 68: (A) Concentration and (B) velocity fields obtained after simulation for AISI D2 [Tabernero, 2010].

Mohagegh et al. also used the CFD software Fluent to study the trajectories of the powder particles at the nozzle outlet [Mohagegh, 2010]. They focused their work on the analysis of the effect that the different process variables have on the efficiency of the filler material deposition. The following conclusions were obtained:

- The increase of the nozzle angle regarding the horizontal axis, brings two benefits:
    - Increases the deposition efficiency.

  - Increases the interaction time between the powder particles and the laser beam, which results in an increase of the temperature of the powder particles.
- The drag flow is the dominant flow in the coaxial nozzles used in the LMD process.

Balu et al. used as well the commercial CFD software Fluent to solve the Navier-Stokes equations [Balu, 2012]. The gas phase is treated as a continuous phase and the powder particles as discrete elements, which diameters follow a Rosin-Rammler distribution. The model is based on the work previously done by Zekovic et al. [Zekovic, 2007] and the following assumptions were considered:

- The continuous phase is supposed to be viscous, compressible and steady-state.
- Constant velocity at the protective and drag gas inlets.
- The discrete phase model is based on a force balance; where drag, inertial and gravitational forces are included.
- The volume fraction of the particles is very small compared to the carrier gas flow, lower than the 10%. Therefore, the interaction between particles and the influence of the particles on the gas flow is omitted.
- The interaction between the laser and the particles is ignored.

They concluded that an increase of the drag gas flow increases the divergence of the powder particles at the nozzle exit and therefore reduces the concentration of the powder particles at the focal plane [Balu, 2012]. Moreover, the velocity of the particles is influenced by the density of the powder material, shape and diameter of the particles and they have a direct influence on the flow stability. A comparison between the modeled powder concentration at the nozzle exit and an image of the real nozzle is shown in Figure II. 69.

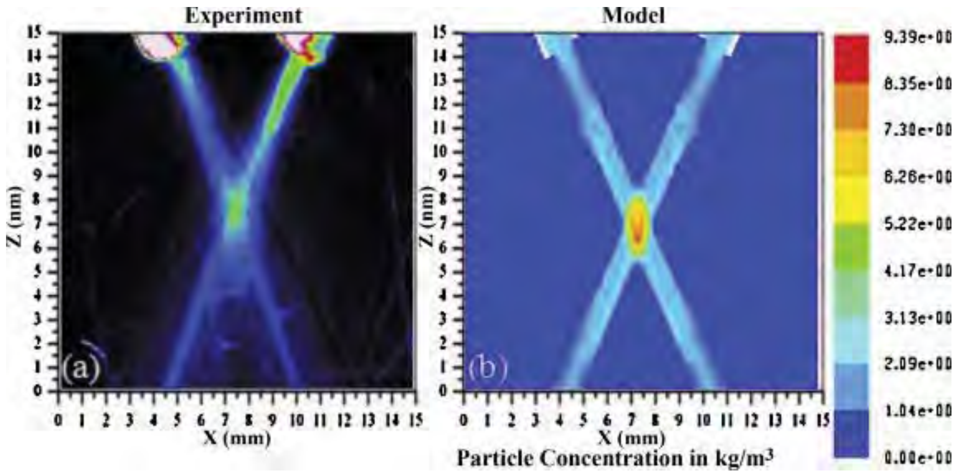

Figure II. 69: NT-20 powder stand-off distance comparison between (a) experimental and (b) numerical results at a carrier gas flow rate of 3.94 × 10^{-5} $m^3 \cdot s^{-1}$ and a powder flow rate of 0.06 $g \cdot s^{-1}$ [Balu, 2012].

Once the numerical model is developed, it has to be validated. Most authors use optical based methods for measuring the powder flux distribution at the nozzle exit [Lin, 1999; Pinkerton, 2007; Balu, 2012], etc. However, the main problem of the optical methods is that they can only give a qualitative value of the concentration. Powder concentration is represented as a percentage regarding the 100% value assigned to the maximum. In Figure II. 70 the experimental setup used by Pinkerton et al. is shown.

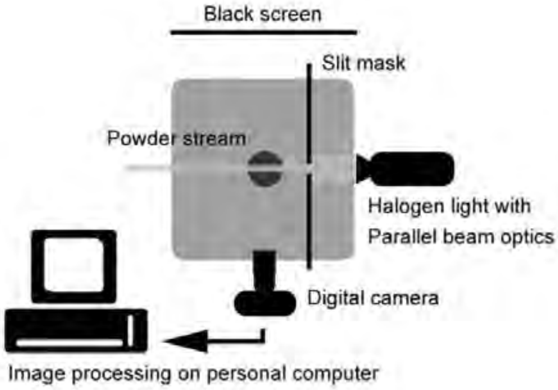
Black screen
Slit mask
Powder stream
Halogen light with
Parallel beam optics
Digital camera
Image processing on personal computer

Figure II. 70: Schematic setup used for obtaining the powder distribution at the nozzle exit and the subsequent digital analysis [Pinkerton, 2007]

Tabernero et al. proposed an alternative method for measuring the powder concentration using a set of cylindrical containers. Each piece of the set has a different inner diameter, ranging from 2 to 20 mm, but they all have an identical external diameter. All containers are placed in a common fixture system. Therefore, powder concentration is obtained on the basis of the weight trapped inside the different diameter holes. In Figure II. 71 the procedure of the developed system is detailed.

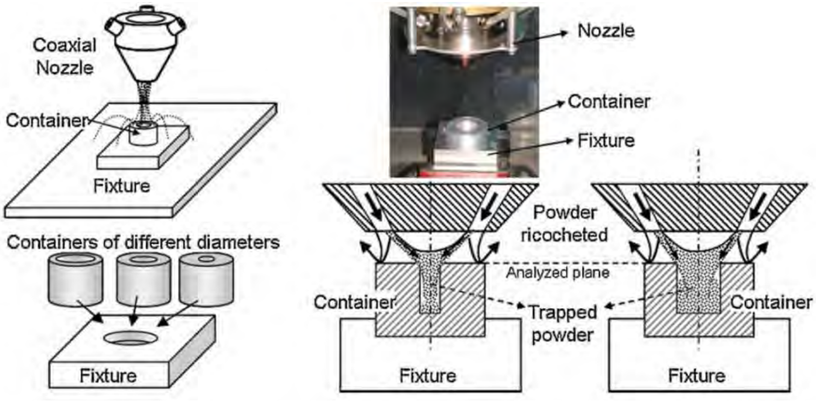
Coaxial Nozzle
Container
Fixture
Containers of different diameters
Fixture
Nozzle
Container
Fixture
Powder ricocheted
Analyzed plane
Container
Trapped powder
Container
Fixture
Fixture

Figure II. 71: Experimental measurement system of the powder flux [Tabernero, 2010]

All the works mentioned until now, model the so called “cold stream” and omit the influence of the laser beam on the powder particles. However, this interaction has a considerable influence on the process and must be considered. On the basis of this statement, many authors have focused their work on the powder particle heating.

Powder particle heating

One of the first works was carried out by Grujicic et al.. They simulated the heating of a single particle during the in-flight time in order to optimize the deposition process [Grujicic, 2001]. Fu et al. simulated the temperature raise of powder particles in the LMD process. They concluded that the powder feeding angle affects significantly to the temperature of the particles and the attenuation of the laser [Fu, 2002].

In the same direction, Liu and Jin developed a simplified approach to solve the thermal problem of the powder flow in coaxial nozzles. Powder particle heating and even melting under the irradiation of a CO_2 laser beam were considered [Liu, 2003]. Authors used a finite-difference method to solve the governing equations of the problem and the developed numerical model was based on the following hypotheses:

- Interaction between powder particles is omitted and, therefore, the heating problem may be reduced to a single particle simulation.
- Powder particles are spherical with constant absorptivity.
- The energy intensity across the laser beam is uniform.
- The protective gas has a constant velocity.
- No interaction between the laser beam and the protective gas is considered.

After the realization of the mentioned research work, Liu and Jin concluded that the velocity of the powder particles has a big influence on the heating process. Besides, the reached maximum temperature is influenced by the size of the particles and laser power. Therefore, these variables must be controlled in order to prevent over-heating problems during the process. In the same direction, more complete models have been proposed by Vetter et al. [Vetter, 1994] and Pinkerton [Pinkerton, 2007]. Both of them calculated the particle temperature rise in coaxial nozzles assuming an average particle radius.

Wen developed a complete model using the commercial CFD software Fluent. The gas phase was treated as a continuous phase and the particle flow was simulated as a discrete phase [Wen, 2009]. A κ-ε turbulent model was considered. The continuous phase was solved using the time-averaged Navier-Stokes equations, whereas the discrete phase was solved using a Lagrangian formulation. The article concludes that at the exit of the nozzle the powder stream can be divided into three zones named as: (a) pre-waist, (b) waist and (c) post-waist.

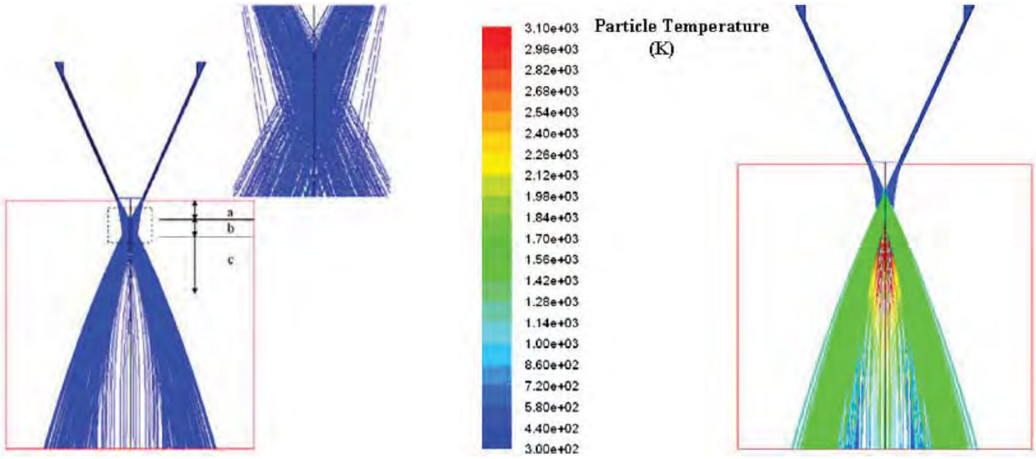

Figure II. 72: Particle stream structure where a) pre-waist; b) waist; c) post-waist stages can be distinguished (left) and powder jet temperature profile for a 300 W laser power and a 1.5 mm laser beam diameter (right) [Wen, 2009].

Ibarra-Medina and Pinkerton modeled the LMD process and considered the interaction between the laser beam, powder particle stream and the substrate [Ibarra-Medina, 2010]. The dynamic behavior of the particles is influenced by the drag force of the carrier gas, gravity and collisions with the solid walls of the nozzle. Special attention was paid to the influence of the substrate. They concluded that the position of the substrate influences both, the distribution of the particles at the powder focal plane and the particle heating due to the particle bounces. Furthermore, the consideration of the substrate in the simulations generates more realistic results and should be considered.

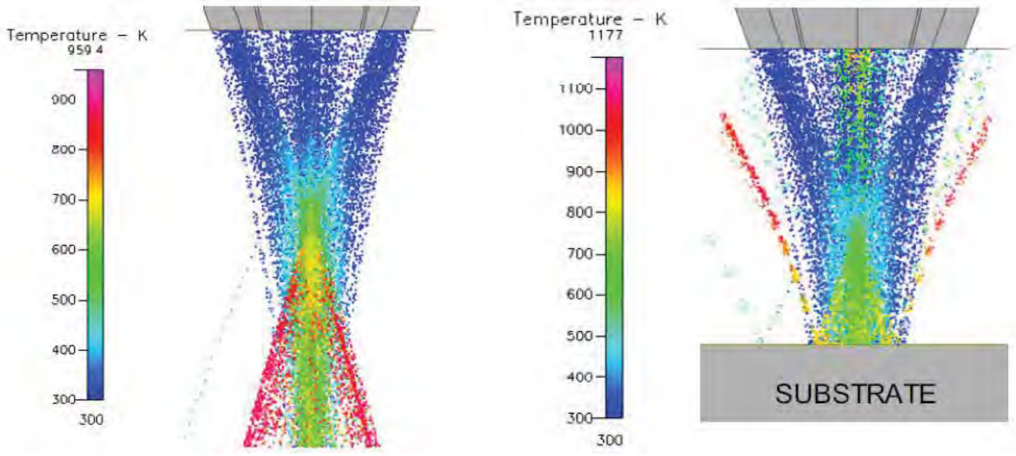

Figure II. 73: Temperature of the particle stream when no substrate is considered (left) and temperature of the particle stream when the substrate is situated at a 10mm distance from the nozzle tip (right). In both cases same process parameters are used. Power 1000 W, powder flow rate: 0.58 g·s^{-1}, carrier gas: 5 l·min^{-1}, protective gas: 4 l·min^{-1} [Ibarra-Medina, 2010].

A discussed point is whether powder particles arrive in solid or melted state to the substrate, fact that has a direct effect on the material deposition process. Kovalev et al. studied both, numerically and experimentally the powder flow characteristics and particle heating due to the laser beam-powder particle interaction [Kovalev, 2010].

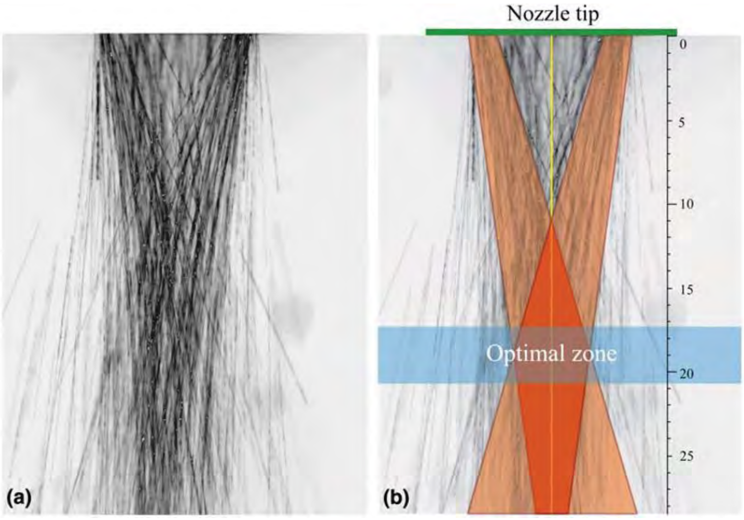

Figure II. 74: a) Powder flux at standard gas flow parameters without laser radiation. b) Optimal zone with the highest concentration of particles formed by crossing divergent particle streams [Kovalev, 2010].

Kovalev et al. distinguished between elastic and non-elastic powder bounces inside the nozzle and developed a numerical model using the commercial software Fluent that studies the effects of considering one or another assumption. The interaction between the powder particles and the walls of the nozzle is controlled by the restitution coefficient, which is divided into normal ($\vec{n}$) and tangential ($\vec{\tau}$) components. If $k_n \approx 1$ the particle bounces are supposed to be elastic. If $k_n \ll 1$ particle bounces are supposed to be non-elastic and, consequently, part of the kinetic energy is lost.

$$\left(V_{pn}\right)_2 = -k_n \cdot \left(V_{pn}\right)_1 = -k_n \cdot \left(\overrightarrow{V_{p1}} \cdot \vec{n}\right) \quad \textbf{(Eq. II. 7)}$$

$$\left(V_{pt}\right)_2 = -k_\tau \cdot \left(V_{pt}\right)_1 = -k_\tau \cdot \left(\overrightarrow{V_{p1}} \cdot \vec{\tau}\right) \quad \textbf{(Eq. II. 8)}$$

Normal and tangential restitution coefficients are calculated based on the work done by Vittal and Tabakoff [Vittal, 1987] and using semi-empiric relations. The incidence angle “α” is the angle between the velocity of the powder particle and the surface.

$$k_n = 1 - 0.4158 \cdot \alpha + 0.4994 \cdot \alpha^2 - 0.292 \cdot \alpha^3 \quad \textbf{(Eq. II. 9)}$$

$$k_t = 1 - 2.12 \cdot \alpha + 3.0775 \cdot \alpha^2 - 1.1 \cdot \alpha^3 \quad \textbf{(Eq. II. 10)}$$

Moreover, Kovalev et al. discussed the influence of the shape and size distribution of the powder particles in the process [Kovalev, 2010]. The article concludes that depending on the LMD conditions (especially the laser power) powder particles may be melted or even vaporized. The temperature of the particles when they reach the surface of the substrate varies within a wide range and depends on the size and trajectories that each particle follows.

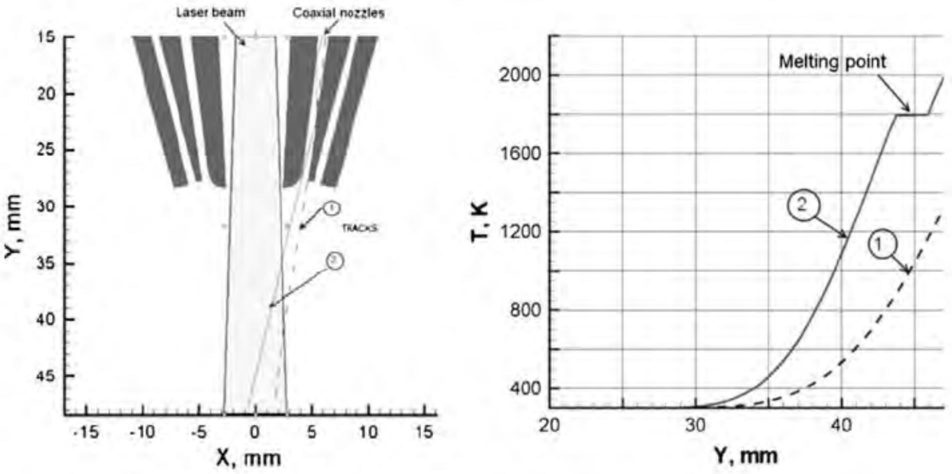

Figure II. 75: Thermal state of the powder particles at the outlet of the nozzle: The schematic of the laser beam interaction with the particles in two different trajectories (left) and the varying particle temperature along their trajectories (right) [Kovalev, 2010].

Due to the complex nature of the above presented models and the subsequent validation difficulties, some simplified models have been presented to calculate the particle heating. With the aim of contemplating the effect of the heated powder particles in the numerical model, Toyserkani et al. introduced a modified absorption coefficient that includes the extra amount of heat introduced to the base material due to the heating of the powder particles [Toyserkani, 2004]. P_1 is the laser power that reaches the surface of the substrate directly in [W], P_2 is the power carried by the powder particles into the substrate in [W] and β is the modified absorption coefficient.

$$P_W = P_1 + P_2 = \beta \cdot P_1 \qquad \textbf{(Eq. II. 11)}$$

Laser beam attenuation

Besides heating, powder particles attenuate the laser beam before it reaches the surface of the substrate. Attenuation values up to the 35% of the laser beam have been measured for lateral LMD nozzles [Partes, 2005] and over the 20% for coaxial nozzles [Tabernero, 2012_1]. Therefore, this phenomenon must be considered when developing a complete LMD model.

Vetter et al. were the first to study the influence of the laser beam attenuation on the LMD process [Vetter, 1993]. They concluded that the main reasons for the laser power attenuation are the beam scattering and the energy absorption by the powder particles. Since then, many authors have studied this phenomenon and have determined the attenuation values for different powders and LMD equipment.

He and Mazumder developed a complete model that simulates the LMD process where the laser beam attenuation and particle temperature rise were considered during the interaction time between the laser beam and the powder particles [He, 2007]. They concluded that particle heating depends mainly on the laser power. Regarding the laser power attenuation, the work concluded that the laser power at the surface of the substrate is reduced between 75-88% of the nominal power. Moreover, the laser beam attenuation resulted to be higher in the center of the beam, where the particle concentration is higher.

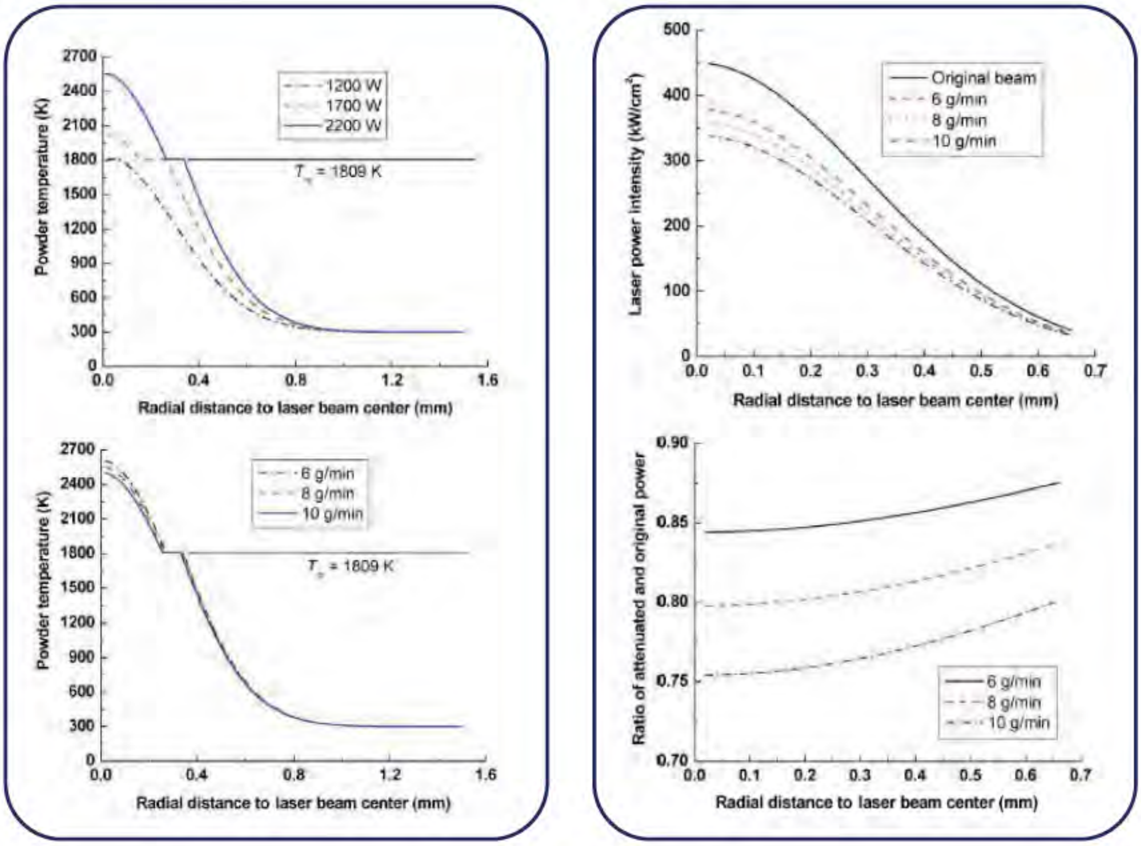

Figure II. 76: Effect of the laser power and the powder mass flow on the particle heating before arriving in to the substrate surface (left) and laser beam attenuation due to different powder mass flows (right) [He, 2007].

Tabernero et al. studied the attenuation of the laser beam for different materials, AISI D2 and Inconel 718, and different grainsizes [Tabernero, 2012_1]. They developed a semi empirical model based on the shadow model. The following hypotheses were considered when developing the model:

1. The laser beam attenuation is proportional to the shadow generated by the powder particles. As the powder concentration is relatively low compared with the gas volume, the shadow between the powder particles is neglected.

2. The attenuation depends on the powder particle concentration and is considered to be independent of the laser power.
3. Powder particles are considered spherical and their projection on the plane can be approximated to a circle.
4. The powder concentration at different planes from the nozzle tip is obtained using the commercial CFD software Fluent.
5. Finally, since particle size variations due to the temperature variation are minimal, the model considers that the size of the powder particles remains constant regardless the temperature.

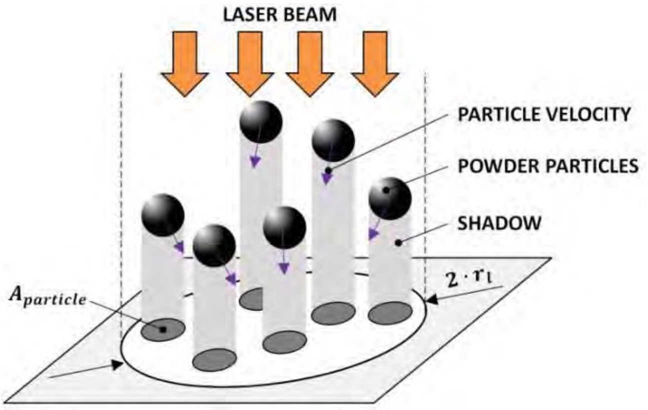

Figure II. 77: Laser beam attenuation.

Taking these assumptions into account, the laser attenuation is considered to be proportional to the ratio between the projected area of the particles and the interaction area (the laser beam transversal area). Furthermore, the attenuation is proportional to the particle velocity, or what is the same: the interaction time between the powder particles and the laser beam. In (Eq. II. 12) "K_{att}" is a dimensionless attenuation factor, which varies between 0 and 1, "$S_{particles}$" is the projected area of the particles per time unit [m^2·s^{-1}], "S_{total}" is the total area occupied by the laser beam [m^2] and "t_{int}" is the interaction time between the laser beam and the particles [s]. The dimensionless material attenuation factor "θ" has to be defined experimentally and includes most of the physical phenomena, such as the scattering effect or the generation of plasma, that are neglected in the model.

$$P_{att} = K_{att} \cdot P_{att} \ ; \quad where \ K_{att} = f\left(\theta, \frac{S_{particles}}{S_{total}}, t_{int}\right) \qquad \textbf{(Eq. II. 12)}$$

On the basis of the first assumption, the area occupied by the powder particles can be considered equal to the number of particles multiplied by their area. In (Eq. II. 13) “$A_{particle}$” is the projected area of a particle in the plane [m^2] and “$N_{particles}$” is the number of particles per unit time [s^{-1}].

$$S_{particles} = N_{particles} \cdot A_{particle} \tag{Eq. II. 13}$$

Additionally, Ya et al. developed a simple model on the basis of the mass concentration to predict the attenuation of the laser power [Ya, 2013]. They used a power meter to measure the laser power attenuation experimentally and a Particle Imaging Velocimetry (PIV) technique for obtaining the average velocity of the particles. The results obtained indicate that the attenuation depends on the nozzle type: coaxial nozzles generate a higher attenuation than lateral nozzles.

Later on, in the 2016 they presented another work entitled “*2D modeling of clad geometry and resulting thermal cycles during laser cladding*” [Ya, 2016]. The energy absorbed by the substrate “Q_{abs}” was defined by the following formula, where “t_{in}” is the interaction time in seconds, α_s and α_p are the substrate and powder absorption coefficients respectively.

$$Q_{abs} = \left[\alpha_s \cdot (P_l - P_{at}) + \alpha_p \cdot P_{at}\right] \cdot t_{in} \tag{Eq. II. 14}$$

With the aim of generating a complete model of the LMD process, Chew et al. developed a mathematical model considering upstream parameters such as the in-flight powder heating and the laser power attenuation [Chew, 2015]. A 2D model based on the Beer-Lambert law was used for the attenuation model. The following assumptions were considered for the powder particle modeling during the in-flight time:

1) The powder stream has a Gaussian distribution at the exit of each of the three discrete injectors of the nozzle.
2) Spherical powder particles are considered with a 70 µm average diameter.
3) Shadowing effects are neglected.
4) Particles have a 4 m·s^{-1} constant velocity at the nozzle exit. Drag and gravity forces are omitted.
5) The laser beam has a Gaussian distribution.
6) Heat transfer due to the protective gas is negligible.

II.8.2. Melt pool model

In the LMD process, the laser beam heats a very small area of the surface of the substrate. Depending on the laser power and the interaction time, material is melted and a melt pool is generated. The generation of a stable melt pool is a key factor to achieve a good quality clad. Therefore, many authors have focused their efforts on the modeling of the geometry of the melt pool and heat transfer inside the workpiece.

The first LMD simulation works are from the early 80s, where the works carried out by Steen´s et al. can be highlighted [Steen, 1991; Li, 1990]. In their works, they calculated the temperature field of a substrate irradiated by a laser beam using a finite-difference method. Moreover, they were able to predict the process parameters based on empirical relations.

In 1994 Picasso et al. proposed a three-dimensional analytical model that solves the heat flow problem in the LMD process [Picasso, 1994]. The model was capable of calculating the process parameters for a determined clad width and height. Furthermore, the model evaluates the powder catchment efficiency of the process.

In the 2004 and 2005 Han et al. presented two articles related with the numerical modeling of the LMD process [Han, 2004; Han, 2005]. In those articles, they worked on the development of a comprehensive mathematical model that includes most of the physical phenomena that take place in the LMD process: Preheating of the powder particles by the laser beam, heat transfer, and fluid flow. The phase change of the material was considered by applying a nonlinear thermodynamic equilibrium to the semisolid region between the molten and the solid material. Moreover, the power attenuation of the laser beam was considered on the basis of the shadow model, subsequently used by Tabernero et al. [Tabernero, 2012_1], and it was found that plays a critical role in the melt pool shape and dimensions.

In the work entitled *"Modeling of Laser Cladding with Powder Injection"*, Han et al. based their research on various simulations and experimental tests [Han, 2004]. They concluded that the LMD process mainly depends on the laser power, mass flow rate and machine feed rate.

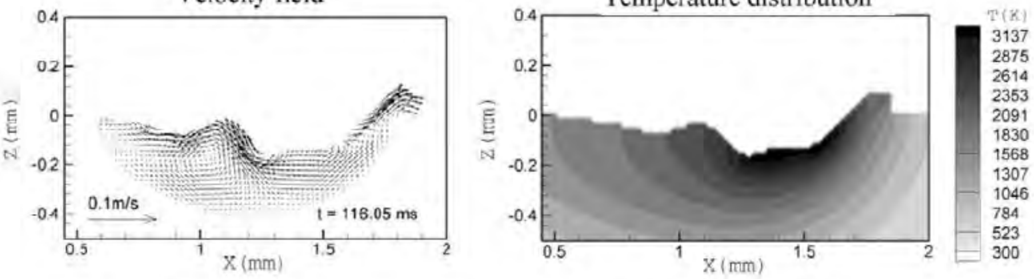

Figure II. 78: Melt pool dynamics without powder injection [Han, 2004].

Dowden concluded in its book that the geometry of the deposited clad is strongly influenced by the temperature gradients inside the melt pool [Dowden, 2009]. Therefore, it is really important to determine the size of the melt pool and temperature field in order to predict the geometry of the clad. Despite the great relevance of the molten material flow inside the melt pool, Dowden highlights that a simple conduction model could be advantageous in many cases, what facilitates the numerical calculation and reduces the computational cost.

The high number of physical phenomena involved in the generation of the melt pool makes its modeling a complex task to achieve. Therefore, the problem is addressed in a simplified way with the aim of reducing the computational cost and facilitate the programming.

One of the classical simplifications when simulating the LMD process is the assumption that the molten material does not move inside the melt pool. For instance, Toyserkani et al. proposed a 3D transient finite element model for powder LMD [Toyserkani, 2004]. This model is based on a modified thermal conductivity coefficient for calculating the boundaries of the melt pool. Once the material is melted, the conductivity is enhanced with an experimentally defined coefficient.

In the same direction, Safdar et al. developed a finite element model using the commercial software ANSYS in order to simulate the thermal transient effects generated by a moving laser beam on an Inconel 718 substrate [Safdar, 2013]. They concluded that an anisotropically enhanced thermal conductivity approach gives a better agreement with the experimental data than an isotropically enhanced thermal conductivity.

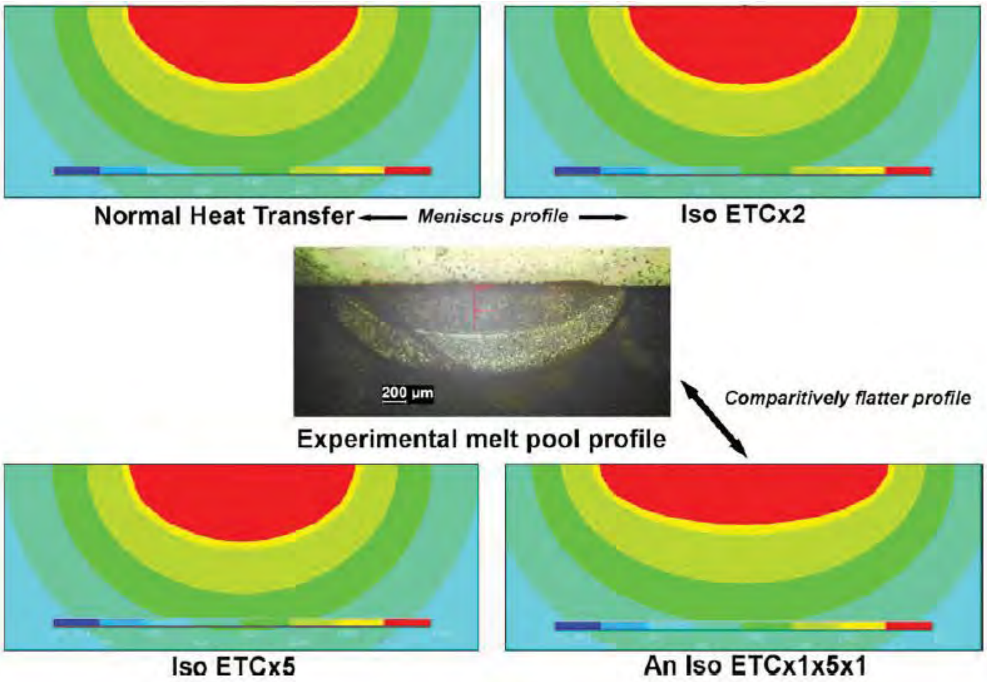

Figure II. 79: Comparison between the predicted and experimental profiles of the melt pool [Safdar, 2013].

Focusing on melt pool modeling, one of the first tasks to define when developing a numerical model is whether a 2D or a 3D model is required. Brückner et al. conducted their research in this direction and they analyzed the influence of using a bi- or three-dimensional model for simulating the LMD process [Brückner, 2007]. They concluded that 2D models can represent the LMD process with high accuracy and lower computational cost than 3D models. Based on that conclusion, Ya et al. developed a 2D model capable of predicting the geometry of the deposited material and thermal cycles in the LMD process using the finite element software Comsol Multiphysics [Ya, 2016]. However, all the previously described models supposed that there is no material displacement inside the melt pool. Furthermore, the shape of the clad is determined as a function of the energy distribution of the laser beam and the powder concentration at the nozzle exit.

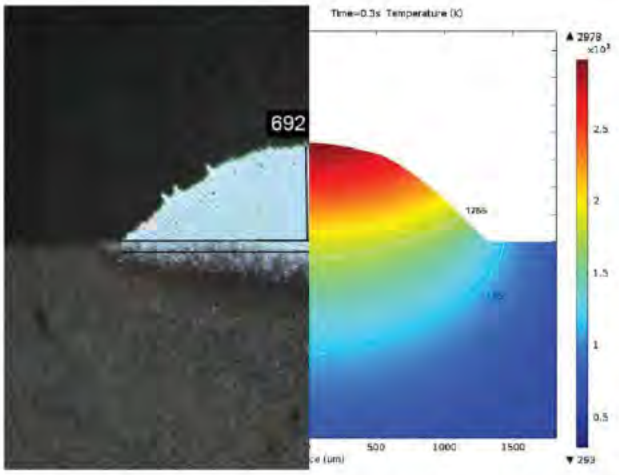

Figure II. 80: Comparison between an experimental cross section and a simulated clad geometry (900 W of laser power, 10 mm·s⁻¹ of cladding speed, 0.1585 g·s⁻¹ of powder feeding rate with 69% of powder efficiency) [Ya, 2016].

Ya et al. used the microhardness profile of the deposited material and the substrate to validate the model. However, the model itself is not able to predict the hardness of the material, what would be a useful tool to predict the mechanical properties of the deposited material.

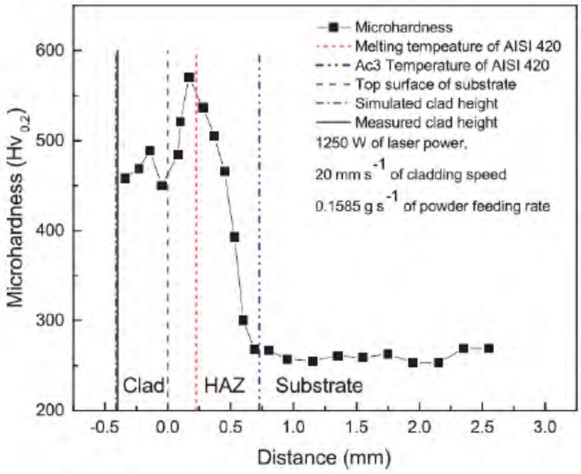

Figure II. 81: Microhardness profile of clad, together with simulated clad height, melt depth and HAZ [Ya, 2016].

Other authors have gone one step beyond and they have modeled the fluid-dynamic phenomena inside the melt pool. Dai and Gu defined the convection currents generated inside the melt pool using the commercial software Fluent [Dai, 2016]. They concluded that as the melt pool is generated, the molten material has moderate convection velocities. Consequently, the convection flow can be assumed to be laminar and it is modeled as a viscous incompressible heat conducting fluid defined by the Boussinesq approximation.

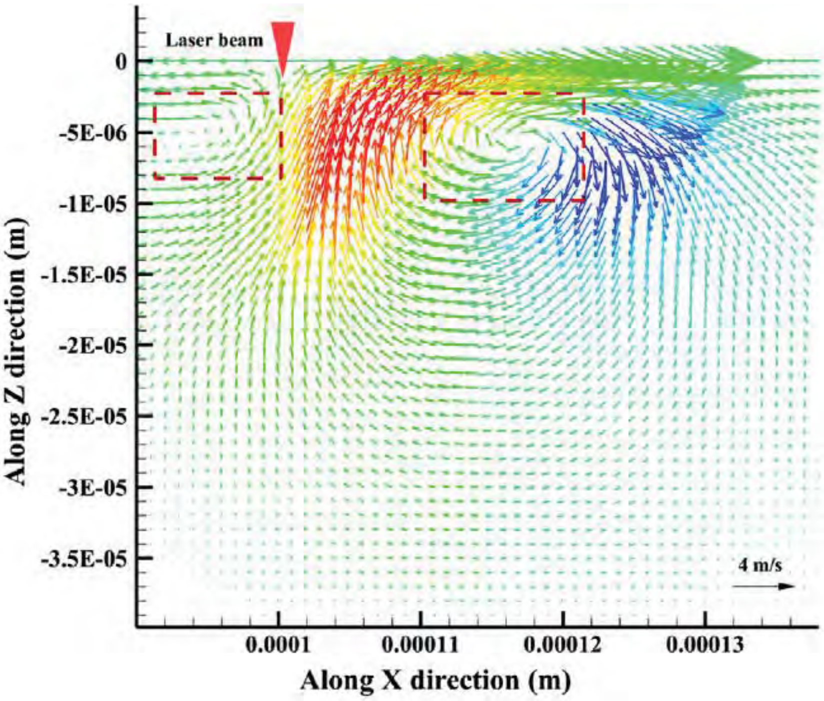

Figure II. 82: Influence of the oxidation on the formation of the multi-vortex in the molten pool (P=180W, v=400mm·s^{-1} and t= 0.275ms) [Dai, 2016].

Moreover, they determined that the existence of rust in the process has a relevant importance in the direction of the generated currents inside the melt pool. The appearance of oxide generates a change in the flow direction of the molten material. On the one hand, when the surface tension variation regarding the temperature ($\partial\sigma/\partial T$) has a negative value, an outward flow of the molten material is generated. On the other hand, when the surface tension variation regarding the temperature ($\partial\sigma/\partial T$) has a positive value, an inward flow of the molten material is generated. The same conclusion was reached by Saldi et al. in in their research [Saldi, 2013].

On the basis of the same assumptions and using the SIMPLE algorithm, Saldi et al. [Saldi, 2013] developed a 2D axisymmetric model that simulates a cross section of the geometry of the melt pool. An artificially enhanced momentum and thermal diffusivity were used in order to include the effect of the flow instabilities that were not modeled. Both, Dai and Gu [Dai, 2016] and Saldi et al. [Saldi, 2013], assumed that the surface of the substrate remains flat and no movement of the interface occurs.

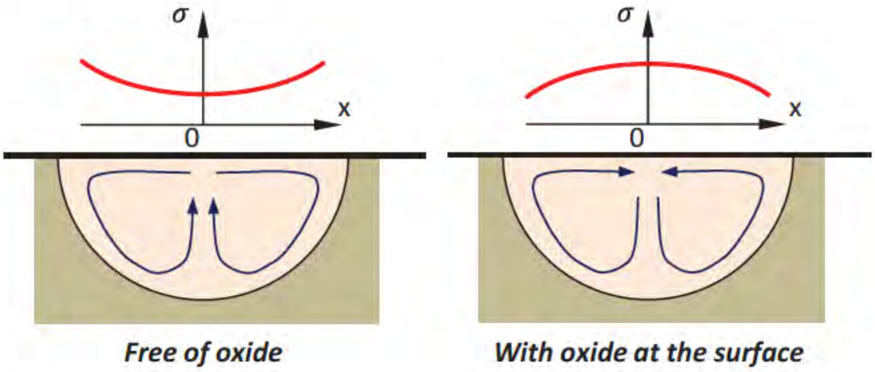

Figure II. 83: Influence of the existence of rust at the surface of the molten material in the surface tension coefficient.

Gibson et al. analyzed experimentally the geometry of the melt pool on an Inconel 625 workpiece using a high speed camera [Gibson, 2009]. Based on the observed surface patterns, they concluded that when a laser with a Gaussian energy distribution is used, the melt pool shows a high intensity ring, which is the oxide being driven towards the outside of the melt pool. When the surface tension variation regarding the temperature is negative, flow direction inside the melt pool is outwards and takes the heat away from the center of the melt pool. Thus, as Chakraborty and Chakraborty concluded, the maximum temperature of the melt pool is lowered, but at the same time the melt pool becomes wider and thinner [Chakraborty, 2005].

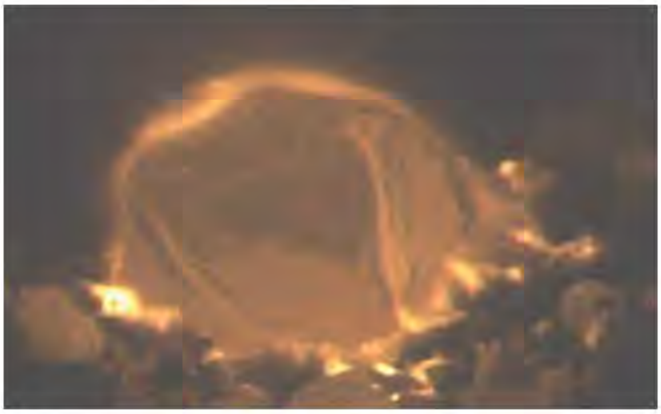

Figure II. 84: Screenshot of the melt pool for a Gaussian intensity distribution laser beam [Gibson, 2009]

Li et al. developed a multiscale methodology based on 3 steps for a fast prediction of the distortions and residual stresses generated in a layer-by-layer LMD process [Li, 2016]. Authors divided the model into 3 submodels: a microscale, a mesoscale and a macroscale model.

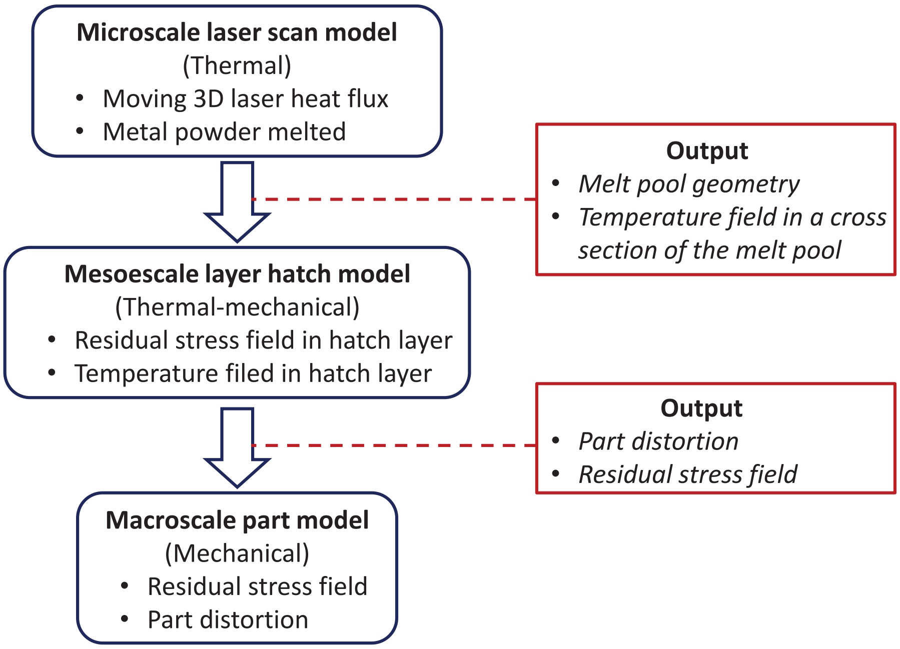
Microscale laser scan model
(Thermal)
Moving 3D laser heat flux
Metal powder melted
Output
Melt pool geometry
Temperature field in a cross section of the melt pool
Mesoescale layer hatch model
(Thermal-mechanical)
Residual stress field in hatch layer
Temperature filed in hatch layer
Output
Part distortion
Residual stress field
Macroscale part model
(Mechanical)
Residual stress field
Part distortion

Figure II. 85: Multiscale methodology for fast prediction of part distortion and residual stress [Li, 2016].

The microscale model was used for solving the thermal problem and defining the geometry of the melt pool. However, neither the displacement of the molten material was considered, nor any conductivity enhancement factor was defined in the model.

Based on the different research works, it is not clear whether the fluid-dynamics phenomena need to be considered or they can be neglected when modeling the geometry of the melt pool in the LMD process. Moreover, none of the mentioned authors have evaluated the influence of the melt pool dynamics in the accuracy of the developed model applied for the LMD process.

II.8.3. Filler material addition and material deposition

Once the melt pool is generated, the next step in order to generate the desired clad, is the addition of the filler material. In the real material addition process, powder particles are directed towards the melt pool and they have to break the surface tension of the molten material in order to penetrate into it. On the contrary, if liquid particles fall outside the melt pool, they would not adhere to the surface of the substrate with a good metallurgical bounding, unless due to the energy transfer the melting temperature of the substrate material is overcome. In this case, a joint with almost no penetration is generated.

Most authors simulate the cladding process with the assumption that all the powder particles that fall inside the melt pool are adhered to the substrate and create a clad [Toyserkani, 2004], [Tabernero, 2012_2; Ya, 2016]. Whereas, powder particles that fall outside the melt pool, bounce instead of adhering to the substrate and, hence, they are lost. However, the generation of the clad can be focused form different points of view and many different models have been developed.

Zhao et al., stated that the transversal profiles of the LMD deposited clads can be controlled by a number of parameters [Zhao, 2003]. They proposed different profiles based on the fact that the free surface of the clad is flat (zero in Figure II. 86 (left) and "x_0-x_s" in Figure II. 86 (right)). The point "x_m" lays on the limit of the melt pool generated on the surface of the substrate.

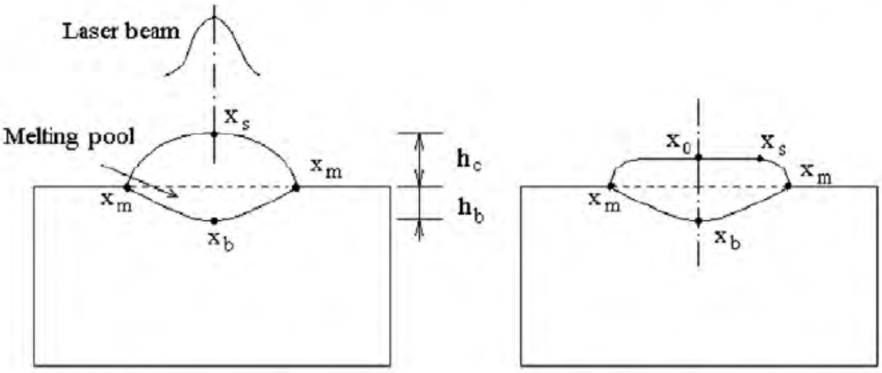

Figure II. 86: Schematic diagram of transverse sections of a clad layer [Zhao, 2003].

One of the parameters used to determine de quality of the deposited material is the contact angle with the substrate. A small contact angle usually entails porosity problems in the overlapping of the subsequent clads, whereas a high contact angle is associated with very low deposition rates. In Figure II. 87 "H" is the clad height, "W" the clad width and "α" is the clad contact angle.

$$\alpha = 180 - 2 \cdot arctan\left(\frac{2 \cdot H}{W}\right) \tag{Eq. II. 15}$$

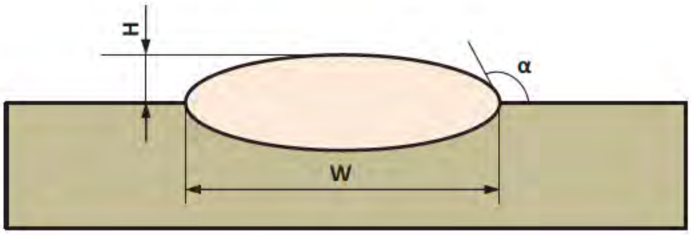

Figure II. 87: Scheme of a typical laser track with its main geometric characteristics.

Thus, Onwubolu et al. developed an exponential model based on the response surface methodology (RSM) that predicts the contact angle of the clad, based on the laser power "P", scanning speed "V" and powder mass flow rate "C" [Onwubolu, 2007]. K, k, l and m are process parameters which values are experimentally obtained.

$$y = K \cdot P^k \cdot V^l \cdot C^m \tag{Eq. II. 16}$$

With the aim of developing a more complex model, El Cheick at al. went one step beyond [El Cheick, 2012]. The developed model, besides obtaining the contact angle, predicts the cross section of the deposited line. The approximation of the profile is based on a circle which dimensions are determined by analytical relations. However, as it is stated at the article itself, it does not give a whole description of the geometry of the depositd line.

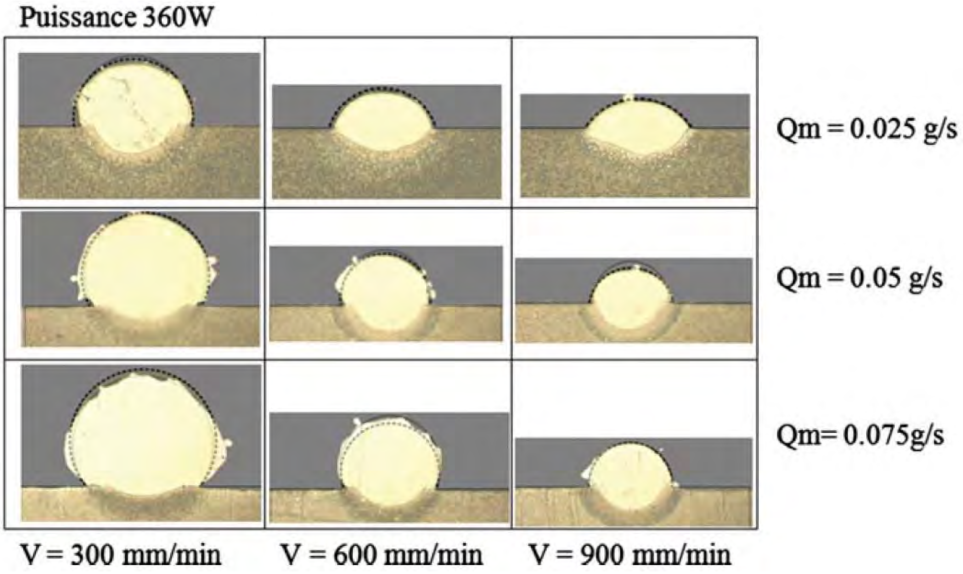

Figure II. 88: Superposition of the experimental results (continuous line) and the simulated results obtained with linear relationships (dashed line) [El Cheick, 2012].

In the same direction, Ocelík et al. presented a recursive model for predicting the profile of the generated coating [Ocelík, 2014]. The model is based on the results obtained in the deposition of single clads. Afterwards, it was applied for predicting the clad height and waviness in different track overlapping situations. Diverse profiles were testes: parabolic, arc, sinusoidal and elliptic. They concluded that the parabolic function gives the most accurate geometry prediction of the generated coating.

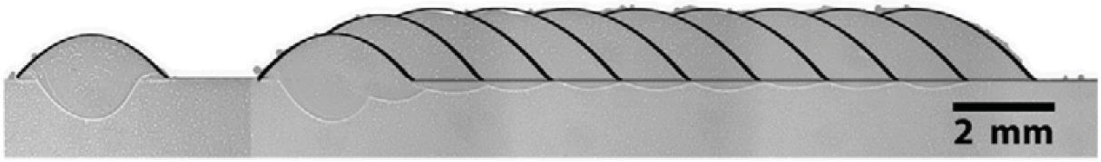

Figure II. 89: Comparison between the experimental and calculated profile (black line) using a parabolic profile function; single clad (left) and multiple clad overlapping (right) [Ocelík, 2014].

Nenadl et al. developed a similar model for predicting the profile of the deposited material [Nenadl, 2014]. The model is based on the following assumptions:

1) The clad width is controlled by the laser beam and remains constant during the entire process.
2) The shape of the generated clad does not vary with the overlapping of the successive clads.
3) The amount of filler material introduced to the clad is constant during the deposition of the successive clads.

Ya et al. used the commercial software Comsol Multiphysics to develop a 2D model for predicting the thermal field and the geometry of the cross section for different cladding conditions. They concluded that the shape of the deposited material is mainly determined by the size of the melt pool and the powder distribution at the surface of the substrate [Ya, 2016]. A parabolic function was proposed to approximate the clad profile:

$$F_0(t) = a \cdot y^2 + b \cdot y + c \qquad \textbf{(Eq. II. 17)}$$

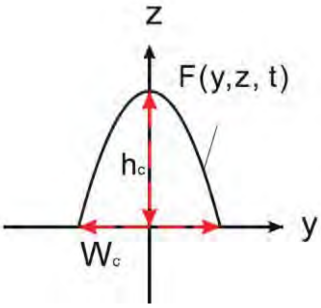

Figure II. 90: Schematic view of the clad profile in 2D [Ya, 2016].

The main disadvantage of all these models that predict the clad profile based on recursive methods is the fact that they require experimental data in order to obtain results. Moreover, all of them are based on the assumption that the filler material addition is constant, which can introduce relevant deviations with regard to the real LMD process, because the filler material deposition rate depends on the thermal field of the substrate.

Toyserkani et al. proposed an alternative two-step model to generate the geometry of the clad [Toyserkani, 2004]. In a first step, the laser beam heats the surface of the substrate and the boundaries of the melt pool are determined based on a thermal model. Afterwards, in a second step, a constant height clad is generated based on the following formula, where “Δh” is the height of the deposited layer, “r” is the radius of the powder flux and “Δt” is the elapsed time.

$$\Delta h = \frac{\dot{m} \cdot \Delta t}{\pi \cdot r^2 \cdot \rho} \tag{Eq. II. 18}$$

The model is based on the assumption that the temperature of the generated layer is equal to the temperature of the substrate below. However, a more realistic approach is the consideration that the temperature of the powder particles when the reach the surface of the substrate, may be different from that of the molten material. In fact, the temperature of the powder particles when they contact with the surface of the substrate differs from the temperature of the melt pool.

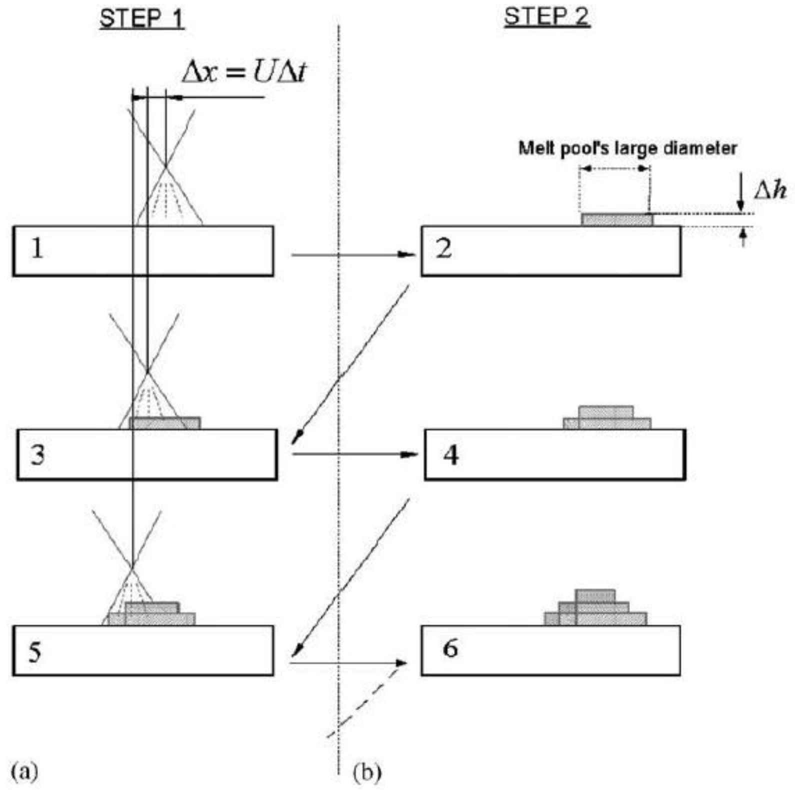

Figure II. 91: Sequence of calculation in the proposed numerical model [Toyserkani, 2004].

He and Mazumder tracked the interface between the molten material and the surrounding gas using the level/set method [He, 2007]. However, the model has an error when predicting the height of the deposited material that reaches almost the 100% of the experimentally measured height.

Tabernero et al. developed a model that calculates the height of the deposited material based on the thermal field. On every node that exceeds the melting temperature, generates a parallelepiped which height is proportional to the introduced amount of powder [Tabernero, 2012_2].

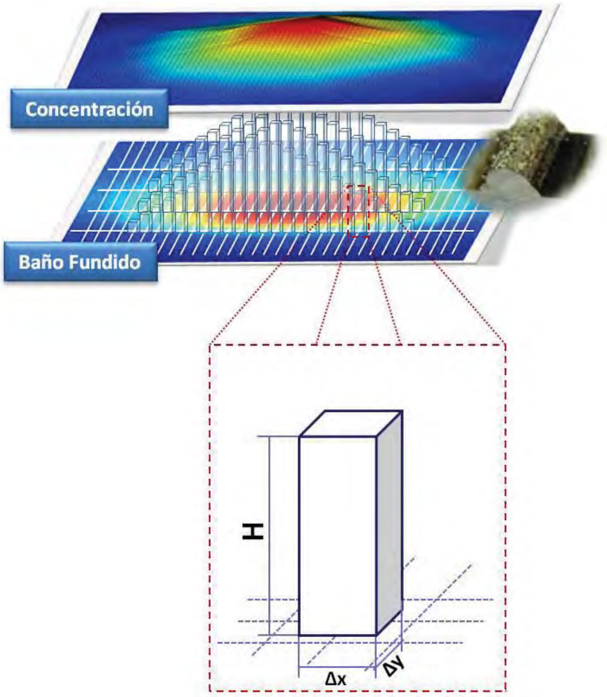

Figure II. 92: Material deposition procedure [Tabernero, 2012_2].

The amount of material injected per element “m_i” is calculated multiplying the mass flow “Φ_i”, that is previously obtained using a CFD model of the LMD nozzle [Tabernero, 2010], by the area of the element “W^2” and the interaction time “t”.

$$m_i = \Phi_i[Kg \cdot m^{-2} \cdot s^{-1}] \cdot W^2[m^2] \cdot t[s] \qquad \textbf{(Eq. II. 19)}$$

Therefore, equaling the injected mass flow and the mass of the created parallelepiped, the height of the deposited material for each element can be calculated by means of the following equation (Eq. II. 20). Where, “Δs” is the length of the discretization step, “ρ” the material density and “V_f” the machine feed rate.

$$H_i = \frac{\Phi_i[Kg \cdot m^{-2} \cdot s^{-1}] \cdot \Delta s[m]}{\rho[Kg \cdot m^{-3}] \cdot V_f[m \cdot s^{-1}]} \qquad \textbf{(Eq. II. 20)}$$

However, the model just predicts the geometry of a single line and actually no material is added to the substrate. Therefore, the model does not add material that in the next steps behaves as a substrate and cannot be applied to layer-by-layer operations.

Chew et al. developed a thermal model using the commercial software ABAQUS for solving the numerical equations [Chew, 2015]. Nevertheless, no material displacement was considered and the convective heat transfer in the melt pool was considered using a modified conductivity value.

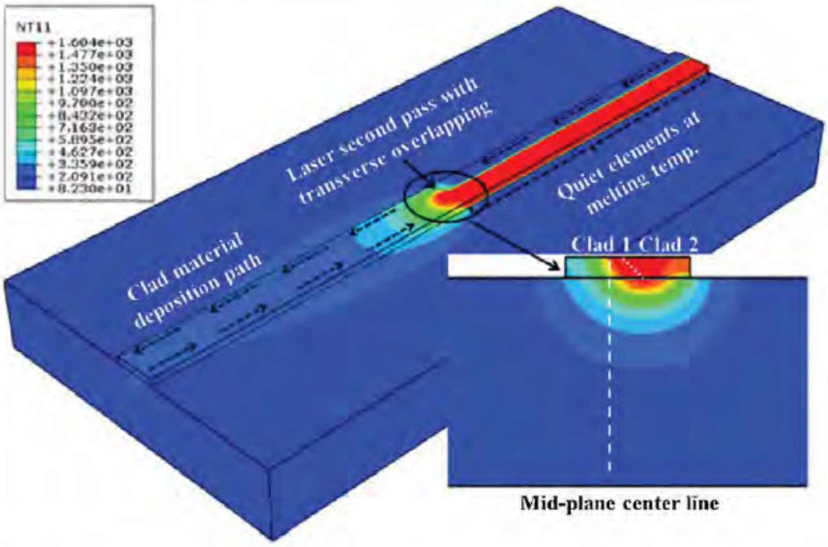
NT11
+1.604e+03
+1.477e+03
+1.350e+03
+1.224e+03
+1.097e+03
+9.700e+02
+8.432e+02
+7.163e+02
+5.895e+02
+4.627e+02
+3.359e+02
+2.091e+02
+8.230e+01
Laser second pass with transverse overlapping
Quiet elements at melting temp.
Clad material deposition path
Clad 1 Clad 2
Mid-plane center line

Figure II. 93: Modeling of continuous double line bead during the second laser heating pass [Chew, 2015].

II.9. Main highlights after the analysis of the state of the art of the Laser Metal Deposition

As a result of the review of the state of the art of the LMD process and the most important published research works related with monitoring and modeling, the following conclusions have been reached:

- The LMD is mainly applied to the coating, repair of high added value components and the generation of entire parts starting from zero. The aeronautical sector can be highlighted as a prominent field where the LMD technology is used.

- Nowadays, one of the main applications of the LMD is the integration of the additive process in machining centers. This way, hybrid machines that are able to manufacture parts by combining additive and subtractive operations are created.

- There is a large amount of research works focused on the experimental study of the LMD process. In these works, various combinations of laser equipment, LMD nozzles, materials and deposition strategies have been tested.

- Regarding the monitoring of the LMD process, there are different works related with the measurement of the geometry of the melt pool, determination of the temperature in different points during the process or the measurement of the powder mass flow. However, there is a need of a robust method that helps to control the process and enables to stabilize the process parameters.

- Most of the developed numerical models are based on a series of simplifications like the assumption that the deposited material has a fixed geometry or the powder that is added to the substrate has a determined temperature. Moreover, many models are orientated towards the achievement of partial results of the LMD process (residual stresses, geometrical distortions, hardness, etc.), but there are few models that consider the LMD process from a holistic point of view.

- The modeling of the melt pool dynamics in the LMD process has been addressed with different levels of complexity. However, no quantitative evaluation of the importance of their consideration or omission is found. Nor the improvement of the accuracy of the model is evaluated when the melt pool dynamics are considered.

- Despite the different works that study the wire and powder LMD processes, no data that compares the mechanical properties of parts produced by both processes have been found.

- There is a lack of background knowledge in the LMD nozzle design field. The most important patents and design developments published during the last years have been studied and it is noticed that no one justifies the design of the nozzle based on CFD simulations.

- In spite of the various control and monitoring systems available in the market or developed in previous research works, no system that controls instantaneously the powder mass flow during the LMD process is found.

Chapter III. Coaxial nozzle design for the Laser Metal Deposition process based on CFD simulation results

Chapter IV. Evaluation of the importance of melt pool dynamics in Laser Metal Deposition process modeling

Chapter V. Development and validation of a 3D model for LMD based on finite differences

Chapter VI. Contributions and future works

Chapter VI. Contributions and future works

In this last chapter, the main contributions of the present research work are summarized. Besides, the future works derived from the realization of the present project are also detailed.

VI.1. Contributions

In the present work a holistic approach of the LMD process is presented with the aim of establishing a landmark in the LMD process setup and modeling, in order to facilitate the industrial integration of this technology. The main contributions of the present research work are presented in detail below.

1. - **A new methodology for the nozzle design is developed:** The nozzle is one of the most important elements in the LMD process, since it is used for focusing the powder particles into the melt pool. Therefore, a proper nozzle design is required in order to ensure good quality parts and enhance the efficiency of the process. With this objective, a benchmarking of the industrial LMD nozzles that are available nowadays is carried out. Besides, the latest patents related with the design of the LMD nozzles are analyzed and their most important characteristics are highlighted. None of these designs is based on the CFD modeling of the powder particles and experimental knowledge is applied in most of the cases. On the contrary, the proposed methodology is based on the powder flux modelling into the nozzle, which helps on the design of internal cavities and chambers in order to obtain the required concentration of powder.

2. - **Development of a new coaxial nozzle design:** In order to validate the methodology for the nozzle design process, a coaxial continuous nozzle for complex LMD operations has been designed. For this purpose, the design of the nozzle is optimized using the CFD model until the initially stablished specifications are accomplished. Afterwards, it has been manufactured and validated. Favorable correlations between the simulations and the experimental results are obtained.

   Moreover, the nozzle is applied successfully for the deposition of different powder materials, such as Inconel 718, Hastelloy X, AISI D2, AISI H13, AISI 304, Stellite 6 or copper.

Different tests, including coating and 5 axis repair operations have also carried out using the designed nozzle.

3. - **Comparison between the powder and wire LMD processes:** A thorough analysis that compares both processes is carried out. For this purpose Inconel 718 tensile test probes are built layer by layer using a longitudinal strategy and the quality of the deposited material is characterized for both, powder and wire, LMD processes. Moreover, factors such as material efficiency, cleanness and robustness of the process are evaluated.

   It is concluded that, both technologies are capable of building high quality parts regarding the material integrity and mechanical properties. However, powder LMD is a more suitable process when complex geometries or all-directional geometries are to be generated. On the other hand, wire LMD results to be in advantage if simple geometries combined with higher deposition rates are required for the repair or manufacture of large parts.

4. - **Improvement of a mechanical system for measuring the powder distribution at the nozzle exit:** A set of containers are re-designed and manufactured for measuring experimentally the powder concentration at different distances from the nozzle tip. On the basis of the different diameters of the entrance holes, the powder distribution can be easily determined. The measurement of the powder distribution is useful not only for validating the manufactured nozzle, but also for verifying whether the nozzle is working properly. This is important when the nozzle suffers a collision or results damaged during the LMD operation.

   The main characteristic of the new design of the containers is the conical shape of the cover, which ensures that the particles that are injected outside the measuring hole do not bounce and fall inside. Moreover, the container includes an exhaust hole with a filter that allows the gas that has entered the container to come out, but not the powder particles. Thus, there is no overpressure inside the container and the gas flow at the nozzle exit is not affected. As a result of these re-design, the accuracy of the experimentally measured powder mass flow is increased.

5. – **Development of an instantaneous powder flux regulation system:** In order to enhance the stability of the process and control the dimensions of the deposited material, the powder mass flow that reaches the surface of the substrate needs to be controlled. The different powder feeding systems and control mechanisms that exist nowadays are

analyzed and it is concluded that most of these system are not capable of regulating the powder flux fast enough.

With this objective, a regulation system based on a solenoid is developed and installed into the nozzle. The powder flux regulation system is proved to be capable of controlling the height of the deposited material, which results to vary proportionally to the duty cycle of the PWM control. Using the appropriate PWM signal, a constant material deposition rate per substrate surface unit area is obtained. Therefore, powder accumulations due to variations of the machine feed rate can be smoothed and constant height depositions can be obtained.

The possibility to switch on or off the powder flow at the nozzle exit enables to stop the powder flux when the process is not depositing material, for example void movements or when the nozzle is approaching to the starting point of the LMD process. The collected powder in the recycling container is completely clean. Besides, as it has not interacted with the laser beam, it has not been re-melted, and maintains its original size and shape. Consequently, it can be reused with no drawbacks to the process. This fact results directly in material saving and a cleaner process.

6. - **Evaluation of the importance of melt pool fluid-dynamics in Laser Metal Deposition modeling:** An analysis of the relevance of the melt pool fluid-dynamics in the LMD process is carried out from an experimental and theoretical approach. On the basis of the obtained results, a process parameter window where the effects of the melt-pool dynamics can be neglected without losing accuracy is determined and justified.

First of all, the developed model is validated for a simple case where the substrate is melted under a static laser beam and no filler material is added. Simulations and experimental results present a good agreement considering the number of involved parameters.

On a second step, the same model is used for predicting the geometry of the deposited material in the LMD process, where filler material is introduced in powder form. On the one hand, a complex model that simulates the thermo-fluid-dynamic phenomena inside the melt pool is used, which results to be able to predict the geometry of the deposited material with an error under the 10%. On the other hand, a simpler thermal model that omits the movement of the molten material inside the melt pool is used to simulate the same tests and the obtained results are compared.

It is demonstrated that even the fluid-dynamic phenomena that occur inside the molten material have a big influence in the resulting shape of the melt pool when no filler material is added; their effect in the LMD process is much smaller. A coefficient named as “MP” that quantifies the importance of the fluid-dynamic phenomena is defined. For values of MP<1, the melt pool fluid-dynamics can be omitted without losing accuracy, what results in a much lower computational cost. All of these conclusions have been experimentally validated.

7. - **Development of a model that predicts the temperature of the powder particles before they are injected into the melt pool:** Powder particles result heated as a consequence of their interaction with the laser beam during the in-flight time from the nozzle to the substrate. A model that predicts the average temperature of the particles when they reach the surface of the melt pool is developed. The model considers phenomena such as the latent heat of fusion and the obtained temperature value of the particles is used as an input value for the LMD process model.

8. - **Development of a 3D model that simulates the complete LMD process and predicts the quality of the deposited material:** On the basis of the statement that melt pool fluid-dynamic phenomena can be neglected, a 3D thermal model that simulates the geometry and the thermal field of the workpiece is developed.

The model can predict the mechanical properties of the deposited material based on the process thermal history. On the one hand, the model is used for predicting the cooling rate of the deposited material. Using experimental equations and the cooling rate, the dendritic arm spacing (DAS) is calculated, which is proved to agree with the experimental measurements. On the other hand, the hardness of the material is predicted based on the sensitivity process that the material undergoes. The hardness value is experimentally validated and good agreement is obtained.

Moreover, a porosity model that predicts the pores apparition based on the probability of trapping gas bubbles or the generation of shrinkage cavities is developed. This model enables to anticipate the quality of the deposited material and therefore, it can be used for choosing the best LMD strategy.

VI.2. Future works

The contributions of the present work have served to pose new challenges, which can be the origin of future works. Below are described the proposed main future works:

- Deposition of reactive materials such as titanium alloys. Due to the reactive nature of these materials a special nozzle design that generates a protective atmosphere is required.
- Development of specific nozzles to be used coupled with galvanometric scanners. The main advantages of these nozzles are the high deposition rates and the increased flexibility due to the use of a mechatronic element such as the galvanometers. However, these nozzles must be capable of controlling automatically the powder flux in different zones of the working volume. These nozzles will present complex designs that could be optimized using CFD modeling.
- Optimize the powder feeding system. Integrate intelligent functions inside the LMD machine that, based on the powder material and powder grainsize, would be capable of calculating the rotation speed of the powder feeder in order to obtain a determined powder mass flow.
- Expansion of the developed model and the inclusion of variables such as the residual stresses generated during the cooling stage.
- Generation of an API or Toolbox that facilitates the 5-axis programming of the LMD process. This solution could be integrated inside a CAD/CAM/CAE module that facilitates the integration of the LMD technology in the industry and minimizes set-up times of the process.

Bibliography

[Albrecht, 2015] B. P. Albrecht, C. Hsu, *Additive manufacturing system for joining and surface overlay,* US0021379A1, 2015.

[Ambit, 2017] http://www.hybridmanutech.com/ (last access: 12/04/2017).

[Andolfi, 2012] A. Andolfi, F. Mammoliti, F. Pineschi. *Advanced laser cladding application for oil and gas components.* GE Oil and Gas company. Technology Insights, 2012.

[Arcam, 2016] *Information from Arcam regarding the tender by GE*, 2016. http://www.arcamgroup.com/investor-relations/2871-2/

[Arrizubieta, 2014] J.I. Arrizubieta, S. Martínez, A. Lamikiz, E. Ukar, I. Tabernero, A. Zugazaga, *Taladrado Láser mediante un Láser convencional*, Revista de Ingeniería Dyna, vol. 89 (3), pp. 338–346, 2014.

[Arrizubieta, 2016] J. I. Arrizubieta, F. Klocke, N. Klingbeil, K. Arntz, A. Lamikiz, S. Martinez, *Evaluation of efficiency and mechanical properties of Inconel 718 components built by wire and powder Laser Material Deposition Process*, Rapid Prototyping Journal, vol. 23 (6) , 2016.

[ASM, 2017] http://www.aerospacemetals.com/ (last access: 12/04/2017).

[ASTM, 2012] ASTM-International, ASTM Standard F2792-12a: Standard Terminology for Additive Manufacturing Technologies, 2012.

[AZOM, 2017] http://www.azom.com/article.aspx?ArticleID=6214 (last access: 12/04/2017).

[Bachmann, 2007] F. Bachmann, P. Loosen, R. Poprawe, *High Power Diode Lasers, Technology and Applications*, Springer Science+Business Media, LLC, 2007. ISBN-13: 978-0-387-34453-9

[Balazic, 2010] M. Balazic, M. Milfelner, J. Kopac, *Repair and Manufacture of High Performance Products for Medicine and Aviation with Laser Technology,* AIJSTPME, vol. 3 (4), pp. 15–22, 2010.

[Balu, 2012] P. Balu, P. Leggett, R. Kovacevic. *Parametric study on a coaxial multi-material powder flow in laser-based powder deposition process*, Journal of Materials Processing Technology, vol. 212, pp. 1598–1610, 2012.

[Bay, 2017] http://www.baystatesurfacetech.com/ (last access: 12/04/2017).

[Belforte, 2016] D. Belforte, *2015 industrial laser market outperforms global manufacturing instability*, Industrial Laser Solutions, February 2016.

[Bhadeshia, 2006] H. Bhadeshia, R. Honeycombe, *Steels: Microstructure and Properties,* 3rd edition, Butterworth-Heinemann, 2006. ISBN: 978-0-7506-8084-4,

[Bi, 2006_1] G. Bi, A. Gasser, K. Wissenbach, A. Drenker, R. Poprawe, *Characterization of the process control for the direct laser metallic powder deposition*, Surface and Coatings Technology, vol. 201, pp. 2676–2683, 2006.

[Bi, 2006_2] G. Bi, A. Gasser, K. Wissenbach, A. Drenker, R. Poprawe, *Investigation on the direct laser metallic powder deposition process via temperature measurement*, Applied Surface Science, vol. 253 pp. 1411–1416, 2006.

[Bi, 2007] G. Bi, B. Schürmann, A. Gasser, K. Wissenbach, R. Poprawe. *Development and qualification of a novel laser-cladding head with integrated sensors*. International Journal of Machine Tools and Manufacture, vol. 47, p. 555–561, 2007.

[Bi, 2011] G. Bi, A. Gasser, *Restoration of Nickel-Base Turbine Blade Knife-edges with Controlled Laser Aided Additive Manufacturing*. Physics Procedia, vol. 12, pp. 402–409, 2011.

[Bitragunta, 2015] V. S. Bitragunta, *Performance metrics for powder feeder systems in additive manufacturing*, Missouri University of Science and Technology, Materials Science and Engineering Department, Master Thesis Paper nº 7461, year 2015.

[Boisselier, 2014] D. Boisselier, S. Sankaré, T. Engel, *Improvement of the laser direct metal deposition process in 5-axis configuration*, Physics Procedia, vol. 56, pp. 239–249, 2014.

[Borges, 2010] B. Borges, L. Quintino, R. M. Miranda, P. Carr, *Imperfections in laser clading with powder and wire fillers*, International Journal of Advanced Manufacturing Technologies, vol. 50, pp. 175–183, 2010.

[Brückner, 2007] F.Brückner, D. Lepski, E. Beyer, *Modeling the influence of process parameters and additional heat sources on residual stresses in laser cladding*, Journal of Thermal Spray Technology, vol. 16, pp. 355–373, 2007.

[Calleja, 2014] A. Calleja, I. Tabernero, A. Fernández, A. Celaya, A. Lamikiz, L. N. López de Lacalle. *Improvement of strategies and parameters for multi-axis laser cladding operations*, Optics and Lasers in Engineering, vol. 56, pp. 113–120, 2014.

[Chakraborty, 2005] N. Chakraborty, S. Chakraborty, *Influences of sign of surface tension coefficient on turbulent weld pool convection in a gas tungsten arc welding (GTAW) process: a comparative study*, Journal of Heat Transfer, ASME vol. 127 (8), pp. 848–862, 2005.

[Chen, 2014] C. Chen, Y. Wang, H. Ou, Y. He, X. Tang. *A review on remanufacture of dies and moulds*, Journal of Cleaner Production, vol. 64, pp. 13–23, 2014.

[Chew, 2015] Y. Chew, J. H. Lye Pang, G. Bi, B. Bin Song, *Thermo-mechanical model for simulating laser cladding induced residual stresses with single and multiple clad beads*, Journal of Material Processing Technology, vol. 224, pp. 89–101, 2015.

[Costa, 2009] L. Costa, R. Vilar, *Laser powder deposition*, Rapid Prototyping Journal, vol. 15, pp. 264–279, 2009.

[Dai, 2016] D. Dai, D. Gu, *Influence of thermodynamics within molten pool on migration and distribution state of reinforcement during selective laser melting of AlN/AlSi10Mg composites*, International Journal of Machine Tools and Manufacture, vol. 100, pp. 14–24, 2016.

[DataRay, 2017] http://www.dataray.com/blog-m2-high-order-modes.html (last access: 12/04/2017).

[de Oliveira, 2005] U. de Oliveira, V. Ocelík, J.Th.M. De Hosson, Analysis of coaxial laser cladding processing conditions, Surface & Coatings Technology, vol. 197, pp. 127–136, 2005.

[Dinda, 2009] G. P. Dinda, A.K. Dasgupta, J. Mazumder, *Laser aided direct metal deposition of Inconel 625 superalloy: Microstructural evolution and thermal stability,* Materials Science and Engineering *A*, vol. 509, pp. 98-104, 2009.

[Ding, 2016] Y. Ding, J. Warton, R. Kovacevic, *Development of sensing and control system for robotized laser-based direct metal addition system*, Additive Manufacturing, vol. 10, pp. 24–35, 2016.

[DMG Mori, 2017] https://www.dmgmori.co.jp/en/ (last access: 12/04/2017).

[Dowden, 2009] J. Dowden, *The Theory of Laser Materials Processing: Heat and Mass Transfer in Modern Technology*, vol. 119. Springer Science & Business Media, 2009.

[El Cheick, 2012] H. El Cheikh, B. Courant, S. Branchu, J. Y. Hascoët, R. Guillén*, Analysis and prediction of single laser tracks geometrical characteristics in coaxial laser cladding process*, Optics and Lasers in Engineering, vol. 50, pp. 413–422, 2012.

[ELB, 2017] http://www.autania-grinding.de/1028.html (last access: 12/04/2017).

[EOS, 2015] https://www.eos.info/press/formnext-2015-eos-continues-course-of-success-growth (last access: 12/04/2017).

[EOS, 2017] https://www.eos.info/en (last access: 12/04/2017)

[FP7, 2014] Additive Manufacturing in FP7 and Horizon 2020. Report from the EC workshop on additive manufacturing held on 18 June 2014, 2014.

http://www.rm-platform.com/linkdoc/EC%20AM%20Workshop%20Report%202014.pdf

[Fu, 2008] J. W. Fu, Y. S. Yang, J. J. Guo, W. H. Tong, *Effect of cooling rate on solidification microstructures in AISI 304 stainless steel*, Materials Science and Technology, vol. 24 (8), pp. 941-944, 2008.

[Fu, 2002] Y. Fu, A. Loredo, B. Martin, A. B. Vannes, *A theoretical model for laser and powder particles interaction during laser cladding*, Journal of Materials Processing Technology, vol. 128, pp. 106–112, 2002.

[Gasser, 2010] A. Gasser, G. Backes, I. Kelbassa, A. Weisheit, K. Wissenbach, *Laser Additive Manufacturing: Laser Metal Deposition (LMD) and Selective Laser Melting (SLM) in Turbo-Engine Applications*, Laser Technik Journal, vol. 7 (2), pp. 58–63, 2010.

[GE Aviation, 2016] GE Aviation, *GE reaches agreement to acquire a 75% stake in Concept Laser GmbH of Germany*, 2016. Available online: http://www.geaviation.com/press/other/other_20161027b.html

[Gibson, 2009] M. Gibson, J. Tyrer, R. Higginson, *Direct Metal Deposition Melt Pool Temperature Distribution Control Through Novel Holographic Beam Shaping, Allowing Improved Mechanical and Corrosion Properties*, 28th International congress, Applications of lasers & electro-optics, Orlando, 2009.

[Grujicic, 2001] M. Grujicic, Y. Hu, G.M. Fadel, D.M. Keicher, *Optimization of the LENS rapid fabrication process for in-flight melting of feed powder*, Journal of Materials Synthesis and Processing, vol. 9 (5), pp. 223–233, 2001.

[Han, 2004] L. Han, F. W. Liou, K. M. Phatak, *Modeling of laser cladding with powder injection*, Metallurgical and Materials Transactions B, vol. 35, pp. 1139-1150, 2004.

[Han, 2005] L. Han, K. M. Phatak, F. W. Liou*, Modeling of laser deposition and repair process*, Journal of Laser Applications, vol. 17 (2), pp. 89–99, 2005.

[Haynes, 2017] http://www.haynes.ch/doc/HASTELLOY_X.pdf (last access: 12/04/2017).

[He, 2007] X. He, J. Mazumder, *Transport phenomena during direct metal deposition*, Journal of Applied Physics, vol. 101, nº 053113, 2007.

[Hecht, 2005] J. Hecht, *Beam: The Race to Make the Laser*, Optics and Photonics News, July/August, pp. 24-29, 2005.

[Heston, 2010] T. Heston, *Analyzing the potential of the solid-state laser. Fiber laser technology begins to penetrate the market*, The FABRICATOR, July 2010.

[HKTDC, 2016] HKTDC Research, 2016. http://economists-pick-research.hktdc.com (last access: 12/04/2017).

[Hofman, 2012] J.T. Hofman, B. Pathiraj, J. van Dijk, D.F. de Lange, J. Meijer, *A camera based feedback control strategy for the laser cladding process*, Journal of Material Processing Technology, vol. 212, pp. 2455–2462, 2012.

[Hosokawa, 2017] http://www.hmicronpowder.com/products/product/mikro-pneumatic-feeder (last access: 12/04/2017).

[Hybrid, 2017] http://www.hybridmanutech.com/news.html (last access: 12/04/2017).

[Ibarmia, 2017] http://www.ibarmia.com/en/ (last access: 12/04/2017).

[Ibarra-Medina, 2010] J. Ibarra-Medina, A. J. Pinkerton, *A CFD model of the laser, coaxial powder stream and substrate interaction in laser cladding*, Physics Procedia, vol. 5, pp. 337–346, 2010.

[Iglesias, 2014] I. Iglesias, I. Tabernero, E. Ukar, J. I. Arrizubieta, A. Lamikiz, *Generación de Recubrimientos Cerámicos Polivalentes mediante Aporte Láser de Material*, XX CNIM, Congreso Nacional de Ingeniería Mecánica, 2014.

[ILT, 2013] *New CAM system for laser material deposition*. Metal Powder Report, vol. 68 (1), pp- 36, January–February 2013.

[ILT, 2017] http://www.ilt.fraunhofer.de/en.html (last access: 12/04/2017).

[IPG, 2015] IPG Photonics, Annual Report 2015. http://investor.ipgphotonics.com/annual-reports.aspx

[IPG, 2017] http://www.ipgphotonics.com/ (last access: 12/04/2017)

[IPT, 2017] http://www.ipt.fraunhofer.de/en.html (last access: 12/04/2017)

[Iwatani, 2014] S. Iwatani, A. Sato, Y. Ishikawa, *Powder cladding nozzle*, EP3012060A1, 2014.

[IWS, 2017] http://www.iws.fraunhofer.de/en.html (last access: 12/04/2017).

[Jeng, 2001] J.Y. Jeng, M.Ch. Lin, *Mold fabrication and modification using hybrid processes of selective laser cladding and milling,* Journal of Materials Processing Technology, vol. 110, pp. 98–103, 2001.

[Jhavar, 2013] S. Jhavar, C.P. Paul, N.K. Jain, *Causes of failure and repairing options for dies and molds: A review,* Engineering Failure Analysis, vol. 34, pp. 519-535, 2013.

[Jones, 2012] J. Jones, P. McNutt, R. Tosi, C. Perry, D. Wimpenny, *Remanufacture of turbine blades by laser cladding, machining and in-process scanning in a single machine*, Proceedings from the 23rd Annual International Solid Freefrom Fabrication Symposium, 2012.

[Kaierle, 2012] S. Kaierle, A. Barroi, C. Noelke, J. Hermsdorf, L. Overmeyer, H. Haferkamp, *Review on Laser Deposition Welding: From Micro to Macro,* Physics Procedia, vol. 39, pp. 336–345, 2012.

[Kievack, 2003] B. Kieback, A. Neubrand, H. Riedel, *Processing techniques for functionally graded materials*, Materials Science and Engineering A, vol. 362, pp. 81–105, 2003.

[Klocke, 2014] F. Klocke, A. Klink, D. Veselovac, D. K. Aspinwall, S. L. Soo, M. Schmidt, J. Schilp, G. Levy, J. P. Kruth, *Turbomachinery component manufacture by application of electrochemical, electro-physical and photonic processes.* CIRP Annals-Manufacturing Technology, vol. 63, pp. 703–726, 2014.

[KMM, 2017] http://www.kmm-vin.info/ (last access: 12/04/2017).

[Koechner, 2006] W. Koechner. *Solid-State Laser Engineering*. Springer Science + Business Media Inc., 2006, ISBN-13: 978-0387-29094-2.

[Koehler, 2010] H. Koehler, K. Partes, T.Seefeld, F.Vollertsen, *Laser reconditioning of crankshafts: From lab to application*, Physics Procedia, vol. 5, pp. 387-397, 2010.

[Kong, 2010] C.Y. Kong, R.J. Scudamore, J. Allen, *High-rate laser metal deposition of Inconel 718 component using low heat-input approach*, Physics Procedia, vol. 5, pp. 379–386, 2010.

[Kovalev, 2010] O. B. Kovalev, A. V. Zaitsev, D. Novichenko, I. Smurov, *Theoretical and experimental investigation of gas flows, powder transport and heating in coaxial laser direct metal deposition (DMD) process,* Journal of Thermal Spray Technology, vol. 20, pp. 465–478, 2010.

[Lamikiz, 2011] A. Lamikiz, I. Tabernero, E. Ukar, S. Martinez, L. N. López de Lacalle, *Current Designs of Coaxial Nozzles for Laser Cladding*, Recent Patents on Mechanical Engineering, vol. 4, pp. 29–36, 2011.

[Laserline, 2017] http://www.laserline.de/ (last access: 12/04/2017).

[Launder, 1972] B. E. Launder and D. B. Spalding, *Lectures in Mathematical Models of Turbulence*, Academic Press, London, England. 1972.

[Layertec, 2017] https://www.layertec.de/en/capabilities/coatings/metallic (last access: 12/04/2017).

[Li, 1990] L. Li, W. M. Steen, R. B. Hibberd, *Computer aided laser cladding,* In: Bergmann HW, Kupfer R (eds): Proc. ECLAT’90, Erlangen (D), Arbeitsgemeinschaft Wärmebehandlung und Werkstofftechnik e.V. (AWT) 1: pp. 355–369, 1990

[Li, 2016] C. Li, C. H. Fu, Y. B. Guo, F.Z. Fang, *A multiscale modeling approach for fast prediction of part distortion in selective laser melting*. Journal of Material Processing Technology, vol. 229, pp. 703–712, 2016.

[Lin, 1999] J. Lin, *Concentration mode of the powder stream in coaxial laser cladding*, Optics & Laser Technology, vol. 31, pp. 251–257, 1999.

[Lin, 2000] J. Lin, *Numerical simulation of the focused powder streams in coaxial laser cladding*, Journal of Materials Processing Technology, vol. 105, pp. 17–23, 2000.

[Liu, 2003] C.Y. Liu, J. Lin, *Thermal processes of a powder particle in coaxial laser cladding*, Optics & Laser Technology, vol. 35 (2), pp. 81–86, 2003.

[Liu, 2005] J. Liu, L. Li, *Effects of powder concentration distribution on fabrication of thin-wall parts in coaxial laser cladding*, Optics & Laser Technology, vol. 37, pp. 287–292, 2005.

[Liu, 2014] S. Liu, P. Farahmand ,R. Kovacevic, *Optical monitoring of high power direct diode laser cladding*, Optics & Laser Technology, vol. 64, pp. 363-376, 2014.

[Liu, 2015] Y. Liu, T. Bobek, F. Klocke, *Laser path calculation method on triangulated mesh for repair process on turbine parts*, Computer-Aided Design, vol. 66, pp. 73–81, 2015.

[M&M, 2017] *Laser Technology Market by Type (Solid-YAG laser ,Fiber laser, Thin Disk Laser, Liquid, Gas-Argon Ion Laser, Excimer, CO2 & Others), Application (Medical, Industrial, Military, Research, Consumer, & Others), and Geography-Trends & Forecast to 2013-2020*, published by MarketsandMarket.
http://www.marketsandmarkets.com/Market-Reports/laser-technology-market-795.html (last access: 12/04/2017)

[Maiman, 1960] T. H. Maiman, *Optical and Microwave-Optical Experiments in Ruby*, Physical Review Letters, vol. 94, pp. 564, 1960.

[Martens, 2010] R. Martens. *MTU Aero engines*. www.mtu.de
(last access: 12/04/2017)

[Martin, 2013] J. Martin, *Australian Additive Manufacturing Technology and Cooperative Research Roadmap.* [Online] Available at: http://amcrc.com.au/aamtsummary, 2013.

[Martinez, 2016] S. Martínez, A. Lamikiz, E. Ukar, I. Tabernero, J. I. Arrizubieta, *Control loop tuning by thermal simulation applied to the laser transformation hardening with scanning optics process*, Applied Thermal Engineering, vol. 98, pp. 49–60, 2016.

[Mazak, 2017] https://www.mazak.com/ (last access: 12/04/2017).

[Medicoat, 2017] http://www.medicoat.ch/ (last access: 12/04/2017).

[Metzger, 2013] J. Metzger, *LMD in production*, Laser-Community; The Laser Magazine from TRUMPF, 2013. Available online: http://www.laser-community.com/en/bmw-and-lufthansa-go-for-additive-laser-metal-deposition/

[Miyagi, 2011] M. Miyagi, T. Tsukamoto, H. Kawanaka, *Laser processing head and laser cladding method*, US0089151A1, 2011.

[Miyagi, 2014] M. Miyagi, T. Tsukamoto, H. Kawanaka, *Laser processing system and overlay welding method*, US8901453B2, 2014.

[Mizar, 2017] http://mizaradditive.com/ (last access: 12/04/2017).

[Mohagegh, 2010] F. Mohagegh, H. Najafian, H. Bisadi, S. M. Hosseinalipour, *Effect of Powder Delivery System Parameters on a Powder Cladding System with one Lateral Nozzle*, 7th International Conference on Multiphase Flow (ICMF), USA, May 30th-June 4th 2010.

[Mok, 2008] S. H. Mok, G. Bi, J. Folkes, I. Pashby, *Deposition of Ti–6Al–4V using a high power diode laser and wire, Part I: Investigation on the process characteristics*, Surface and Coatings Technology, vol. 202 (16), pp. 3933–3939, 2008.

[Morsi, 1972] S. A. Morsi, A. J. Alexander, *An Investigation of Particle Trajectories in Two-Phase Flow Systems*, Journal of Fluid Mechanics, vol. 55 (2), pp. 193–208, 1972.

[Naebe, 2016] M. Naebe, K. Shirvanimoghaddam, *Functionally graded materials: A review of fabrication and properties*, Applied Materials Today, vol. 5, 2016, pp. 223–245, 2016

[Navas, 2005] C. Navas, A. Conde, B.J. Fernández, F. Zubiri, J.de Damborenea, *Laser coatings to improve wear resistance of mould steel*, Surface & Coatings Technology, vol. 194, pp. 136–142, 2005.

[Nenadl, 2014] O. Nenadl, V. Ocelík, A. Palavra, J. Th. M. D. Hosson, *The prediction of coating geometry from main processing parameters in laser cladding*, Physics Procedia, vol. 56, pp. 220–227, 2014.

[Nowotny, 2011] S. Nowotny, *Current use of laser technology for build-up welding applications*, Surface Engineering, vol. 27 (4), pp. 231–233, 2011.

[Nowotny, 2012] S. Nowotny, A. Schmidt, S. Scharek, T. Naumann, F. Kempe, *Machining head with integrated powder supply for deposition welding using laser radiation*, US8129657B2, 2012.

[Ocelík, 2007] V. Ocelík, U. de Oliveira, M. de Boer, J.Th.M. de Hosson, *Thick Co-based coating on cast iron by side laser cladding: Analysis of processing conditions and coating properties*, Surface & Coatings Technology, vol. 201, pp. 5875–5883, 2007.

[Ocelík, 2014] V. Ocelík, O. Nenadl, A. Palavra, J.Th.M. De Hosson, *On the geometry of coating layers formed by overlap*. Surface & Coatings Technology, vol. 242, pp. 54–61, 2014.

[Ocylok, 2014] S. Ocylok, E. Alexeev, S. Mann, A. Weisheit, K. Wissenbach, I. Kelbassa, *Correlations of melt pool geometry and process parameters during laser metal deposition by coaxial process monitoring*, Physics Procedia, vol. 56, pp. 228–238, 2014.

[Oerlikon, 2017] https://www.oerlikon.com/metco/en/ (last access: 12/04/2017).

[Onwubolu, 2007] G. C. Onwubolu, J. Davim, C. Oliveira, A. Cardoso, *Prediction of clad angle in laser cladding by powder using response surface methodology and scatter search*. Optics & Laser Technology, vol. 39, pp. 1130–1134, 2007.

[Overton, 2016] G. Overton, A. Nogee, D. Belforte, C. Holton, *Annual laser market review & forecast: can laser markets trump a global slowdown?*, Laser Focus World, February 2016.

[Pang, 2016] S. Pang, X. Chen, W. Li, X. Shao, S. Gong, Efficient multiple time scale method for modeling compressible vapor plume dynamics inside transient keyhole during fiber laser welding, Opt. Laser Technol. 77 (2016) 203–214.

[Parishram, 2007] P. Parishram, *Laser assisted repair welding of H13 tool steel for die casting,* University of Arkansas, United States, publication number 1452334, 2007.

[Partes, 2005] K. Partes, T. Seefeld, G. Sepold, F. Vollersten, *Increased efficiency in laser cladding by optimization of beam intensity and travel speed*, *Proceedings SPIE* 6157, Workshop on Laser Applications in Europe, 2005.

[Patankar, 1980] S. V. Patankar, *Numerical Heat Transfer and Fluid Flow*, McGraw-Hill Book Company, 1980. ISBN-13: 978-0891165224.

[Pavlov, 2010] M. Pavlov, M. Doubenskaia, I. Smurov, *Pyrometric analysis of thermal processes in SLM technology*, Physics Procedia, vol. 5, pp. 523–531, 2010.

[Pavlov, 2011] M. Pavlov, D. Novichenko, M. Doubenskaia, *Optical Diagnostics of Deposition of Metal Matrix Composites by Laser Cladding*, Physics Procedia, vol. 12, pp. 674–682, 2011.

[Peng, 2007] L. Peng, J. Shengqin, Z. Xiaoyan, H. Qianwu, X. Weihao, *Direct laser fabrication of thin-walled metal parts under open-loop control*, International Journal of Machine Tools and Manufacture, vol. 47, pp. 996–1002, 2007.

[Picasso, 1994] M. Picasso, C. F. Marsden, J.-D. Wagniere, A. Frenk, M. Rappaz*, A simple but realistic model for laser cladding*. Metallurgical and Materials Transactions B, vol. 25, pp. 281–291, 1994.

[Pinkerton, 2004] A. J. Pinkerton, L. Li, *Multiple-layer cladding of stainless steel using a high-powered diode laser: an experimental investigation of the process characteristics and material properties*. Thin Solid Films, vol. 453-454, pp. 471–476, 2004.

[Pinkerton, 2007] A.J. Pinkerton, *An analytical model of beam attenuation and powder heating during coaxial laser direct metal deposition*, Journal of Physics D: Applied Physics, vol. 40, pp. 7323–7334, 2007.

[Prakash, 2015] K. Prakash, P. Santanu, S. Ramesh, Y. Wenyi*, Experimental characterization of laser cladding of CPM 9V on H13 tool steel for die repair applications*, Journal of Manufacturing Processes, vol. 20 (3), pp. 492–499, 2015.

[Precitec, 2017] http://www.precitec.de/en/products/joining-technology/processing-heads/yw30/ (last access: 12/04/2017).

[Propawe, 2011] R. Poprawe, *Tailored Light 2, Laser Application Technology*, Springer-Verlag Berlin Heidelberg, 2011. ISBN 978-3-642-01236-5.

[Pugsley, 1996] T.S. Pugsley, B.J. Milne, F. Berruti*, An innovative non-mechanical feeder for high solids mass fluxes in circulating fluidized bed risers*, Powder Technology, vol. 88, pp. 123–131, 1996.

[Purtonen, 2014] T. Purtonen, A. Kalliosaari, A Salminen, *Monitoring and adaptive control of laser processes*, Physics Procedia, vol. 56, pp. 1218–1231, 2014.

[Rahamood, 2012] R. M. Mahamood, E. T. Akinlabi, M. Shukla and S. Pityana, *Functionally Graded Material: An Overview*, Proceedings of the World Congress on Engineering 2012 Vol III WCE 2012, July 4 - 6, 2012, London, U.K.

[Reis, 2017] http://rp-lasertec.com/ger/varioclad.html (last access: 12/04/2017).

[Renishaw, 2017] http://www.renishaw.com/en/additive-manufacturing-systems--15239 (last access: 12/04/2017).

[Richter, 2004] K.-H. Richter, S. Orban, S. Nowotny, *Laser cladding of the Titanium alloy Ti6242 to restore damaged blades*, Proceedings of ICALEO 2004: 23rd International Congress on Applications of Lasers and Electro-Optics, San Francisco, USA, 2004.

[Richter, 2008] K. H. Richter, *Laser Material Processing in the Aero Engine Industry. Established Cutting-Edge and Emerging Applications*, Proceedings of the 3rd Pacific International Conference on Application of Lasers and Optics, 2008.

[Richter, 2010] K. H. Richter, *Using the Laser for Build-Up. Established and Emerging Applications at MTU Aero Engines*, International Laser Technology Congress AKL'10, Aachen, 2010.

[Riedelsberger, 2013] H. Riedelsberger, *Laser cladding in ship and other offshore applications*, The Laser User, vol. 69, pp. 8, 2013.

[Safdar, 2013] S. Safdar, A. J. Pinkerton, L. Li, M. A. Sheikh, P. J. Withers*, An anisotropic enhanced thermal conductivity approach for modelling laser melt pools for Ni-base super alloys*, Applied Mathematical Modelling, vol. 37, pp. 1187–1195, 2013.

[Saldi, 2013] Z.S. Saldi, A. Kidess, S. Kenjereš, C. Zhao, I.M. Richardson, C.R. Kleijn, *Effect of enhanced heat and mass transport and flow reversal during cool down on weld pool shapes in laser spot welding of steel*, International Journal of Heat and Mass Transfer, vol. 66, pp. 879–888, 2013.

[Sciaky, 2017] http://www.sciaky.com/ (last access: 12/04/2017)

[Sciencedirect, 2016] http://www.sciencedirect.com/ (last access: 12/04/2017)

[Sexton, 2002] L. Sexton, S. Lavin, G. Byrne, A. Kennedy, *Laser cladding of aerospace materials*, Journal of Materials Processing Technology, vol. 122, pp. 63-68, 2002.

[Siemens, 2017] http://www.plm.automation.siemens.com/en_us/products/nx/for-manufacturing/cam/hybrid-additive-manufacturing.shtml
(last access: 12/04/2017).

[Smurov, 2013] I. Smurov, M. Doubenskaia, A. Zaitsev. *Comprehensive analysis of laser cladding by means of optical diagnostics and numerical simulation,* Surface & Coatings Technology, vol. 220, pp. 112–121, 2013.

[Song, 2008] R. Song, S. Hanaki, M. Yamashita, H. Uchida, *Reliability evaluation of a laser repaired die-casting die*, Material Science and Enginering A, vol. 483–484, pp. 343–345, 2008.

[Steen, 1991] W. M. Steen, *Laser surface cladding*, edit. Springer London, 1991. ISBN 978-1-4471-3820-4.

[Suri, 2009] A. Suri, M. Horio, *A novel cartridge type powder feeder*. Powder Technology, vol. 189, pp. 497–507, 2009.

[Tabernero, 2010] I. Tabernero, A. Lamikiz, E. Ukar, L.N. López de Lacalle, C. Angulo, G. Urbikain, *Numerical simulation and experimental validation of powder flux distribution in coaxial laser cladding*, Journal of Materials Processing Technology, vol. 210, pp. 2125–2134, 2010.

[Tabernero, 2011] I. Tabernero, A. Lamikiz, S. Martínez, E. Ukar, J. Figueras, *Evaluation of the mechanical properties of Inconel 718 components built by laser cladding,* International Journal of Machine Tools & Manufacture, vol. 51, pp. 465-470, 2011.

[Tabernero, 2012_1] I. Tabernero, A. Lamikiz, S. Martínez, E. Ukar, L.N. López de Lacalle, *Modelling of energy attenuation due to powder flow-laser beam interaction during laser cladding process,* Journal of Materials Processing Technology, vol. 212, pp. 516-522, 2012.

[Tabernero, 2012_2] I. Tabernero, A. Lamikiz, S. Martínez, E. Ukar, L.N. López de Lacalle, *Geometric Modelling of Added Layers by Coaxial Laser Cladding*, Physics Procedia, vol. 39, pp. 913–920, 2012.

[Tagliaferri, 2013] F. Tagliaferri, G. Leopardi, U. Semmler, M. Kuhl, B. Palumbo, *Study of the Influences of Laser Parameters on Laser Assisted Machining Processes*, Procedia CIRP, vol. 8, pp. 170–175, 2013.

[Tan, 2010] H. Tan, J. Chen, F. Zhang, X. Lin, W. Huang, *Process analysis for laser solid forming of thin-wall structure*, International Journal of Machine Tools and Manufacture, vol. 50, pp. 1–8, 2010.

[Tao, 2015] W. Tao, D. Huapeng, T. Jie, W. Hao, *Recent Repair Technology for Aero-Engine Blades*, Recent Patents on Engineering, vol. 9, pp. 132–141, 2015.

[Thayalan, 2006] V. Thayalan, R. G. Landers, *Regulation of Powder Mass Flow Rate in Gravity-Fed Powder Feeder Systems*, Journal of Manufacturing Processes, vol. 8 (2), pp. 121–132, 2006.

[Thompson, 2015] S. M. Thompson, L. Bian, N. Shamsaei, A. Yadollahi, *An overview of Direct Laser Deposition for additive manufacturing; Part I: Transport phenomena, modeling and diagnostics*, Additive Manufacturing, vol. 8, pp 36–62, 2015.

[Tolochko, 2004] N. K. Tolochko, S. E. Mozzharov, M. K. Arshinov, K. I. Arshinov, and M. B. Ignat’ev, *Laws governing vibrating feeding of finely dispersed powder into a laser sintering zone*, Powder Metallurgy and Metal Ceramics, vol. 43, pp. 9–10, 2004.

[Torims, 2012] T. Torims A. Ratkus, M. Zarins, V. Brutans, J, Vilcans, *In-Situ Laser Build-Up Welding Of Shipboard Crankshafts*, Applied Mechanics and Materials, vol. 234, pp. 39–46, 2012.

[Toyserkani, 2004] E. Toyserkani, A. Khajepour, S. Corbin, *3-D finite element modeling of laser cladding by powder injection: effects of laser pulse shaping on the process*, Optics and Lasers in Engineering, vol. 41, pp. 849–867, 2004.

[Toyserkani, 2005] E. Toyserkani, A. Khajepour, S. Corbin, *Laser Cladding*, CRC Press LLC, 2005. ISBN-13: 978-0849321726.

[Triantafyllidis, 2003] D. Triantafyllidis, L. Li, F. H. Stott, *Mechanisms of porosity formation along the solid/liquid interface during laser melting of ceramics*, Applied Surface Science, vol. 208-209, pp. 458–462, 2003.

[Trumpf, 2015] TRUMPF GmbH + Co. *Trumpf attentive annual report 2014/2015.* Corporate Communications and Public Affairs, 2015.

[Uddeholm, 2017] https://www.acerosuddeholm.com/2318.htm(last access: 12/04/2017).

[Udupa, 2014] G. Udupa. S. S. Rao, .K.V. Gangadharan, *Functionally Graded Composite Materials: An Overview*, Procedia Materials Science, International Conference on Advances in Manufacturing and Materials Engineering, ICAMME 2014, vol. 5, pp. 1291-1299, 2014.

[Urtasun, 2014] J. Urtasun, *Far-reaching technology for aircraft manufacture that pollutes less*, Elhuyar, basque research, 2014. Available online: http://www.basqueresearch.com/new/far-reaching-technology-for-aircraft-manufacture-that-pollutes-less

[Vetter, 1993] P. A. Vetter, J. Fontaine, T. Engel, L. Lagrange, T. Marchione, *Characterization of laser-material interaction during laser cladding process,* Transactions on Engineering Sciences, vol. 2, pp. 185–194, 1993.

[Vetter, 1994] P.A. Vetter, T. Engel, J. Fontaine, *Laser cladding: the relevant parameters for process control*, Proceedings of SPIE, vol. 2207, pp. 452-462, 1994.

[Vittal, 1987] B.V.R. Vittal, W. Tabakoff, *Two-Phase Flow Around a Two Dimensional Cylinder*, AIAA Journal, vol. 25 (5), pp. 648–654, 1987.

[Wang, 2011] W. Wang, L. Li, *High-quality high-material-usage multiple-layer laser deposition of nickel alloys using sonic or ultrasonic vibration powder feeding*, Proceedings of the Institution of Mechanical Engineers, Part B: Journal of Engineering Manufacture, vol. 225, pp. 130–139, 2011.

[Weber, 2013] C.L. Weber, V. Pena, M.K. Micali, E. Yglesias, S.A. Rood, J. A. Scott, B. Lal, *The Role of the National Science Foundation in the Origin and Evolution of Additive Manufacturing in the United States*, Science & Technology Policy Institute, 2013.

[Weisheit, 2001] A. Weisheit, G. Backes, R. Stromeyer, A. Gasser, K. Wissenbach, R. Poprawe, *Powder injection: the key to reconditioning and generating components using laser cladding*, Proceedings of International Congress on Advanced materials and Processes, Munich, Germany, 2001.

[Wen, 2009] S. Y. Wen, Y. C. Shin, J. Y. Murthy, P.E. Sojka, *Modeling of coaxial powder flow for the laser direct deposition process*, International Journal of Heat and Mass Transfer, vol. 52, pp. 5867–5877, 2009.

[WFL, 2017] http://www.wfl.at/Home (last access: 12/04/2017).

[Whitfield, 2016] R. P. Whitfield, *Laser cladding device with an improved nozzle*, US9352420B2, 2016.

[Wholers, 2014] T. Wholers, T. Caffrey, *Wholers Report 2014 - 3D Printing and Additive Manufacturing State of the Industry*, Wholers Associates, 2014.

[Wohlers, 2016] T. Wholers, et al., *Wholers Report 2016 - 3D Printing and Additive Manufacturing State of the Industry*, Wholers Associates, 2016.

[Xu, 2006] G. Xu, M. Kutsuna, Z. Liu, L. Sun. *Characteristic behaviours of clad layer by a multi-layer laser cladding with powder mixture of Stellite-6 and tungsten carbide*. Surface and Coatings Technology, vol. 201, pp. 3385-3392, 2006.

[Ya, 2013] W. Ya, J. Hernandez Sanchez, B. Pathiraj, A. Huis in't Veld, *A study on attenuation of a Nd:YAG laser power by co-axial and off-axial nozzle powder stream during cladding*. Proceedings of ICALEO'13, pp. 453-546, 2013.

[Ya, 2016] W. Ya, B. Pathiraj, S. Liu, *2D modelling of clad geometry and resulting thermal cycles during laser cladding*, Journal of Materials Processing Technology, vol. 230, pp. 217-232, 2016.

[Yang, 2009] N. Yang, *Concentration model based on movement model of powder flow in coaxial laser cladding*, Optics and Laser Technology, vol. 41, pp. 94–98, 2009.

[Zekovic, 2007] S. Zekovic, R. Dwivedi, R. Kovacevic, *Numerical simulation and experimental investigation of gas–powder flow from radially symmetrical nozzles in laser-based direct metal deposition*, International Journal of Machine Tools and Manufacture, vol. 47, pp. 112–123, 2007.

[Zhao, 2003] G. Zhao, C. Cho, J. D. Kim, *Application of 3-D finite element method using Lagrangian formulation to dilution control in laser cladding process*, International Journal of Mechanical Sciences, vol. 45, pp. 777-796, 2003.

[Zhong, 2015] C. Zhong, A. Gasser, T. Schopphoven, R. Poprawe, *Experimental study of porosity reduction in high deposition-rate Laser Material Deposition*, Optics and Laser Technology, vol. 75, pp. 87–92, 2015.